JMEMT

www.jmemt.jarap.org

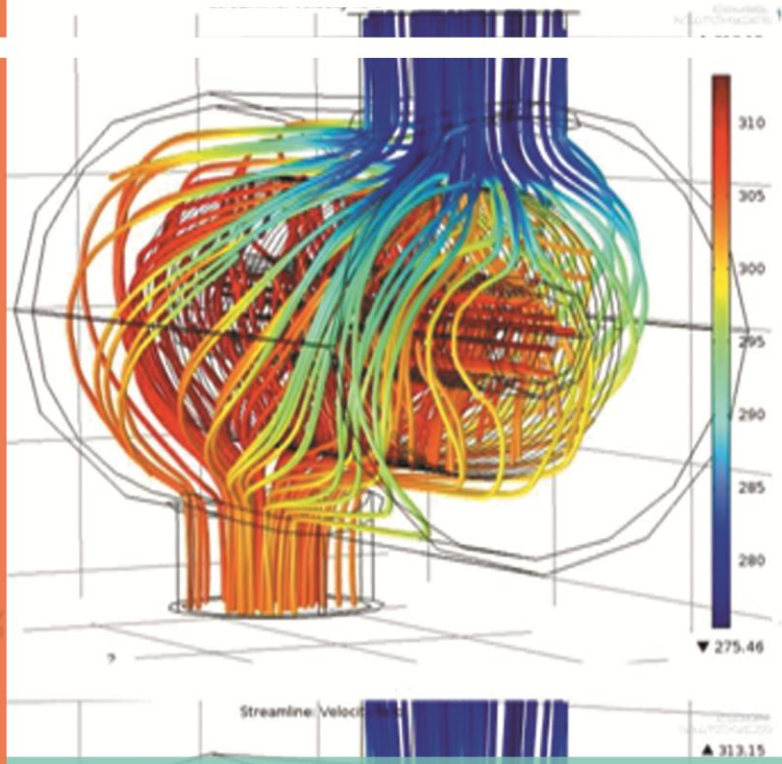

Journal of Mechanical Engineering & Modern Technology

Volume 1
Issue 1
30 June 2018

Jhand Advanced Research Analysis & Publication (JARAP)

www.jarap.org

Journal of Mechanical Engineering and Modern Technology

Editor Board

Publisher **:** Jhand Advanced Research Analysis & Publication, Vill. Khela, P.O. Chohan, Teh & Dist Amritsar, Punjab, India- 143149.

***Journal Customer Services*:** For ordering information, claims and any enquiry concerning your journal subscription please go to www.jarap.org/contact.aspx

Contact Email Address **:** ems@jarap.org & jaraporg@gmail.com

Website of Journal **:** www.jmemt.jarap.org

Website of Publisher **:** www.jarap.org

Contact Number **:** +91 7347265430

Journal of Mechanical Engineering and Modern Technology

INDEX

(Volume 1, Issue 1, 30 June 2018)

Journal of Mechanical Engineering & Modern Technology
www.jmemt.jarap.org
Volume 1 Issue 1, 30 June 2018
PP. 1-8

A CONTRIBUTION TO THE STUDY OF THERMAL LOAD OF TRUCKS POWERTRAIN SUSPENSION SYSTEM DUE TO VIBRATIONS

Miroslav D. DEMIC *[1] & Djordje M. DILIGENSKI [2]

[1] Engineering Academy of Serbia, Belgrade, Serbia.
[2] University of Belgrade, Vinča Institute of Nuclear Sciences, Centre for I.C. Engines and Vehicles, Belgrade, Serbia.
* Corresponding author; E-mail: demic@kg.ac.rs ; Tel.: +381642415367

Key words

vehicle,
vibration parameters,
degradation,
thermal load powertrain mounting system

Abstract

Dynamic simulation, based on modelling, has a significant role during to the process of vehicle development. It is especially important in the first design stages, when relevant parameters are to be defined. Powertrain mounting system is exposed to thermal loads which can lead to its damage and degradation of characteristics. Therefore, this paper attempts to analyse a conversion of mechanical work into heat energy by use of a method of dynamic simulation. Bearing in mind the most frequent application of classic - mechanical and hydraulic powertrain suspension in modern trucks, this paper will present analyses of thermal load of a vehicle manufactured by the domestic manufacturer FAP. The issue of heat dissipation from the powertrain mounting system has not been taken into consideration. The experimental verification of the results will be done in next investigations.

1. INTRODUCTION

As it is known, the vibration and noise from the powertrain of the vehicle are transmitted to the vehicle structure. In order to reduce this effect to a satisfactory measure, the powertrain is to be elastically linked to the vehicle structure. In the opposite direction, the same system absorbs vibration excitations coming from the road, and passing through the vehicle suspension system to the powertrain. Kinetic energy of the powertrain, which is a result of vibration, causes a mechanical work in powertrain mounts which is transformed into thermal energy [1].

In practice, in the stage of vehicle development, powertrain mounting system are chosen from the condition of damping of vehicle vibrations, but in order to avoid the negative impact on the function, thermal loads should be taken into consideration [2, 3]. The goal is to convert, as much as possible, the mechanical work received from the ground and powertrain into thermal energy which will be transferred to the environment and thus provide the cooling of powertrain mounting system. Wrong selection of mount characteristics, from the standpoint of thermal loads, can cause rapid degradation of its properties during service life. Excessive amount of heat energy, eventually kept "inside" the mounts, would cause rapid deterioration of sealing elements and loss of function of the damping element.

Tests have shown that the mechanical work is partly converted into the heat which is transferred to the mounts, and the remaining amount of heat delivery is transferred to the environment, thus cooling the powertrain mounting system. Mathematically, it can be displayed by the formula [3-7]:

$$A = Q_t + Q_f + Q_e \qquad (1)$$

where:

– A - mechanical work (equal to the quantity of heat),

- Q_t - quantity of heat transferred to the mount body,
- Qf - quantity of heat transferred to the working fluid (in the case that it exists), and
- Qe - quantity of heat transferred to the environment.

The work of the force in the mount is of relevance because it enables the analysis of its transformation into heat energy. The work of force in the mount is experimentally measurable, but it is hard to measure the amount of heat released from the mount [1, 2]. This phenomenon is complex and difficult to measure in test conditions because it is known that a part of the generated energy is distributed to the mount elements, working fluid (in case it exists), etc. In addition, the nature of heat transfer from the mount to the environment is very complex. Heat transfer is carried out by convection, as dominant, also by conduction and radiation [2].

From the point of maximal cooling, proper selection of mounts requires a comprehensive analysis of the transformation of mechanical energy into heat. Method of transformation of mechanical energy into heat is largely determined by the mount design. It is not possible to influence directly on the conduction of heat and radiation from the mount. It is necessary to increase the influence of the heat transfer by convection from the mounts to the surrounding environment, as dominant appearance. The idea is to utilize convection flow of air around the mount with the least complexity of the structure. In practice, this solution is rarely used, but can be applied. Making some kind of air deflectors on the elements of the body should increase the effect of convective heat transfer to the environment.

Note that the objective of this study was not to analyse the cooling of the powertrain mounts, but only thermal load to which it is exposed. Therefore, it was deemed expedient to analyse the heat which is obtained by converting mechanical work into heat energy per time unit. Mechanical work in powertrain mounting system was calculated by use of mechanical powertrain model, which will be discussed below.

This research does not take into account thermal load caused by the engine combustion process, which is transmitted to the mounts, because this load does not arise from vibration. To be more specific, only thermal stresses that result from mechanical work of elasto-damping forces in mounts were analysed.

As it is known, conventional mounts consist of rubber-metal elements, with the damping effect coming from the tire hysteresis, and further having hydraulic damping of the oil flow.

It is well known that vibrations of the power train are investigated in detail [8,14]. However, there are very rare cases of research of the power train mounts thermal loads. Classic power train mounts consist of metal-rubber elements, with damping coming from rubber hysteresis and additional hydraulic damping from the oil streaming through them. Considering the presence of classic – mechanical and hydraulic power train mounting systems in modern trucks, analysis of power train mounting thermal loads of a FAP 1213 vehicle [8] was conducted. Bearing in mind that cooling of the powertrain mounts is very complicated, the experimental verification of the thermal powertrain mounts will be done in next investigation.

2. MODEL OF POWERTRAIN

In the literature, depending on the task to be solved, we can find different models of mechanical powertrains. From [9,10-15] it is well known that during the analysis of the problem of transferring dynamic loads from the powertrain to the freight vehicle frame, vibration of cab and cargo box may be neglected. To be more precise, the analysis shall include only the vibration motion of the vehicle powertrain and related
excitations of the vehicle frame For the sake of illustration, Fig. 1. shows scheme of powertrain suspension of a FAP freight vehicle [8].

Powertrain, as a rigid body in space, has six degrees of freedom (three translations and three rotations) [9,10, 11-13, 15-20]. In order to describe its spatial movement, a Cartesian coordinate system with the origin in the CG of the powertrain will be adopted, initially in steady state. One of axis is parallel to the axis of the engine crankshaft, while the other two are perpendicular to the first one [9,21-24]. The adopted coordinate axes will be called CG geometric axes, and they are, at the same time coinciding with the axes which are often used by powertrain manufacturers [8,9]. It should be pointed out that the use of geometric CG axes leads to the application of centrifugal moments of inertia, but in order to simplify the analysis, it was found appropriate to introduce the assumption that they are, at the same time, the major axes of inertia. Powertrain performs spatial vibrations as a result of the excitations from the frame (originally coming from the road unevenness and frame vibration as an elastic system), as well as uneven engine running, inertial forces and torques of rotating masses, etc.

For describing the vibrational motion of the powertrain, two coordinate systems will be adopted [9, 14], see Fig. 2:

• stationary, and

• movable, fixed to the powertrain.

The motion of the powertrain in the space is defined with three coordinates X, Y, Z, and rotation of the powertrain around CG (as a fixed point) is defined by three angles: φ-roll, θ-pitch and ψ-yaw.

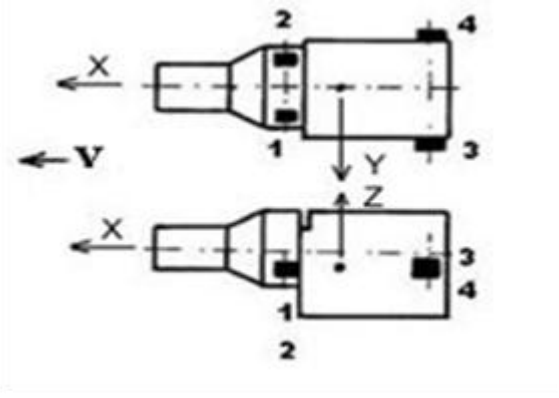

Fig. 1 Scheme of powertrain suspension of the observed freight vehicle

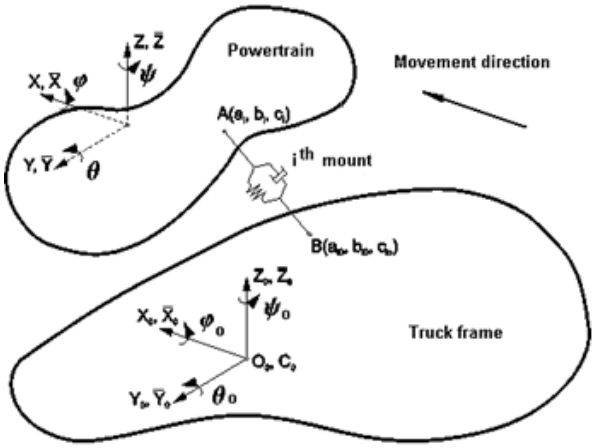

Fig. 2 Coordinate systems introduced to describe motion of the powertrain

Newton-Euler equations are applied to describe spatial motion of the powertrain [11].

$$M\ddot{X}_C = \sum X_i \quad (2)$$

$$M\ddot{Y}_C = \sum Y_i \quad (3)$$

$$M\ddot{Z}_C = \sum Z_i \quad (4)$$

$$I_u\dot{\omega}_u - I_{uv}\dot{\omega}_v - I_{uw}\dot{\omega}_w + (I_w\omega_w - I_{uw}\omega_u - I_{vw}\omega_v)\omega_v - (I_v\omega_v - I_{uv}\omega_u - I_{vw}\omega_w)\omega_w = \sum M_u^{F_i} \quad (5)$$

$$I_v\dot{\omega}_v - I_{uv}\dot{\omega}_u - I_{uw}\dot{\omega}_w + (I_u\omega_u - I_{uv}\omega_v - I_{uw}\omega_v)\omega_w - (I_w\omega_w - I_{uv}\omega_u - I_{vw}\omega_v)\omega_u = \sum M_v^{F_i} \quad (6)$$

$$I_w\dot{\omega}_w - I_{uv}\dot{\omega}_u - I_{vw}\dot{\omega}_v + (I_v\omega_v - I_{uv}\omega_u - I_{vw}\omega_w)\omega_u - (I_u\omega_u - I_{uv}\omega_v - I_{uv}\omega_w)\omega_v = \sum M_w^{F_i} \quad (7)$$

where:

M - powertrain mass,

- $\ddot{X}_C, \ddot{Y}_C, \ddot{Z}_C$ –projections of powertrain accelerations on axes of the moving coordinate systems,
- X_i, Y_i, Z_i – projection of excitation forces and reactions of respective powertrain mounts,
- I_u, I_v, I_w, I_{uv}, I_{uw}, I_{vw} – moments of inertia for the respective coordinate axes,
- $\omega_u, \omega_v, \omega_w, \dot{\omega}_u, \dot{\omega}_v, \dot{\omega}_w$ -the angular velocities and accelerations for axes u, v and w,
- M_u , M_v, M_w – projections of torques of the excitations, engine torque, and mounts of the powertrain for axes *u*, *v* and *w*.

For the sake of simplification, it will be assumed that the angular motions of the powertrain are small [14] what may enable the application of the relations [9, 11, 18, 21-23]:

$$\omega_u = \dot{\varphi}\ \omega_v = \dot{\theta}\omega_w = \dot{\psi}$$

In order to calculate forces in the mounts, it is necessary to define their deformations and deformation velocities. Bearing in mind the adopted coordinate systems, motion of any point on the powertrain is given in the equation in a matrix form [9-11]:

$$r = r_C + Lr_A \quad (8)$$

where:

$$r_C = \begin{bmatrix} X \\ Y \\ Z \end{bmatrix} \quad (9)$$

$$r_A = \begin{bmatrix} a_i \\ b_i \\ c_i \end{bmatrix} \quad (10)$$

$$L = \begin{bmatrix} c2c3 & s1s2c3 & s1s3 - c1s2c3 \\ -c2s3 & -s1s2s3 & c1s2s3 \\ s2 & -s1c2 & c1c2 \end{bmatrix} \quad (11)$$

In the expression (11) ***s*** and ***c*** are cosine and sinus of the respective angles, respectively.

For small angles the following expression can be written:

$$L = \begin{bmatrix} 1 & \psi & -\theta \\ -\psi & 1 & \varphi \\ \theta & -\varphi & 1 \end{bmatrix} \quad (12)$$

Similarly, and bearing in mind the low vibration of a vehicle, the expression can be written:

$$r_0 = r_{c0} + L_0 r_B \quad (13)$$

$$r_{c0} = \begin{bmatrix} X_0 \\ Y_0 \\ Z_0 \end{bmatrix} \quad (14)$$

$$r_B = \begin{bmatrix} a_{Bi} \\ b_{Bi} \\ c_{Bi} \end{bmatrix} \quad (15)$$

$$L_0 = \begin{bmatrix} 1 & \psi_0 & -\theta_0 \\ -\psi_0 & 1 & \varphi_0 \\ \theta_0 & -\varphi_0 & 1 \end{bmatrix} \quad (16)$$

where X_O, Y_O and Z_O - coordinates relative to the origin of the movable coordinate system of the vehicle frame.

Since the dimensions of the mounts are small relative to the powertrain, the following can be written:

$$r_A \approx r_B \rightarrow r_i = \begin{bmatrix} a_i \\ b_i \\ c_i \end{bmatrix} \quad (17)$$

Deformation of the *i*-th mount is defined by the following matrix equation [9, 11]:

$$\Delta_i = r - r_0 = (r_c - r_{c0}) + (L - L_0) r_i \quad (18)$$

Substituting the corresponding expressions and rearranging leads to the expressions:

$$\Delta X_i = X - X_0 + b_i(\psi - \psi_0) - c_i(\theta - \theta_0) \quad (19)$$
$$\Delta Y_i = Y - Y_0 + a_i(\psi - \psi_0) + c_i(\varphi - \varphi_0) \quad (20)$$
$$\Delta Z_i = Z - Z_0 - a_i(\theta - \theta_0) - b_i(\varphi - \varphi_0) \quad (21)$$

Mount deformation velocities can be obtained by differentiating the previous expressions:

$$\Delta \dot{X}_i = \dot{X} - \dot{X}_0 + b_i(\dot{\psi} - \dot{\psi}_0) - c_i(\dot{\theta} - \dot{\theta}_0) \quad (22)$$
$$\Delta \dot{Y}_i = \dot{Y} - \dot{Y}_0 + a_i(\dot{\psi} - \dot{\psi}_0) + c_i(\dot{\varphi} - \dot{\varphi}_0) \quad (23)$$
$$\Delta \dot{Z}_i = \dot{Z} - \dot{Z}_0 - a_i(\dot{\theta} - \dot{\theta}_0) - b_i(\dot{\varphi} - \dot{\varphi}_0) \quad (24)$$

In the literature [19, 20] there are many mathematical models of powertrain mounts, which are essentially more or less complicated. Bearing in mind the objective of this study was a comparative analysis of thermal loads in mounts, it was estimated to be acceptable to apply more simplified expressions for approximation of forces in the mounts.

Forces in elastic mounts are assumed in the form [9]:

$$F_{ci} = c_{i1}\Delta_i + c_{i2}\Delta^2 + c_{i3}\Delta^3 \quad (25)$$

where:

- c_i, c_{i1}, c_{i2} and c_{i3} – stiffness coefficients, and
- Δ_i – relative deformation of the mount.

Damping forces in the mounts are assumed in the form [9]:

$$F_{ai} = k_{i1}\dot{\Delta} + k_{i2}\dot{\Delta}^2 sign(\Delta) \quad (26)$$

where:

- k_{i1}, k_{i2} –damping coefficients,
- $\dot{\Delta}$ - relative velocity of the mount deformation, and
- *sign* - respective mathematical function.

Powertrain vibrations also depend on the unbalance of the running engine (torques and inertial forces).

In the specific case of a four-stroke four-cylinder in-line diesel engine was used with a crankshaft whose kranks lie in the same plane (the angle 180°). Forces occur in the reciprocating mechanisms [24] that drive the piston (gas forces and inertial forces of the piston group), and centrifugal and tangential forces acting on the movable bearing of the crank shaft knee. When balancing the inertial forces of the piston group mass (in the ideal case, if a force is developed into Fourier series), the inertial forces of the second and higher orders stay unbalanced. It is noted that in case when there are differences in the masses of the piston groups for each cylinder, there are also unbalanced forces of the first order (in this considered case, the masses have been equal to each other).

Assuming that harmonics of a higher order can be ignored, the unbalanced inertial force of the observed engine can be expressed in the form [14, 24]:

$$F_{in} = 4 m_r \omega^2 \lambda \cdot \cos 2\omega t \quad (27)$$

where:

- m_r – reduced mass of the piston group,
- r – radius of the crankshaft crank,
- ω - angular velocity of the engine crankshaft,
- λ - crankshaft radius and connecting rod ratio, and
- t – time.

Using basic knowledge of the vector theory and postulates of statics, and taking into account Figs 2 and 3, the torque resulting from the inertial force is defined by the equation (8) [9]:

$$\overrightarrow{M_{Fin}} = \begin{bmatrix} \overrightarrow{u_0} & \overrightarrow{v_0} & \overrightarrow{w_0} \\ a_E & b_E & c_E \\ -F_{in} sin\gamma & \gamma & F_{in} cos\gamma \end{bmatrix} \quad (28)$$

wherein the expressions in (9) are harmonized with the Fig. 3.

Centrifugal force is partially balanced the counter-weights, or by use of other methods, of which there will be no more to say, but readers are advised to see [24].

Tangential force causes engine torque, which, due to its variation has a variable value (unevenness is partially reduced by the engine flywheel) [24].

In the absence of precise information, it will be assumed that the torque acting on the powertrain can be described by expression [9]:

$$M = -M_e \cdot i_0 \cdot i_m (0.95 + 0.1 \cdot rnd) \quad (29)$$

where:

- M_e – engine torque,
- i_0 – driving axle ratio,
- *rnd* – random numbers uniformly distributed in the interval [0,1].

The vibration of powertrain impacts the vibration of the vehicle frame, which is of random nature [9,14]. Bearing in mind that

the complexity of the vehicle spatial model exceeds the needs of this study, it is estimated to be appropriate in this specific case not to use the frame vibration excitations based on the vehicle model, but to use already adopted broadband excitation functions in the following form:

excitation = max (*rnd*- 0.5) (30)

where:

- max = 0.01 m, rad
- *rnd*- has the same meaning as mentioned in description of the engine torque.

Projections of the generalized forces include all the components of forces and torques of the corresponding mount in the direction of the observed axes (for mounts 1 to 4), the engine inertial forces and torques and unbalanced inertial forces, as well as the active suspension force which, does not have the corresponding torque due to the assumption that it acts in the powertrain C.G.

Bearing in mind the expressions (1-27), differential equations of motion of the powertrain can be written in the form:

$$M\ddot{u} = \sum X_i \quad (31)$$

$$I_u\ddot{\varphi} = \sum M_F^u \quad (32)$$

$$M\ddot{v} = \sum Y_i \quad (33)$$

$$I_v\ddot{\theta} = \sum M_F^v \quad (34)$$

$$M\ddot{w} = \sum Z_i \quad (35)$$

$$I_w\ddot{\psi} = \sum M_F^w \quad (36)$$

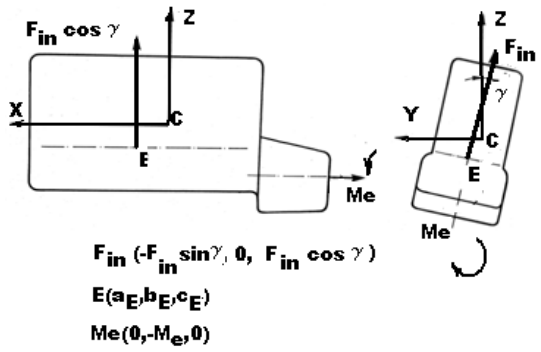

Fig. 3 Inertial force and engine torque

where:

F_{in} – resulting inertial force of piston group,

M_e – engine torque,

E – acting point of the resulting force and its coordinates related to the moving coordinate system,

γ - engine inclination (in the observed case 0°).

3. THERMAL LOAD OF MOUNTING SYSTEM

Due to the relative motion of sprung and unsprung masses, mechanical work is being done in mounts, which is equivalent to the amount of produced heat, Q [2]. Mechanical work (the amount of heat) is defined by the expression [2-7]:

$$A = \int_0^s F_m(t) \cdot dz_{rel} = \int_0^T F_m(t) \cdot \dot{z}_{rel} \cdot dt\,, \quad (37)$$

where:

- $F_m(t)$ - is elasto-damping force in the mount,
- z_{rel} – is deformation of the mount, eqns (19 - 21),
- $\dot{z}_{rel}$ - relative velocity of deformation (time derivatives of displacements) given by eqns (22-24) and
- t – is time.

Mechanical power, $P(t)$, that is equivalent to heat flux, is the first derivative of mechanical work with respect to time:

$$P(t) = \frac{dA}{dt} \quad (38)$$

Average power, P_{av}, is given by expression [10]:

$$P_{av} = \frac{A}{T} = \frac{1}{T}\int_0^T P(t) \cdot dt\,, \quad (39)$$

where T is the monitoring period. Average power turns into heat, with dominant convection [10]:

$$P = \alpha \cdot S \cdot \Delta\tau\,, \quad (40)$$

where:

- α - is heat transfer coefficient,
- S - convection area and
- $\Delta\tau$ - is temperature difference between the mounts and surrounding air.

As already noted, the analysis of heat transfer from the mount has not been carried out in the paper, because the values of α_i and S_i are not known, and it requires very extensive experimental studies to determine these values, which will certainly be the subject of special attention in the future.

Since all four power train unit mounts had the same characteristics, the analysis of collective thermal loads was conducted.

4. NUMERICAL SIMULATION AND ANALYSIS OF RESULTS

On the basis of the expressions (1-40), it can be seen that the differential equations describing the spatial vibration of the vehicle powertrain are non-linear and should be solved numerically, by use of the method Runge-Kutta, and by use of a software developed by the authors, in Pascal. The integration was carried out with the time increment of 0.0001 s, in 524288 points. This enabled reliable analysis in the domain 0.019-5000 Hz [25]. It is obvious that the domain is much broader than range of excitations from the running engine and the entire vehicle powertrain. Integration of differential equations is carried out in case of using conventional and hydraulic mounts.

The parameters of the observed vehicle and its powertrain given in Tab. 1, and the coordinates of the connection points (mounts) in Tab. 2.

Table 1. Characteristic parameters of the vehicle FAP 1213 and its powertrain

Maximal engine power, kW	100
Maximal engine speed, min^{-1}	2600
Maximal engine torque, Nm	428
Engine speed at max. engine torque, min^{-1}	1300
Vehicle mass, kg	12000
Powertrain mass, kg	1680
Moments of inertia Ix/Iy/Iz, kgm^2	85/35/72
Driving axle gear ratio, -	3.83
Transmission ratio in direct gear, -	1

Table 2. Engine mounts coordinates

Mount position →	a, m	b, m	c, m
Mount 1	0.5	0.4	0.1
Mount 2	0.5	-0.4	0.1
Mount 3	-0.5	0.4	0.1
Mount 4	-0.5	-0.4	0.1

Mechanical and hydraulic mounts have identical stiffness in the direction of the axes X, Y and Z, which are determined by the tests performed in FAP [8], as shown in Table 3.

Table 3. Stiffness of the applied conventional and hydraulic mounts

	c_{i1}, N/m	c_{i2}, N/m^2	c_{i3}, N/m^3
X	1200000	250000	60000
Y	1200000	250000	60000
Z	1200000	250000	60000

In the absence of accurate data, damping characteristics of the mounts are approximately defined on the basis of the support stiffness and mass carried by those [11], and are given in Tab. 4.

Table 4. Assumed damping characteristics of the mounts

	k_{i1} (mechanical/ hydraulic), Ns/m	k_{i2} (mechanical/ hydraulic), Ns^2/m^2
X	620/62000	1/100
Y	620/62000	1/100
Z	620/62000	1/100

In this paper it is assumed that the frame has six identical excitations in the time domain (eq. 30). For the illustration, vertical vibration excitations of the powertrain, derived from the frame vibration are shown in Fig. 4. It is obvious that the excitations are very dynamic, and so large thermal load of the powertrain mounts should be expected.

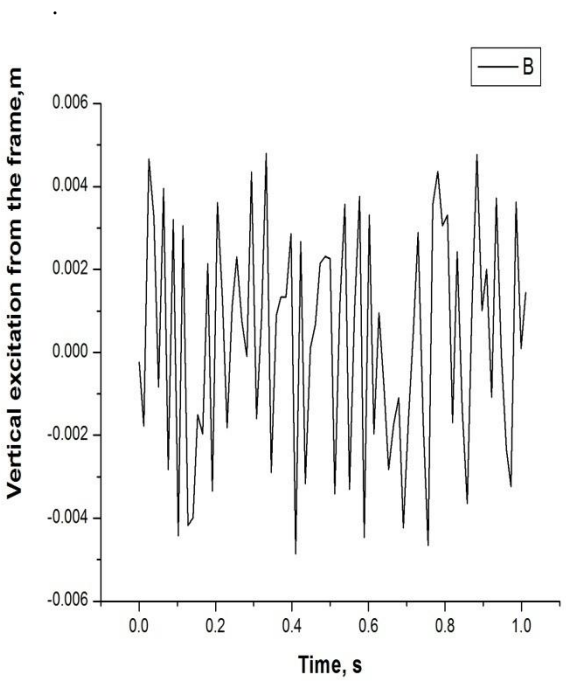

Fig. 4 Illustration of the frame excitation

Results of the dynamic simulation are shown in the time domain. To illustrate, Fig. 4 gives the variation of displacements in case of use of hydraulic mounts. Analysis of the data concerning classical and hydraulic mounts, partially shown in Fig. 5, in the time domain, shows that the type of the applied mounts affects the character and the amplitude of the monitored displacement of the powertrain.

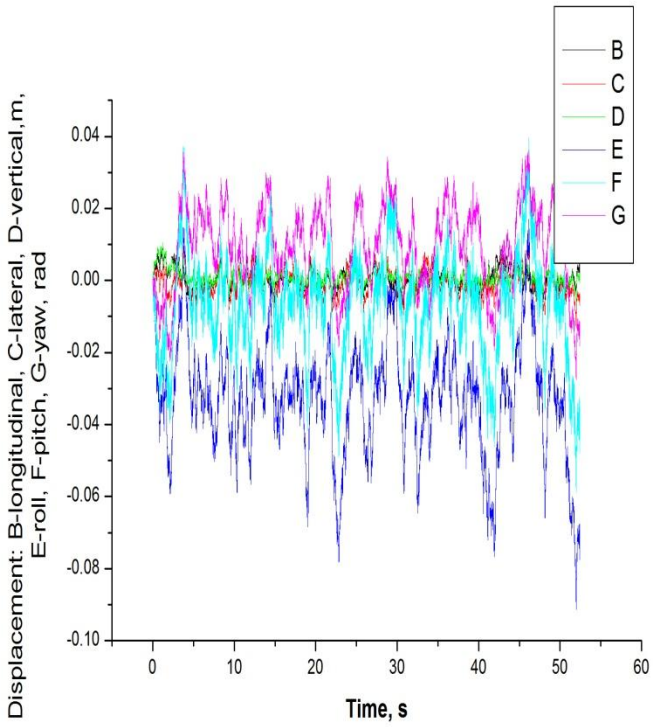

Fig. 5 Powertrain displacements in case of hydraulic mounts

Summarized thermal loads (for all forces and torques components and for all four mounts) are calculated using the Eqs (2-40) and the results are shown in Figs 6 and 7, wherein the values in Fig. 6 for the amount of heat are given in the log scale.

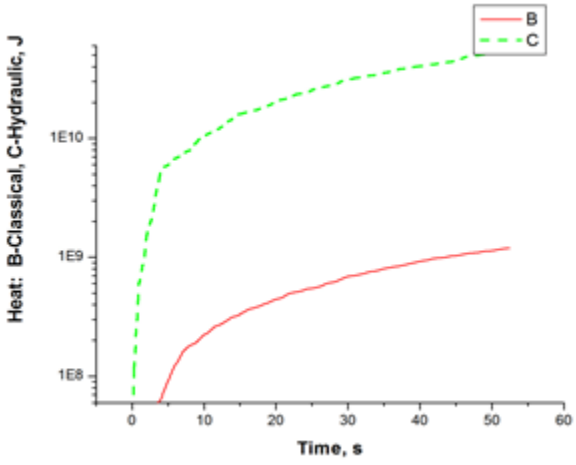

Fig. 6 Quantity of heat (mechanical work) depending on the type of mount

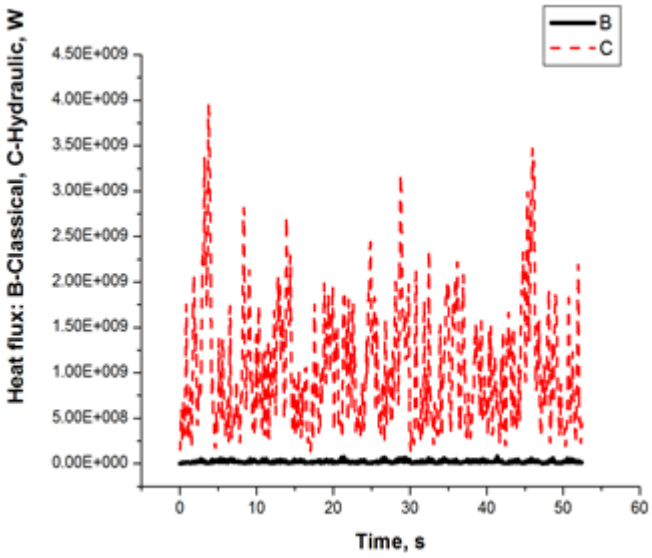

Fig. 7 Heat flux depending on the type of mounts

Table 5. Statistical data on heat flux

Mounts	Min, W	Max, W	Mean value, W	Effective value, W
Classical	2.494 10^2	2.973 10^8	2.271 10^7	3. 438 10^7
Hydraulic	2.570 10^2	1347 10^{10}	1.038 10^9	1. 609 10^9

The analysis of Fig. 6 shows that mechanical mounts suffer from approximately 45 times lower thermal loads then the hydraulic (for 52 s, classical about 1.19x109 J, and hydraulic about 53.69x109 J). This is understandable bearing in mind that hydraulic mounts, in addition to hysteresis in the rubber, have the additional fluid flow within the mount. Fig. 6 shows that the amount of heat increases with time and that in the absence of cooling, they would experience a degradation of the shape and characteristics.

Fig. 7 shows how the heat flux depends on the time. It is obvious that it changes stochastically over time, so for the sake of the analysis, it is necessary to calculate some characteristic statistical values given in Tab. 5 [25,26].

Analysis of the data from Tab. 5 shows that the heat flux is much higher in hydraulic, that in the conventional suspension of powertrain. This indicates a greater possibility of degradation of characteristics of hydraulic mounts compared to the classical. Therefore they are bigger in size than the classical. It should be pointed out that such high values of thermal flow are a result of rigorous excitations of vehicle frame that were used in the simulation. In practice, they are significantly milder, and consequently the real thermal load of the

powertrain mounts. However, the research is carried out to determine the ratio of the thermal load of classic and hydraulic supports, with by use of models, so the obtained results can be adopted only as an orientation, which is acceptable in the initial design phase of the truck. It should be mentioned that hydraulic mounts have significantly better performance when vibrations of the powertrain are in question [9].

5. CONCLUSIONS

The research shows that mechanical models can perform analyses of the impact of powertrain supports features on their thermal loads. Analyses showed that the hydraulic supports are significantly more exposed to heat load than the conventional. Bearing in mind the thermal loads, as well as a more complex structure, the less frequent application of hydraulic supports at the freight vehicles powertrain is expected. In order to verify the obtained results the experimental research should be carried out in the future.

Based on the research results the following conclusions can made:
The proposed model of powertrain can be used for the simulation of thermal load of freight vehicle powertrain mounts,
The hydraulic mounts of powertrain are subjected to a significantly greater thermal load than the conventional, and
Bearing in mind the extent of the existing thermal loads, as well as a more complex design, the application of hydraulic powertrain mounts is understandably less frequent in freight vehicles powertrain suspension.

Nomenclature
z- vertical vibration, [m]
A – work, [J]
Iu, I_v, I_w - moment of inertia, [kgm^2]
f – frequency, [Hz],
t – time, [s],
Q - quantity of heat, [J]
Fm -force in the shock absorber, [N]

Greek symbols:
φ - roll, [rad]
θ - pitch, [rad]
ψ- yaw of the powertrain, [rad]
x – reference for x-axis, y – reference for y-axis, and z – reference for z-axis

REFERENCES

[1] Demić, M., Diligenski, Đ. (2016) Numerical simulation of shock absorbers heat load for semi-active suspension system, Therm Sci, 20, 5: 1725-1739, doi 10.2298/TSCI150624005D
[2] Mitschke, M. (1997) Kraftfahrzeugkonstruktion, Teil D. TU Braunschweig, Forlesung, Germany,
[3] Atkins, P. (2010) The Laws of Thermodynamics (A Very Short Introduction), Oxford, UK
[4] Bojić, M. (2011) Thermodynamics (in Serbian). University of Kragujevac, Mechanical Engineering Faculty
[5] Ilić, G., et al (1996) Thermodynamics II, Basics of heat transfer (in Serbian), University of Niš, Mechanical Engineering Faculty
[6] Moran, M.J., et al (2010) Fundamentals of Engineering Thermodynamics, John Wiley and Sons
[7] Fermi, E. (2011) Thermodynamics, Dover Books on Physics
[8] FAP Informations (2017) (in Serbian), Priboj, Serbia
[9] Demić M. (1990) A contribution to the optimization of the position and the characteristics of passenger cars powertrain mounts, Int J of Vehicle Des, 1: 87-103
[10] Mitschke M. (1972) Dynamik der Kraftfahrzeuge (in German), Springer Verlag, Germany
[11] Pars, L. (1971) A Treatise on Analytic Dynamics, Heinemann, London, UK
[12] Rotenberg R. (1972) Motor Vehicle Suspension (in Russian), Mashinostroenie, Moscow, Russia
[13] Simić D. (1988) Motor Vehicle Dynamics (in Serbian), Naučna knjiga, Belgrade, Serbia
[14] Simić, D., Demić, M. (1992) Mounting of the power train (monograph), MVM, Kragujevac, Serbia
[15] Shanguan, W.B., et al (2016) Design method of automotive powertrain mounting system based on vibration and noise limitations of vehicle level, Mech Syst Signal Pr, 677-695
[16] Demić M. (1997) Identification of Vibration Parameters for Motor Vehicles, Vehicle Syst Dyn, 27: 65-88
[17] Demić M. (1997) The Optimization of Vibratory Systems of Motor Vehicles (monograph, in Serbian) – Mechanical Engineering Faculty, Kragujevac, Serbia
[18] Frolov K.V., Furman F.A., (1980) Applied theory of vibration protection systems (in Russian), Mashinostroenie, Moscow, Russia
[19] Ravi, K. et al (2016) Study of Engine Mountings: A Review, The International Journal of Science & Technoledge, 4 10: 38-46
[20] Kadam V.V., Kulkarni N. (2016) Modelling & Analysis of Engine Mount System for Vibration Reduction, International Journal of Latest Trends in Engineering and Technology, 7 3: 53-60
[21] Genta A. (2003) Motor Vehicle Dynamics, Politecnika di Torino, Torino, Italy
[22] Gillespie T.D. (1992) Fundamentals of Vehicle Dynamics, SAE
[23] Miliken W., Miliken D. (19959 Race Car Dynamics, SAE
[24] Mahalec, I., et al. (2015) Z., Engine Constructions (in Croatian), FSB Zagreb, Croatia
[25] Bendat J.S., Piersol A.G. (2000) Random Data-Analysis and measurement procedures, John Wiley and Sons Inc., London, UK
[26] Demić, M., (2003) ANALSIGDEM: Software for signal analysis. Available online at www.ptt.yu/korisnici/i/m/imizm034/

Journal of Mechanical Engineering & Modern Technology
www.jmemt.jarap.org
Volume 1 Issue 1, 30 June 2018
PP. 9-17

HEAT EXCHANGER REGULATION BASED ON METHOD OF INVARIANT ELLIPSOIDS

Vojislav Filipovic[1], Dragutin Lj. Debeljkovic[2], Milan Matijevic[1] &Vladimir Đorđevic[1]

[1]University of Kragujevac, Serbia

[2]Faculty of civil engineering, Megatrend University of Belgrade, Serbia

Key words

Heat exchangers
uniform bounded disturbance
invarinat ellipsoids
optimal regulator
convex optimization
solvers
YALMIP
SeDuMi

Abstract

The paper proposes a new method for heat exchanger regulation. At the first, a lumped parameter mathematical model for heat exchanger is proposed. The model is linear and includes a disturbance which can be categorized as an almost arbitary disturbance. Overall a priori knowledge about disturbance is contained in the fact that the disturbance is uniformly bounded. Regulator design is based on (in discrete case) or (in continuous case) optimisation. These methodologies belong to the class of serious problems in control engineering. In this paper is used the latest results based on method of invarinat ellipsoids which relax the above problems. The problem of regulator design comes down to minimizing the size of the invariant ellipsoids of the dynamic system. Numerical solution isbased on application of convex analysis (semidefinite programming and linear matrix inequalities). To solve these problems, there are powerful solvers (YALMIP and SeDuMi) so practical regulator implementation is significantly simplified. Intensive simulations give verification of regulator efficiency and its superiority over the well-known LQ regulator. Energy efficiency and quality of HVAC system is in strong correlation with regulator performances.

1. INTRODUCTION

In recent years, Heating, Ventilation and Air Conditioning (HVAC) systems integrated into building automation systems have become very popular.

Their popularity results from their ability to quickly set and retain demanded temperature by using various sensors in combination with a sophisticated feedback-control system. In addition, efficient control strategies play an essential role in developing improved energy control systems for buildings. The most important criteria for designing HVAC plants are energy efficiency and indoor climate conditions. Heat exchangers are standard components within HVAC systems [1-3]. To improve energy efficiency, there is a growing interest in developing techniques that compute control signals that minimize energy consumption. Such control techniques require a model of heat exchangers that relates the control signals to the space temperature. The mathematical model based on the fundamental principles is in the form of partial differential equations [4]. Regulator design, in this case, is a non-trivial task [5]. The alternative is obtaining and exploitation of models with lumped parameters [6].

In this paper we use the last option for mathematical model of heat exchangers. Under real conditions there are temperature variations as well as heating fluid flow variations. Such phenomena will be modeled as uniformly bounded disturbances. This is a deviation from the dominant assumption that the disturbances are stochastic signals. From point of view of practical application it is very important that required a priori information about disturbances is minimal.

Regulator design based on models of uniformly bounded disturbances belongs to a set of the very difficult problems in control engineering. In the case of discrete models, the problem is solved in [7-8] (l^1 optimization). In continuous domain, the problem is solved in [9-10] (L^1 optimization). By aforementioned methodology, results are regulators with very high order.

In continuous domain, which is discussed in this paper, infinitely dimensional regulator is result of the L^1 norm minimization. These facts prevent the application of l^1 and L^1 the optimal regulators.

The latest studies of regulator design in the presence of bounded disturbances access from positions of invariant sets [11].

Invariant ellipsoid as a special form of the invariant set is considered, which significantly facilitates troubleshooting [12-13], which consists in minimizing the size of the invariant ellipsoid of dynamic system.

The original L^1 optimization comes down to the use of LMI (Linear Matrix Equation) [14], and semidefinite programming [15]. For these methodologies, there are very efficient solvers (YALMIP, SeDuMi, CVX) and they will be used in the simulations.

A new model of the heat exchanger is proposed by this paper.

The model is linear and includes bounded disturbance. The linear part of the model is second order in derivatives.

Heat exchanger description is provided in the state space form. Applying the method of invariant ellipsoids the regulator is designed.

The regulator has a simple structure and is obtained using modern solvers based on the convex analysis [16]. At this manner designed regulator is a step towards energy savings.

The last part of the paper presents simulation results concerning of the heat exchanger regulation.

2. THE CONCEPT OF INVARIANT ELLIPSOIDS FOR DYNAMICAL SYSTEMS

Suppose that the LTI (Linear Time Invariant) dynamic system is described by the continuous time stationary linear system.

$$\dot{\mathbf{x}}(t) = A\mathbf{x}(t) + B\mathbf{u}(t) + D\mathbf{w}(t)$$
$$\mathbf{y}(t) = C\mathbf{x}(t) \quad (1)$$

where $\mathbf{x}(t) \in \mathbb{R}^n$ is the vector of the system phase state, $\mathbf{y}(t) \in \mathbb{R}^l$ is the vector of the system output, $\mathbf{w}(t) \in \mathbb{R}^m$ are the exogenous disturbances bounded at each time instant,

$$\left\|\mathbf{w}(t)\right\| \le 1, \ \forall t \ge 0 \quad (2)$$

where $\left\|\cdot\right\|$ is the Euclidean norm of the vector.

Therefore, we consider the L^∞ bounded exogenous disturbances $w(t)$.

$$\left\|\mathbf{w}(t)\right\|_\infty = \sup_{t\ge 0}\sqrt{\mathbf{w}^T(t)\mathbf{w}(t)} \le 1 \quad (3)$$

We assume that system (1) is stable, that is, A is Hurwitzian matrix with negative real parts, the pair (A, B) is controllable, and C is the maximum-rank matrix.

We determine the family of invariant ellipsoids of this system.

The ellipsoid $\mathcal{E}_x$ with the center at the origin

$$\mathcal{E}_x = \left\{\mathbf{x}(t) \in \mathbb{R}^n : \ \mathbf{x}^T(t)P^{-1}\mathbf{x}(t) \le 1\right\}, \ P > 0 \quad (4)$$

is invariant to the variable $\mathbf{x}(t)$ (in state) for dynamic system (1)-(2), if it follows from the condition $\mathbf{x}(0) \in \mathcal{E}_x$ that $\mathbf{x}(t) \in \mathcal{E}_x$ for all time instants $\forall t \ge 0$.

P is called the matrix of the ellipsoid $\mathcal{E}_x$.

The ellipsoid invariant to the variable $\mathbf{y}(t)$, that is, system output, is determined from (1) and (4) by

$$\mathcal{E}_y = \left\{\mathbf{y}(t) \in \mathbb{R}^m : \ \mathbf{y}^T(t)\left(CPC^T\right)^{-1}\mathbf{y}(t) \le 1\right\} \quad (5)$$

The invariant ellipsoids may be regarded as the characteristic of the impact of the exogenous disturbances on the trajectories of the dynamic system.

Since the invariance of the ellipsoid $\mathcal{E}_y$ and its size are the measure of disturbances $\mathbf{w}(t)$ effects on the system outputs $\mathbf{y}(t)$, a natural criterion for regulator synthesis is to minimize the ellipsoid $\mathcal{E}_y$.

In this paper it will be used the criterion

$$f(P) = tr\left[CPC^T\right] \quad (6)$$

which is the sum of squares of axis of the invariant ellipsoid.

3. HEAT EXCHANGER MODEL IN THE STATE SPACE

The tubular counter-current heat exchanger is presented on Fig. 1.

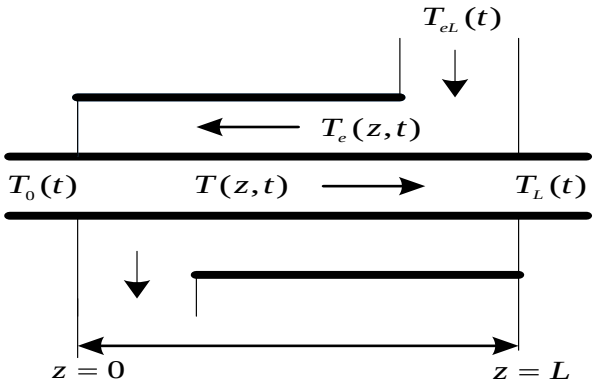

Figure 1: Counter-current heat exchanger

The short description of the heat exchanger follows [17].

A liquid fluid of constant density ρ and heat capacity c_p flows through the internal tube of length L with **constant**velocity w. Input fluid has temperature T_0.

This fluid exchanges heat with the **second liquid** of constant density ρ_e and the heat capacity c_{pe} which flows counter-currently in the jacket with a time varying velocity $w_e(t)$.

The input temperature of this fluid is T_e and output inter fluid temperature is T_L.

Both temperatures depend on time and special position along the tube.

The dynamic of heat exchanger can be described with two partial differential equations.

$$\frac{\partial T(z,t)}{\partial t} + w\frac{\partial T(z,t)}{\partial z} = \wp\left(T_e(z,t) - T(z,t)\right) \quad (7)$$

$$\frac{\partial T_e(z,t)}{\partial t} - w_e(t)\frac{\partial T_e(z,t)}{\partial z} = \wp_e\left(T(z,t) - T_e(z,t)\right) \quad (8)$$

where the coefficients $\wp$ and $\wp_e$ are known and defined by geometry of heat exchangers and its fluid characteristics.

Regulator design and implementation, based on the model (7) - (8), is a very complex problem.

Because of that, in this paper, the heat exchanger will be considered as a process with lumped parameters.

In accordance with [18] fluid that is heated can be regarded as a disturbance.

The change of its flow occurs as a disturbance.

Process diagram of the heat exchanger is shown in the following figure

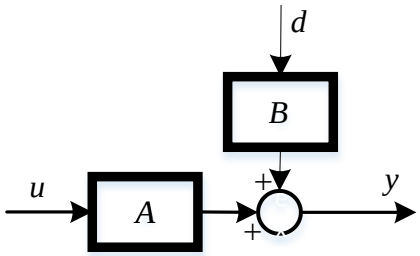

Figure 2: Process diagram of the heat exchanger.
A – fluid for heating of process fluid.
B – process fluid.

At Fig.2, the input signal $u(t)$ represents the flow of heating fluid, disturbance $d(t) = w(t)$ is a change of flow rate of process fluid (i.e. heated fluid), and $y(t)$ is the temperature of the heated process fluid.

Experimental studies in [6] have showed the following

a) in the case of constant flow of process fluid (heated fluid), input $u(t)$ - flow of heating fluid – output $y(t)$ - the temperature of the heated process fluid) model is linear

b) in the case of constant flow of heating fluid $u(t)$, under changes of flow rate of process fluid (i.e. heated process fluid, disturbance input $d(t) = w(t)$, output $y(t)$ - the temperature of the heated process fluid) model is nonlinear

Based on the experiment [6], it is concluded that the model on Fig.2. consists of linear block A and nonlinear block B (correct nonlinear model is Hammerstein model).

Nonlinear Hammerstein model is BIBO (bounded input bounded output) stable [19]. Since disturbances (*d*) are uniformly bounded then the output of Hammerstein model (*w*) is bounded.

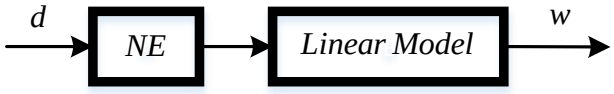

Figure 3: Hammerstein model of disturbance effect on system output

Based on Fig.2 and Fig.3, the final model of the heat exchanger is obtained and shown on Fig.4.

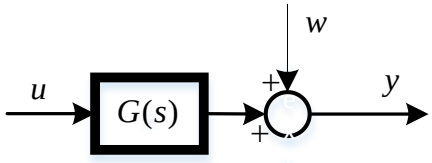

Figure 4: Heat exchanger model

In [6] transfer function $G(s)$ (see Fig.4) is identified as

$$G(s) == \frac{-65.22s - 11.23}{s^2 + 2.664s + 0.604} = -\frac{65.22s + 11.23}{s^2 + 2.664s + 0.604} \quad (9)$$

Problem of regulator synthesis based on plant model presented in Fig.4 with uniformly bounded disturbance we will solve using methodology of invariant ellipsoids [12].

In order to apply methodology of invariant ellipsoids it is necessary to transfer the model (9) into the state space model.

$$\dot{\mathbf{x}}(t) = A\mathbf{x}(t) + B_1\mathbf{u}(t) \quad (10)$$

$$\mathbf{y}(t) = C\mathbf{x}(t) + B_2\mathbf{u}(t) \quad (11)$$

where:

$$A = \begin{pmatrix} -2.664 & -0.604 \\ 1.000 & 0.000 \end{pmatrix}, \quad B_1 = \mathbf{b}_1 = \begin{bmatrix} 1 \\ 0 \end{bmatrix}, \quad C = \begin{pmatrix} 0 & 0 \\ 0 & 1 \end{pmatrix}, \quad B_2 = \mathbf{b}_2 = \begin{bmatrix} 1 \\ 0 \end{bmatrix}$$

According to Fig.4 complete model of heat exchanger has the form

$$\begin{aligned} \dot{\mathbf{x}}(t) &= A\mathbf{x}(t) + \mathbf{b}_1 u(t) + \mathbf{d}w(t) \\ \mathbf{y}(t) &= C\mathbf{x}(t) + \mathbf{b}_2 u(t) \end{aligned} \quad (12)$$

$$\mathbf{d} = \begin{bmatrix} 0 \\ 1 \end{bmatrix} \quad (13)$$

It should be noted, a well-known fact, that there is freedom (not uniqueness) in the selection of the second relation in (12).

The key feature of the model (12) - (13) that there is only information about disturbances that ones are bounded.

$$\left\|\mathbf{w}(t)\right\| \le 1, \ \ \forall t \ge 0 \tag{14}$$

Such a description of the disturbances is extremely general which is very important for practice. It belongs to the class of almost arbitrary disturbances [20].

The condition (14) defines methodology of regulator design, which is a very difficult problem for the given case of application. Methodology is exposed in the next chapter.

4. REGULATOR DESIGN BASED ON THE METHODOLOGY OF INVARIANT ELLIPSOIDS

In this section, the regulator design approach will be considered under conditions of persistent disturbance based on the methodology of invariant ellipsoids and linear matrix inequalities. State feedback regulator will be determined. The basic requirement is that the designed regulator performs stabilization, and that, in turn, minimizes the corresponding invariant ellipsoid.

A linear continuous system is described in the following way

$$\dot{x}(t) = Ax(t) + B_1u(t) + Dw(t), \ \ x(0) = x_0 \tag{15}$$

$$y(t) = Cx(t) + B_2u(t) \tag{16}$$

where are $A \in \mathbb{R}^{n\times n}$, $B_1 \in \mathbb{R}^{n\times 1}$, $D \in \mathbb{R}^{n\times 1}$, $B_2 \in \mathbb{R}^{n\times 1}$, $C \in \mathbb{R}^{n\times n}$ corresponding matrices and vectors, $x(t) \in \mathbb{R}^n$ is the system phase state, $y(t) \in \mathbb{R}^n$ is the system output, $u(t) \in \mathbb{R}^1$ is the control, and $w(t) \in \mathbb{R}^1$ is the exogenous (uniform limited) disturbance satisfying the constraint

$$\left\|w(t)\right\| \le 1, \ \ \forall t \ge 0 \tag{17}$$

where $\left\|\cdot\right\|$ Euclidean norm of the vector. It is also required that the

a) (A, B_1) is controllable pair

b) $B_2^TC = 0$

It is not necessary that the matrix A is Hurwitzian which means that the regulator can be applied to unstable systems.

The fundamental elements of the theory are exposed in [12]. The regulator has the form

$$u(t) = Kx(t) \tag{18}$$

The system with closed feedback loop (15) - (18) has the following form

$$\dot{x}(t) = (A + B_1K)x(t) + Dw(t) \tag{19}$$

$$y(t) = (C + B_2K)x(t) \tag{20}$$

The problem of designing a static regulator by state (18) which rejects optimally (in the sense of the trace that is output-invariant to the ellipsoid) the exogenous disturbances is equivalent to that of minimization of

$$tr\left[CPC^T + B_2ZB_2^T\right] \to \min \tag{21}$$

under constraints

$$AP + PA^T + \alpha P + B_1Y + Y^TB_1^T + \frac{1}{\alpha}DD^T \le 0, \ \ \alpha > 0 \tag{22}$$

$$\begin{bmatrix} Z & Y \\ Y^T & P \end{bmatrix} \ge 0 \tag{23}$$

$$P > 0 \tag{24}$$

The regulator (18) is obtained as

$$\hat{K} = \hat{Y}\hat{P}^{-1} \tag{25}$$

where $\hat{P}$, $\hat{Y}$ and $\hat{Z}$ the solution of the problem (21) - (24)

Minimum invariant ellipsoid is

$$C\hat{P}^TC^T + B_2\hat{Z}B_2^T \tag{26}$$

The graphical representation of control system is given on the next figure

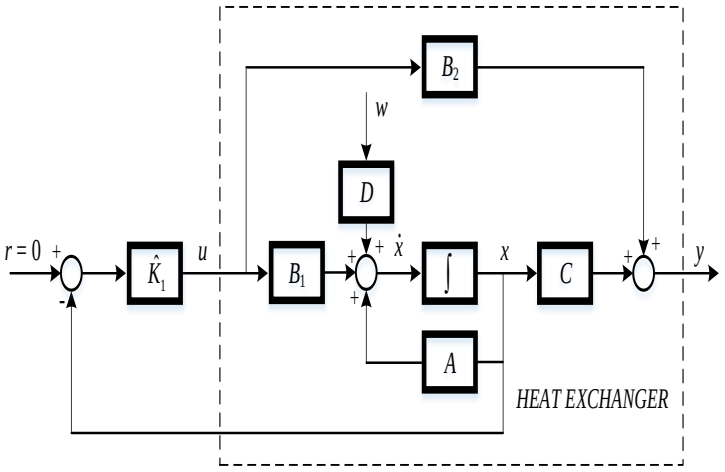

Figure 5: Control system for heat exchanger ($\hat{K}_1 = -\hat{K}$)

Remark 1. The condition $B_2^TC = 0$ can be avoided [21]. In this case, the criterion (21) se is replaced by the following

$$tr\left[CPC^T + CY^TB_2^T + B_2YC^T + B_2ZB_2^T\right] \to \min \tag{27}$$

In other details, the new procedure is identical to the procedure (21) - (24).

Remark 2. The presence of $B_2u(t)$ in relation (16) provides, in minimizing the output signal, avoiding large control signals. It follows

that the matrix B_2 has the same role as the matrix S in LQ regulator design

$$J=\int_0^{\infty}\left(x^T(t)Rx(t)+u^T(t)Su(t)\right)dt \tag{28}$$

The alternative is to explicitly introduce limitations to the control signal.

5. SIMULATION RESULTS AND DISCUSSION

Let consider the model (12)-(13) where A, B_1, C and B_2 the same as in the relations (10)-(11). It is easy to verify that (A,B_1) is controllable pair and that $B_2^TC=0$. Using the optimal regulator $\hat{K}$; which is obtained by solving of relations (21)-(24), the invariant ellipsoid of output is minimized. In order to solve problem (21)-(24), it is used software packages SeDuMi and YALMIP based on MATALB software package. Numerical problem is solved by use of semidefinite programming (21) under constraints (22)-(24).

In the simulations is very important, prior to calculating the vector regulator gain, to define parameter α ($\alpha>0$). For this purpose is defined segment $\alpha\in[\varepsilon,k_\alpha]$, for $\exists\varepsilon>0$ and $k_\alpha>0$. Simulations are conducted for $k_\alpha\le 5$. The segment $[\varepsilon,k_\alpha]$ is subdivided into the collection of subsegments, and by YALMIP is searched value α for that value is obtained minimum value criteria

$$tr(C\hat{P}^TC^T+B_2\hat{Z}B_2^T)$$

If the lowest value α is on the border segment $[\varepsilon,k_\alpha]$, then the segment should be extended until within the segment finds α for that the above criteria is minimal. In the first step is carried out a rough division of the segment $[\varepsilon,k_\alpha]$. When it finds the best value α, then defines a small segment containing α, and the search procedure for the best α repeats with a finer division of this segment. At this manner, relatively quickly, we can receive value α.

Below we will illustrate the behavior of the closed-loop system under various disturbances.

A) The disturbance is given by $w(t)=\sin(t/2)$. In this case the solution of the problem (21) - (24) is

$$\alpha=1.1569,\ \hat{K}=\begin{bmatrix}-0.9035 & -2.2924\end{bmatrix}$$

On Fig.6 and Fig.7 it is shown the minimum invariant output ellipse of the system (Fig.6), and both control and disturbance signal (Fig.7)

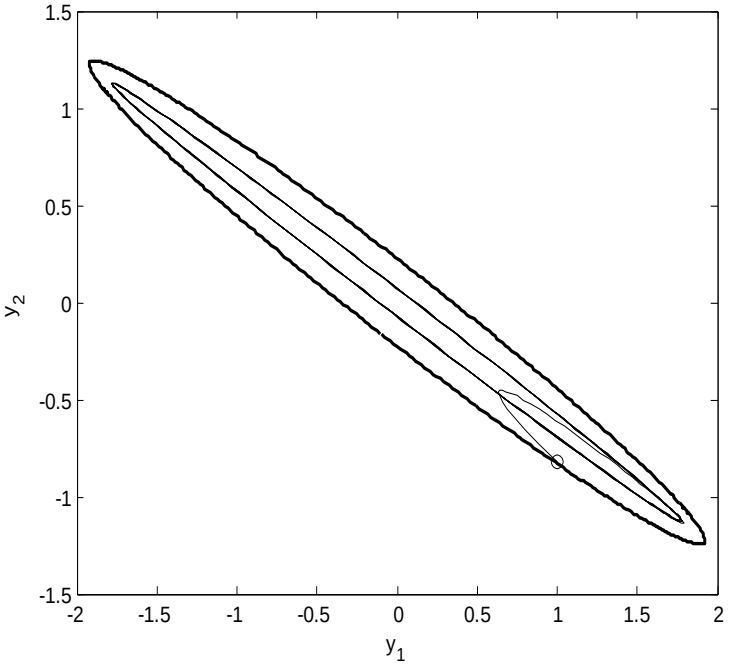

Figure 6: Minimum invariant output ellipse for $B_2=\begin{bmatrix}1\\0\end{bmatrix}$,

$$w(t)=\sin\frac{t}{2}.$$

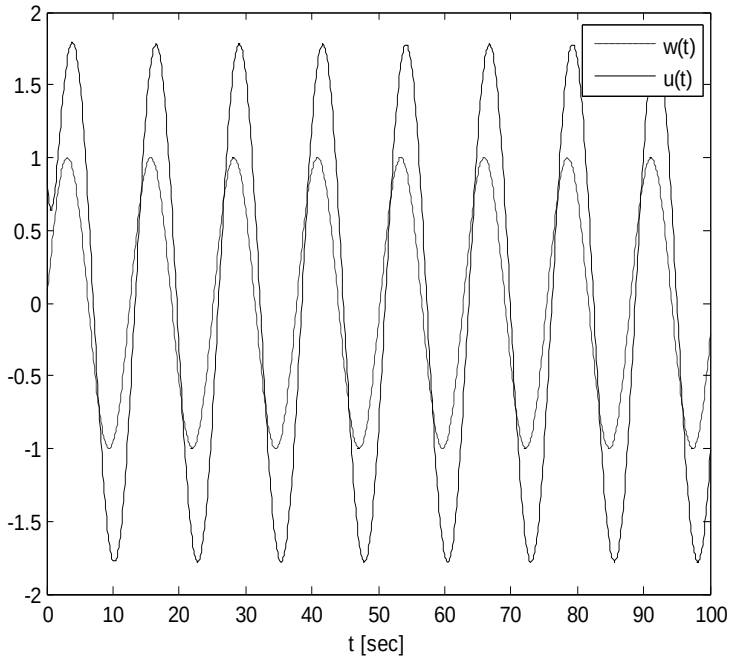

Figure 7: Control $u(t)$ and disturbance $w(t)$

In accordance to remark 2, using the vector B_2, it can be influenced on the control signal magnitude. If the vector B_2 is adopted as $B_2^T=\begin{bmatrix}2.5 & 0\end{bmatrix}$, for solution of the problem (21) - (24) is obtained

$$\alpha=0.3716,\ \hat{K}=\begin{bmatrix}-0.1197 & -0.3037\end{bmatrix}$$

and behavior of the system is shown on Fig.8 and Fig.9.

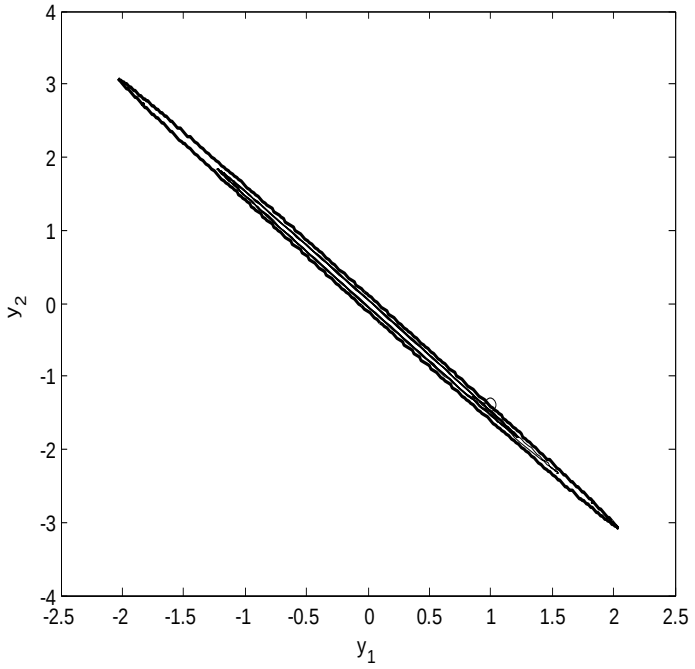

Figure 8: Minimum invariant output ellipse for $B_2^T = \begin{bmatrix} 2.5 & 0 \end{bmatrix}$.

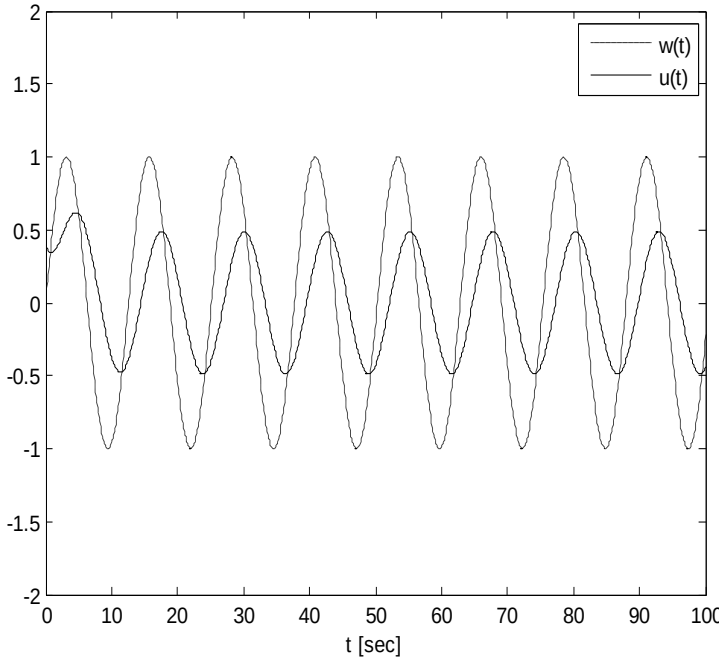

Figure 9: Control $u(t)$ and disturbance $w(t)$

With Fig.8 can be seen how is increased the coordinate y_2, and with Fig.9 how is reduced amplitude of the control signal $u(t)$. If the vector B_2 is adopted as $B_2^T = \begin{bmatrix} 0.1 & 0 \end{bmatrix}$, for solution of the problem (21) - (24) is obtained

$$\alpha = 4.3284, \ \hat{K} = \begin{bmatrix} -6.5375 & -24.6378 \end{bmatrix}$$

The behavior of the system is shown in Fig.10 and Fig.11

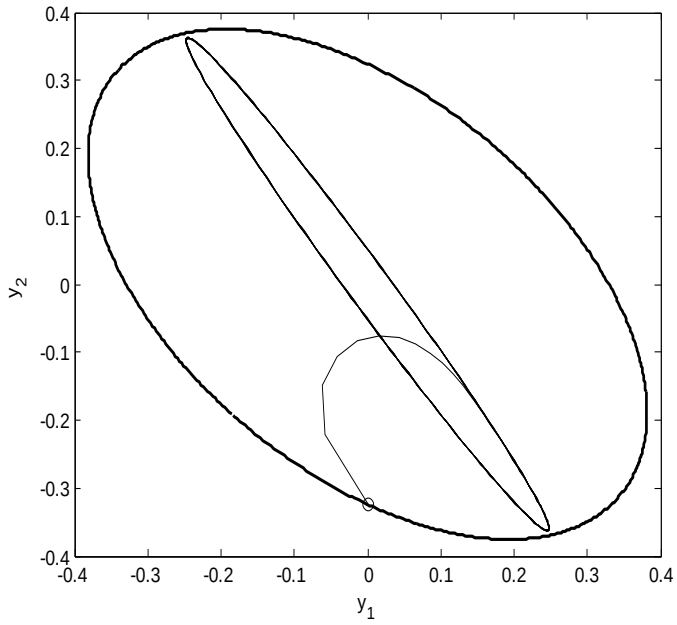

Figure 10: Minimum invariant output ellipse for $B_2^T = \begin{bmatrix} 0.1 & 0 \end{bmatrix}$.

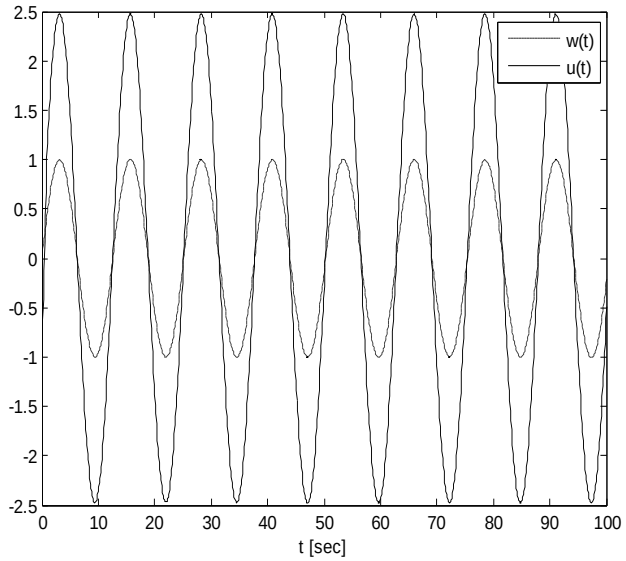

Figure 11: Control $u(t)$ and disturbance $w(t)$ for $B_2^T = \begin{bmatrix} 0.1 & 0 \end{bmatrix}$

With Fig.8 it can be seen how is decreased size of the invariant output ellipse, which is convenient from a position of control. But, on the other hand, with Fig.11. it can be seen that is significantly increased the amplitude of control signal, which is disadvantageous.

B) The disturbance is given by $w(t) = \text{sgn}(\sin(t/2))$. In this case, the solution of the problem (21) - (24) is

$$\alpha = 1.1569, \ \hat{K} = \begin{bmatrix} -0.9035 & -2.2924 \end{bmatrix}$$

The behavior of the system is shown in Fig.12 and Fig.13.

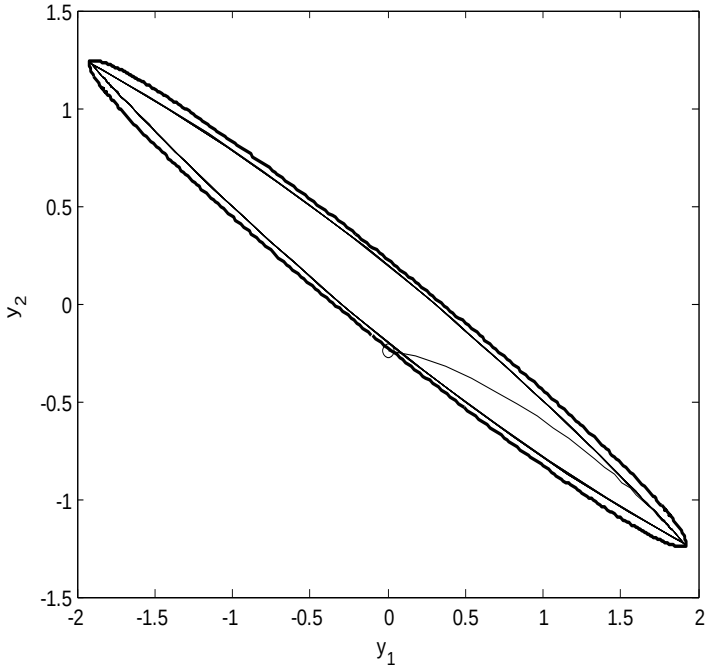

Figure 12: Minimum invariant output ellipse

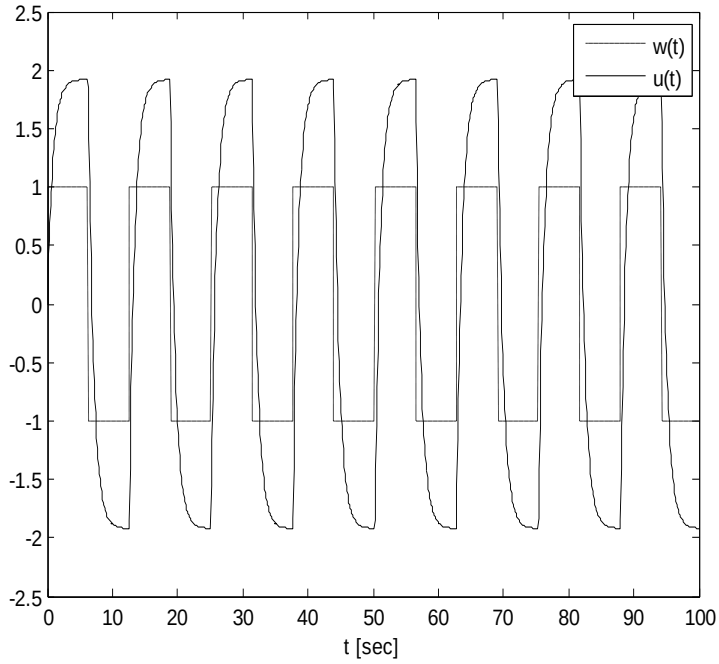

Figure 13: Control $u(t)$ and disturbance $w(t)$

The simulations also show that by changing the vector B_2 it is obtained similar results as in the case under A

C) Disturbance $w(t)$ is step function, and in that case

$$\alpha = 1.1569,\ \hat{K} = \begin{bmatrix} -0.9035 & -2.2924 \end{bmatrix}$$

Minimum invariant output ellipse is shown at Fig.14, and disturbance $w(t)$ and control signal $u(t)$ are shown at Fig.15.

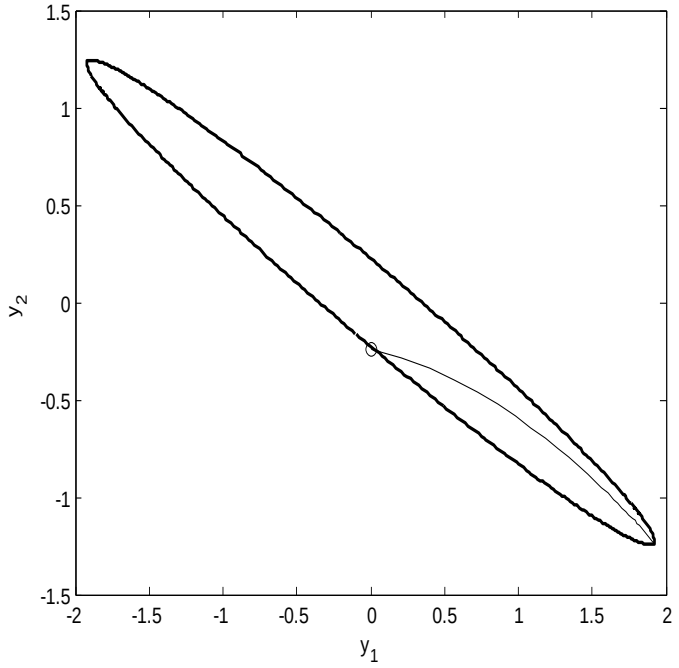

Figure 14: Minimum invariant output ellipse

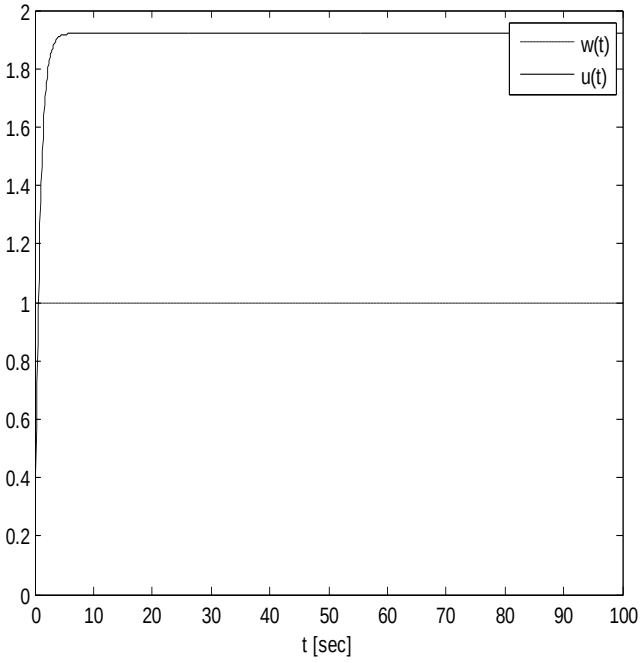

Figure 15: Control $u(t)$ and disturbance $w(t)$

The behavior of the state vector is shown in Fig.16.

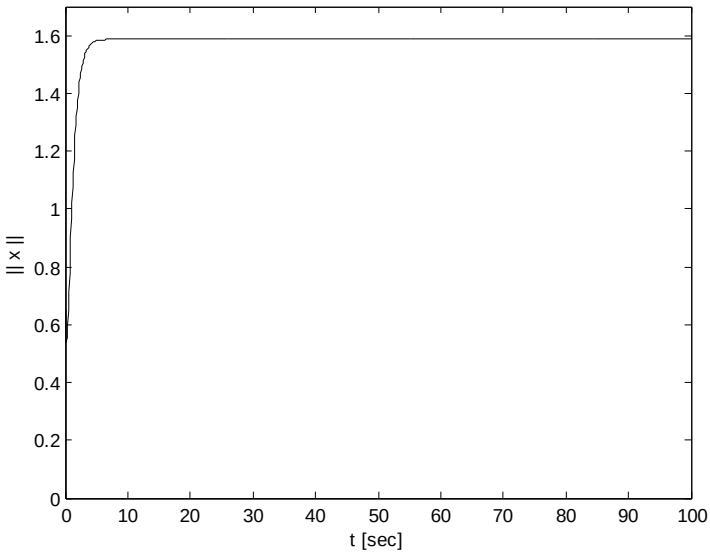

Figure 16: Norm of the system state vector

D) Disturbance $w(t) = 0$, and in tator based on methodology of invariant ellipsoids (for system (15)-(16)) is

$$\alpha = 1.1569,\ \hat{K} = \begin{bmatrix} -0.9035 & -2.2924 \end{bmatrix}$$

For the case $w(t) = 0$ and system (15)-(16), optimal regulator is LQ regulator, which can be obtained by minimisation of functional (28). For adopted matices in (28)

$$R = \begin{bmatrix} 1 & 0 \\ 0 & 1 \end{bmatrix} \text{ i } S = 1.6$$

LQ regulator is defined by

$$K_{LQ} = \begin{bmatrix} -0.251 & -0.3909 \end{bmatrix}$$

Comparison of the above regulator is given in the following figure 17.

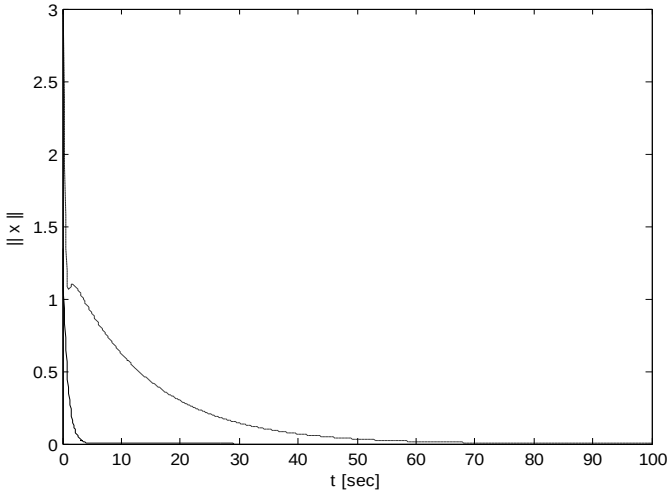

Figure 17: Norm of the system state vector

Legend:

——— *Regulator based on methodology of invariant ellipsoids*

- - - - - *LQ regulator*

It can be seen that the dynamic behavior of the system with regulator based on the ideology of invariant ellipsoid is significantly superior in comparision to behavior of the system with LQ regulator. This can be explained by the higher values of the elements of the vector $\hat{K}$ in comparison to the LQ gain vector K_{LQ}.

6. CONCLUSIONS

The paper discusses the problem of regulator design for linear systems under effects of uniformlybounded disturbances. This assumption about the external disturbances is very general and embraces the minimum a priori information about ones. It is very realistic and very important for practical applications. The problem of regulator synthesis comes down on the minimization of the specified criteria (semidefinite programming) under constraints in the form of linear matrix inequalities. Intensive simulations for different types of disturbances verify good regulator properties. In the case of disturbance absence, regulator based on the methodology of invariant ellipsoid has superior characteristics compared to LQ regulator. Potentials for further work on the problem are: i) extension of problems on discrete case, ii) the design of the regulator with L^{∞} limit on the control signal.

ACKNOWLEDGMENT

This paper is a result of two project activities: (1) project TR33026, (2) project TR33047. The both project are financed Ministry of Education, Science and Technological Development of Republic of Serbia. We would like to thank to Ministry of Education, Science and Technological Development of Republic of Serbia for financial support during these investigations.

REFERENCES

[1] T. Salsbury, A survey of control technologies in the building automation industry, in:16th Triennial World Congress, Prague, Czech Republic, 2005, pp. 90-100

[2] W. Cho, D. Song, S. Hwang, S. Yun, Energy-efficient ventilation with air-cleaning mode and demand control in a multi-residental building, Energy and Building 90 (2013) 6-14

[3] T. Gao, M. David, J. Geer, R. Schmidt, B. Sommakia, Experimental and numerical dynamic investigation of an energy efficient liquid cooled chiller-less data center test facility, Energy and Buildings 91(2015) 83-96

[4] M. A. Arbadut, L. Veruieres, D. Seguin, M. A. Abdelghenc-Idrissi, Counter–current tubular heat exchanger: modelling and adaptive predictive functional control, Applied Thermal Engineering 27 (2007) 2332-2338

[5] P. D. Cristofiedes, Nonlinear and Robust Control of PDE Systems: Methods and Applications to Transport-Reaction Processes, Birkhauser, Boston, 2001

[6] E. Eskinat, S. Johnson, W. Luyben, Use of Hammerstein models in identification of nonlinear systems, AICHE Journal 37 (1991) 255-268

[7] A. E. Barabanov, O. N. Granichin, Optimal controller for linear plants with bounded noise, Automtion and Remote Control 44 (1984) 39-46

[8] M. A. Dahleh, J. B. Pearson, l^1 – optimal feedback controllers for MIMO discrete-time systems, IEEE Transactions on Automtic Control 32 (1987) 314-322

[9] M. A. Dahleh, J. B. Pearson, L^1 – optimal compensators for continous – time systems, IEEE Transactions on Automtic Control 32 (1987) 889-893

[10] A. E. Barabanov, Design of Minmax Controllers, Sankt Peterburg University, Sankt Peterburg, 1996 (in Russian)

[11] F. Blanchini, Set invariance in control-a survey, Automatica 35 (1999) 1747-1767

[12] S. A. Nazin, B. T. Polyak, M. V. Topunov, Rejection of bounded exogenous disturbances by the method of invariant ellipsoids, Automtion and Remote Control 68 (2007) 106-125

[13] A. Z. Poznyak, A Plyakov, V. Azhmaykov, Attractive Ellipsoids in Robust Control, Birkhauser, Basel, 2014

[14] S. Boyd, L. El Ghaoui, E. Ferron, V. Balakrishnan, Linear Matrix Inequalities in Systems and Control Theory, SIAM, Philadelphia, 1994

[15] B. Gartner, J. Matousek, Approximation Algorithms and Semidefinite Programming, Springer, Berlin, 2012

[16] S. Boyd, L. Vandenberghe, Convex Optimization, Cambridge University Press, Cambridge, 2004

[17] A. Maidi, M. Diaf, J-P. Corrion, Boundary geometric control of a counter–current heat exchanger, Journal of Process Control, 19(2009) 297-313

[18] F. G. Shinskey, Process Control Systems, McGrow Hill, New York, 1979

[19] M. Vidyasagar, Nonlinear Systems Analysis, SIAM, Philadelphia, 2002

[20] O. Granichin, Z. Volkovich, D. Toledano-Kitai, Randomized Algorithms in Automatic Control and Data Mining, Springer, Berlin, 2015

[21] M. V. Khlebnikov, B. T. Polyak, V. M. Kuntsevitson, Optimization of linear systems subject to bounded exogenous disturbances: The invariant ellipsoid technique, Automtion and Remote Control 72 (2011) 2227-2275

Journal of Mechanical Engineering & Modern Technology
www.jmemt.jarap.org
Volume 1 Issue 1, 30 June 2018
PP. 18-30

3D FLOW SIMULATION OF A SHELL AND TUBE HEAT EXCHANGER WITH NANO-DIAMOND FLUID

Hamidreza Ghasemi Bahraseman [1*], Cody Secor [2], Michael McDaniel [2], Chris Okimoto [2], Michael Guerero [2], Maxwell Thatcher [2] & George Tanner [2]

[1] Mechanical Engineering Department, San Diego State University, San Diego, 92182, CA, USA
[2] Mechanical Engineering Department, California State Polytechnic University, Pomona, 91768, CA, USA
*Corresponding authors: Hamidreza Ghasemi Bahraseman, hghasemibahraseman@sdsu.edu

Key words

Shell and tube heat exchanger
Diamond Nanofluid
Forced convection
Laminar
Baffles

Abstract

The purpose of this inspection is to identify the heat transfer effects of an incremental addition of diamond nanoparticles to hot engine oil in a structural steel shell and tube heat exchanger using forced convection to heat cooler air. The shell and tube heat exchanger is constructed with one tube containing hot engine oil, which is positioned symmetrically inside a larger tube containing colder air. The outlet air temperature was examined for relative changes in temperature for each concentration of nano-diamond added (i.e., 0, 0.5, 1.0, and 2.0% respectively). Additionally, a comparison study was performed to show the difference between a model with no baffles and a model with containing several baffles that demonstrate maximum efficiency for a pure oil control. The COMSOL simulation investigates the stationary laminar flow solutions for all cases considered. Dynamic viscosity, thermal conductivity, density, and specific heat are modified to simulate the various oil compositions; an experimental investigation from 2012, by M. Ghazvini, et.al [1], was used in obtaining the material properties for this report at 313.15 K. The simulation expresses a maximum increase in air outlet temperature of 1.06% and 0.98% for an engine oil additive of 2.0% nano-diamond. These percentages are respective of a no baffle model, and the baffle case that demonstrated maximum efficiency, 17 baffles. Additionally, the increase in outlet air temperature for pure oil between the two geometries was found to be 1.28%. These two methods to increase heat transfer efficiency are seen to have a comparable effect on this geometry.

1. INTRODUCTION

Shell and tube heat exchangers are the most common type of industrial heat exchanger used, Galal stated they are commonly used in oil refineries and chemical plants [2]. A frequent application of shell and tube heat exchangers is in petroleum refinery plants to preheat the crude oil before it is refined into numerous advantageous petroleum products stated by Kundnaney & Kushwaha [3]. Additionally, since the shell and tube heat exchangers are used for such large-scale operations it is desired that they have high efficiency, a low overall cost, and easy maintainability. The modeling and simulation of a shell and tube heat exchanger is one possible solution for increasing efficiency at a relatively low cost. Moreover, the modeling and simulation process holds an importance in the engineering design process because it has the capability of demonstrating an estimated efficiency of a design before prototyping or manufacturing a singleunit; modeling and simulation has a proposed benefit of lower cost relative to testing an unknown number of prototypes.

Diamond is a particularly effective additive due to its high thermal conductivity, low electrical conductivity, low density, and high hardness. In a 2013 article, *Nano-diamond Nanofluids for Enhanced Thermal Conductivity* by Branson, et al., it is expressed that ultra-dispersed diamond powder (UDD) or detonation nano-diamond is a common source for commercial use nano-diamonds [4]. Detonation nano-diamond gets its name from the fact that explosives are used in a cavity containing diamond where nanoparticles are produced from the explosion. Adding nano-diamonds to the oil will increase the specific heat, thus, increasing its thermal conductivity.

The addition of very small particles in the fluid can be thought to be suspended evenly through the fluid adding a higher conductivity, to a degree, like what is present in solids. In theory, higher concentrations of the nano-diamond will increase the heat transfer in the shell and tube heat exchanger; between the hot oil and the cool air by air convection from the surface of the pipe containing the oil, though empirically this is true only to a certain concentration, after which the heat transfer rate will begin to decrease. This is partially due to the increasing viscosity impeding convection. A few assumptions were made while performing the simulation and analysis. The assumptions were: the outer wall of the shell is an adiabatic barrier, stationary simulation not transient, laminar flow, for time equal to zero the oil tube is all hot oil at the initial hot temperature, and the air and shell are initially at the air inlet temperature.

In *Heat Transfer Properties of Nano-diamond–Engine Oil Nanofluid in Laminar Flow,*

M. Ghazvini, et al. [1] in 2012 notes that the recent developments in technology allow for the possibility of composing new fluids with enhanced heat transfer properties by the addition of either metallic or non-metallic nanoparticles, in these early stages of development these nanofluids have been perceived as possibly being revolutionary in heat transfer improvement techniques. The same study conducts experiments on diamond nano additive in laminar flowing engine oil, using a 6mm pipe. It is from the documentation of the study's experimentally found material properties that this report forms its basis of analysis. There are four cases considered for the engine oil in this investigation; pure oil, oil with 0.5% nano-diamond particle, oil with 1.0% nano-diamond particle, and oil with 2.0% nano-diamond particle. A simulation was done for each case showing an increase in temperature percent difference. It is possible for manyproperties to change with the addition of the nano-diamond, pertaining to the shell; property changes due to wear or corrosion resistance alterations from the flowing particles, however, only dynamic viscosity, thermal conductivity, specific heat, and density of the oil are considered in the physical model due to their initial importance.

The introduction of nanoparticles to traditional base fluids, such as, ethanol glycol, water, or oil composes a new fluid category referred to as a nanofluid first coined by Choi [5].

Although, nanofluids increase heat transfer, they can also have certain negative effects on a thermal system. The unfavorable effects include: erosion of shell and tube material, increased power requirements, and possible blockages in smaller diameter pipes observed by Hu and Dong [6]. Corrosion occurs more with diamond nanoparticles compared to other nanoparticles such as titanium because of the large difference in hardness between a steel shell and diamond, reported by Hu, Z. S., and Dong, J. X. in *Study on Anti Wear and Reducing Friction Additive of Nanometer Titanium Oxide*. Additionally, the increased wear of the material that is to be in direct contactto the continuously flowing fluid is a topic of concern of many researchers in and of itself. Also, the desired levels of thermal conductivity are more difficult to achieve practically than one would ideally perceive [6, 7]. When testing UDD in ethylene glycol, Branson, et al. [4] found there was only a slight increase to the base fluid's conductivity, which was said to be due to the poor dispersibility of the nanoparticles in the base fluid throughout the entire system of the heat exchanger. In Branson's experiment it was specifically stated, "...achieving stable ND/base fluid dispersions usually requires ND surface modification via gas annealing techniques or the addition of surfactant-based or covalently bound functional groups." However, the concern is not apparent in this COMSOL analysis because the additional thermal conductivity created from the additions of percent nano-diamond particle is already ideally added to the base fluid before the simulation was commenced. Although, in practice this does present a practical hurtle for a sustained continuous uniform circulation of the nano-diamond throughout a system.

2. MATERIALS AND METHODS

2.1 Geometry

COMSOL was used in both the creation of the model geometry and the simulation of the basic shell and tube heat exchanger. The primary focus of the simulations is in evaluating the added performance of the nanoparticles, thus, the dimensions of the model were created arbitrarily, and the final model geometry can be seen in figure 1 & 2. The model was created on the mm scale to reduce solving time, where in previous larger designs elongated solving times was a challenge encountered with ANSYS taking more than 4 to 5 hours to complete a calculation for an industrial size heat exchanger with baffles, and a more complex 19 hot tube construction. Additionally, sudden expansions were eliminated around the oil tube to help with convergence issues. The requirement for simulating three distinct materials from a three-dimensional model is that there exists three separate model sections: one for the shell (structural steel), one for the hot fluid (engine oil/engine oil nanofluid), and one for the cooler fluid to be heated (air). Lastly, the surface area density was calculated as 382.78 m^2/m^3, which is simply the ratio of heat transfer surface area to heat exchanger volume (the volume was interpreted as the volumetric air space).

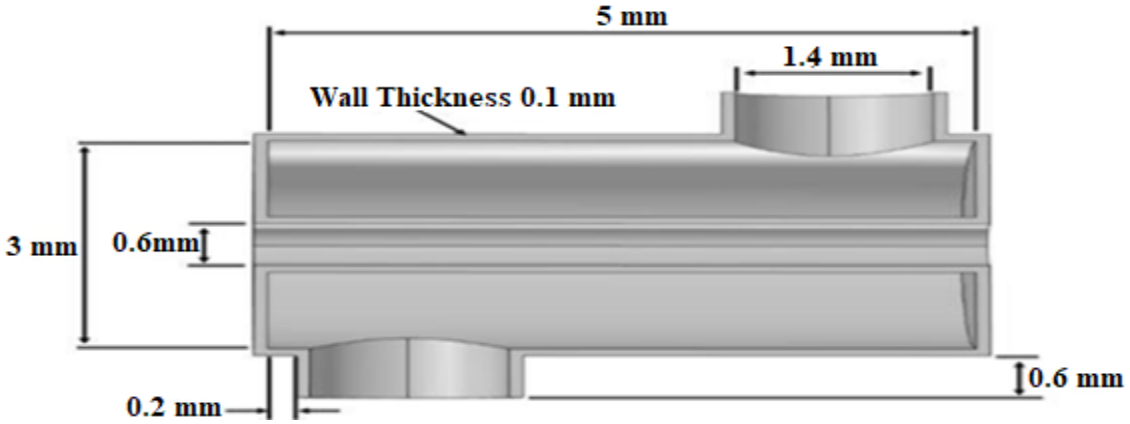

Figure 1: **Figure 2 :** Dimensions of shell and tube heat exchanger

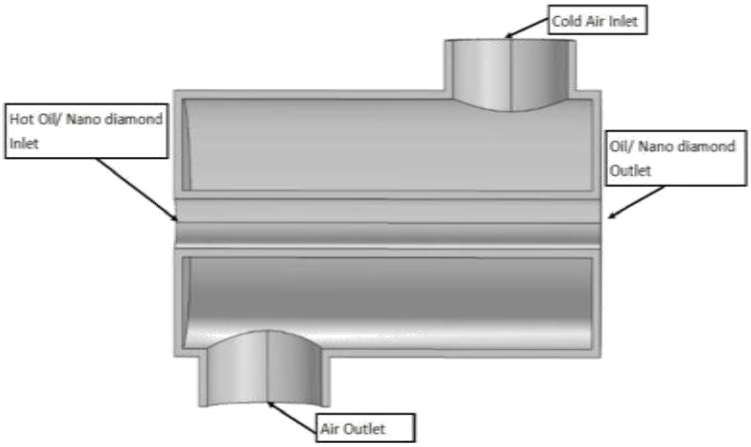

Cross Sectional Diagram of Inlets and Outlets

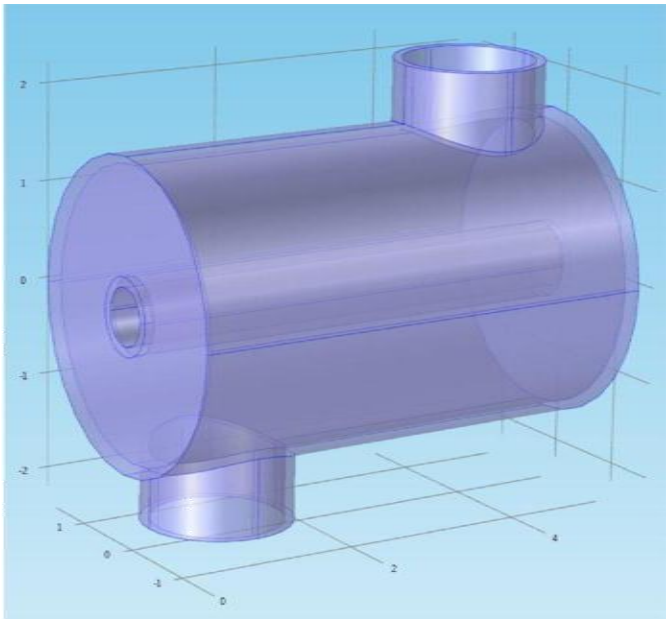

Shell and Tube

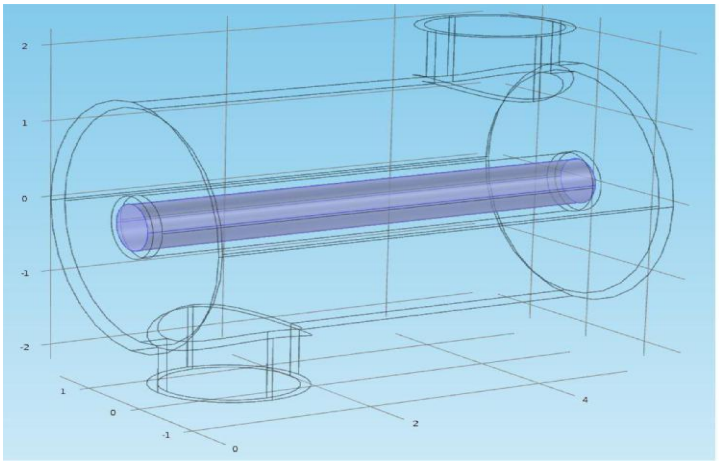

Oil

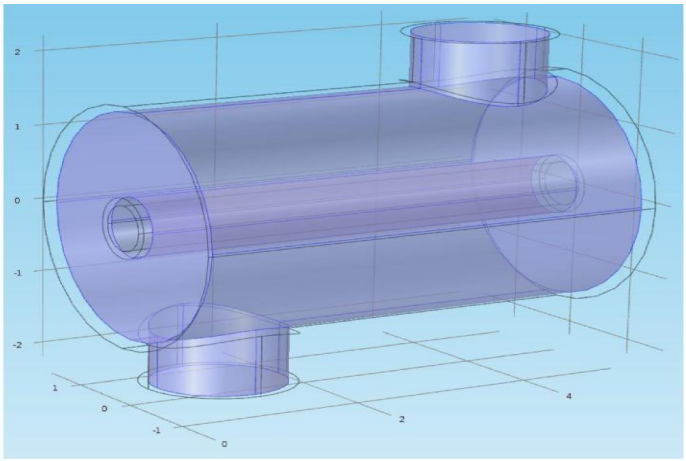

Air

Figure 2 : Geometry

2.2 Materials

The COMSOL study performed utilizes the default material assignments within the material fluid and solids database including: Structural steel, air, and engine oil. The breakdown of the material properties are viewed in figures 5-6, as well as initial conditions for the boundaries. However, the modifications to the oil, to simulate the nanofluid, were basedon the experimental study performed by M. Ghazvini, M. A. Akhavan-Behabadi, E. Rasouli&M. Raisee in 2012 where they use 20W50 motor oil with a nano-diamond particle additive [1]. Figures 3 and 4 are linear regressions derived from the study at 40 centigrade where this study obtains its values for the respective material properties; similarly, thermal conductivity is obtained from the studies experimental findings at 0, 0.5,1, & 2% nano-diamond particle in oil. The density of pure motor oil was assumed to be 810 kg/m^3 and the nano-diamond 3500 kg/m^3. The respective blend densities were summations derived via percentages of the pure values just stated, which is derived from conservation of mass. It can be added that constant oil density is linked to its defined incompressible flow. COMSOL uses equation-based material properties for air and engine oil, however, for the time independent study the material properties of the nanofluid are considered here as constant. The projected maximums of the oil property increases were 35% in thermal conductivity and 20% in specific heat [1]. In contrast, the maximum increases calculated relative to pure oil for this simulation can be seen in figure 7, which are 36% for thermal conductivity and 15% for specific heat. Additionally, for dynamic viscosity the max increase was 17% and the density increased a maximum of 7 % for the 2% nano-diamond addition. The near proximity or equivalence to the observed published maximums yield the notion that this study is taking full advantage of the nano-diamond benefit seen in the Ghazvini, M.,et.al study [1]. It is this studies goal to utilize the nano-particles maximum superior qualities in conjunction with the discussed base fluid

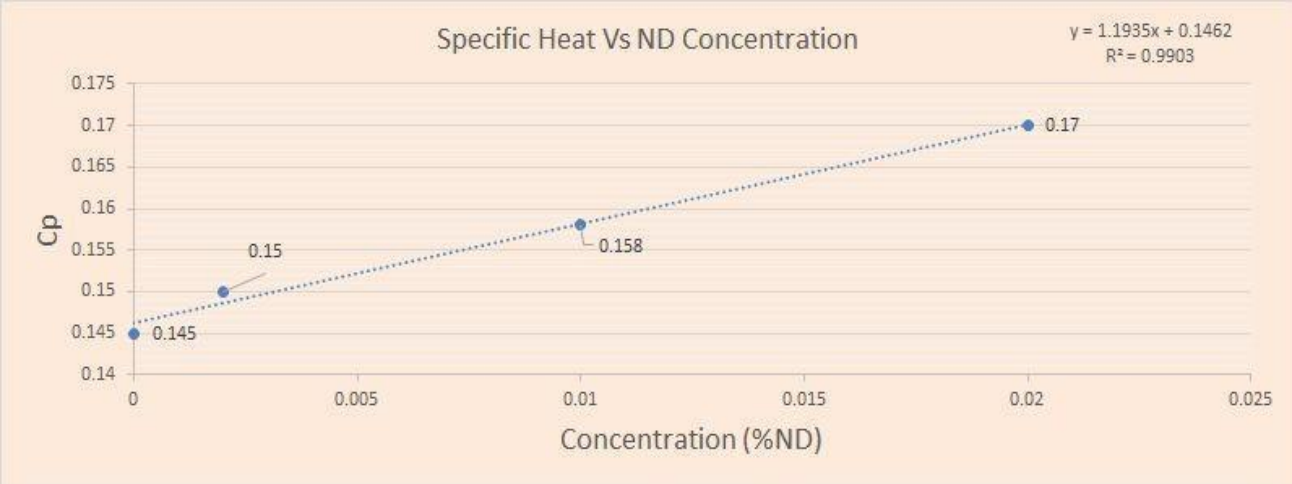

Figure 3: Material Properties for the used concentrations based on Ghazvini, M., et al 2012 study [1]. (Specific heat, linear trend with concentration 40°C.)

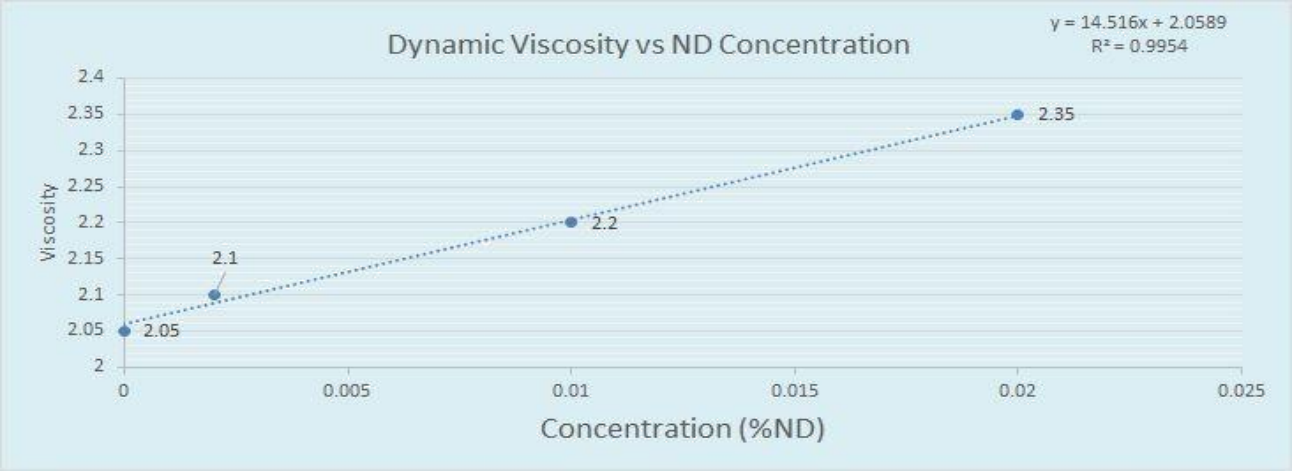

Figure 4: Material Properties for the used concentrations based on Ghazvini, M., et al 2012 study [1] (Viscosity, linear trend with concentration 40°C.)

Table 1: Air and Steel Properties (COMSOL Default) [8]

MATERIAL PROPERTIES Air & Steel Shell			
Material		Air	Structural Steel Shell
Relative Permeability		1	1
Relative Permittivity		1	1
Dynamic Viscosity	[Pa s]	a1	-
Ratio Of Specific Heats		1.4	-
Electrical Conductivity	[S/m]	0	4.03E+06
Heat Capacity At Constant Pressure	[J/ (kg K)]	a2	475
Density	[kg/m^3]	a3	7850
Thermal Conductivity	[W/(m K)]	a4	44.5
Poisson's Ratio		-	0.33
Young's Modulus	[Pa]	-	2.00E+11
Coefficient of Thermal Expansion	[1/K]	-	1.23E-05
Inlet Temperature	[K]	276.15	-
Initial Operating Conditions	[K]	276.15	276.15
Initial Velocity	[m/s]	1	-
*a1={(-8.38278e-7)+(8.35717342e-8)*T^1 - (7.69429583e-11)*T^2+(4.6437266e-14)*T^3-(1.06585607e-17)*T^4}*			
*a2={(1047.63657)-(0.372589265)*T^1 + (9.4530421e-4)*T^2-(6.02409443e-7)*T^3+(1.2858961e-10)*T^4}*			
*a3=pA*0.02897/8.314/T*			
*a4={(-0.00227583562)+(1.15480022e-4)*T^1 - (7.90252856e-8)*T^2+(4.11702505e-11)*T^3-(7.43864331e-15)*T^4}*			

Table 2: Oil with Nano Diamond Concentration Properties [1,8]

MATERIAL PROPERTIES Oil With Varied Nano Diamond Concentration					
Material		C1: Oil (pure) 0%ND	C2: Oil 0.5%ND	C3: Oil 1%ND	C4: Oil 2%ND
Relative Permeability		1	1	1	1
Relative Permittivity		1	1	1	1
Dynamic Viscosity	[Pa s]	0.1462	0.74295	1.3397	2.5332
Ratio Of Specific Heats		1	1	1	1
Electrical Conductivity	[S/m]	0	0	0	0
Heat Capacity At Constant Pressure	[J/ (kg K)]	2.0589	9.3169	16.5749	31.0909
Density	[kg/m^3]	810	823.45	836.9	863.8
Thermal Conductivity	[W/(m K)]	0.126	0.152	0.160	0.1715
Poisson's Ratio		-	-	-	-
Young's Modulus	[Pa]	-	-	-	-
Coefficient of Thermal Expansion	[1/K]	-	-	-	-
Inlet Temperature	[K]	313.15	313.15	313.15	313.15
Initial Operating Conditions	[K]	313.15	313.15	313.15	313.15
Initial Velocity	[m/s]	100	100	100	100

Table 3: Oil & Nanofluid Diamond Concentration Properties Percent Increases

PERCENT INCREASES IN THE MATERIAL PROPERTIES RELATIVE TO PURE OIL				
% Weight	Dynamic Viscosity	Thermal Conductivity	Specific Heat	Density
0.00%	0%	0%	0%	0%
0.50%	3%	21%	2%	2%
1.00%	9%	27%	7%	3%
2.00%	17%	36%	15%	7%

2.3 Boundary Conditions

If one used a compressible flow model the isentropic stalled temperature would be defined, which is a function of both Mach number and the ratio of specific heat. Although in this model, due to the non-isothermal incompressible flow the inlet temperatures must be specified. The diamond nanoparticles were introduced into engine oil through a central tube with an inlet temperature of 313.15 K. In the exterior cavity inlet air at 276.15 K is passed over the outer diameter of the engine oil tube, as seen in the cross-sectional diagram of figure 2. The outlets were both set to zero pressure, for a compressible model this would result in non-physical results, but for an incompressible simulation with inlet velocities defined the choice with zero gradient and magnitude is often assumed for the environment of fluid exiting the defined system.

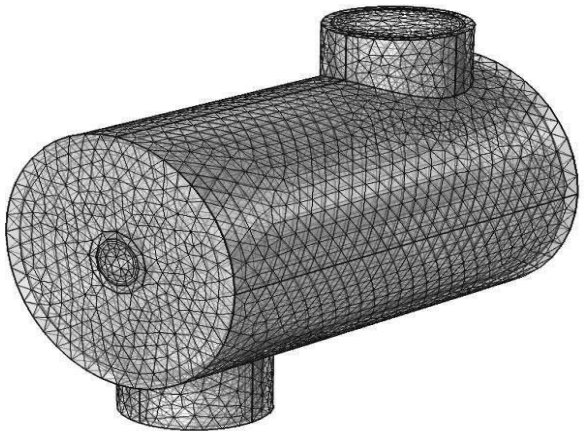

Figure 5: COMSOL Mesh (Normal Default)

Additionally, the outer shell is assumed adiabatic and with the stationary simulation, also, the initial temperatures of the cavities of the model (t_0 =0) corresponds to the oil and air temperatures, respectively as stated before. Moreover, it is assumed that the air fluid component has an initial velocity of 1 m/s, while the oil fluid component is pumped in the tube inlet at 100 m/s, displayed in Table 1-2. The model is further defined with the default mesh configurations for normal mesh size and the physics-controlled option is activated for additional properties such as inflation or a boundary layer on fluid shell boundaries; mesh independence was found for the
model, but normal was used for a higher calculation speed, seen in figure 5.

2.4 Setup

Subject to Ghazvini, M.,et. al, this was a steady state laminar study as the experimental properties for the nanofluid was performed with a laminar flow [1]. Additionally, the study was defined as non-isothermal, apart from the inlets, the temperature throughout the structure andfluids will vary. Also, the overall solution was fully coupled, the combined elements of the model are solved simultaneously together; for the physical phenomenon of the model are all connected through heat transfer, thus, appropriate for the simulation. PARDISO (Parallel Sparse Direct Linear Solver) was chosen for its superior speed in comparison to the other COMSOL direct solvers available, such as MUMPS or SPOOLES. The solver is capable of bridging the work over multiple cores on the computer, while simultaneously having the capability of storing the solution partially on the computer hard disk [3]. The preorder algorithm was defined as a multi-threaded nested dissection. Additionally, the

simulation was configured to run to with a limit of 1000 iterations relative to a tolerance factor of 1. The simulation converged to the tolerance factor in all cases, generally less than 70 iterations, but for most of the trials the solver converges in around 10 iterations (figure 6).

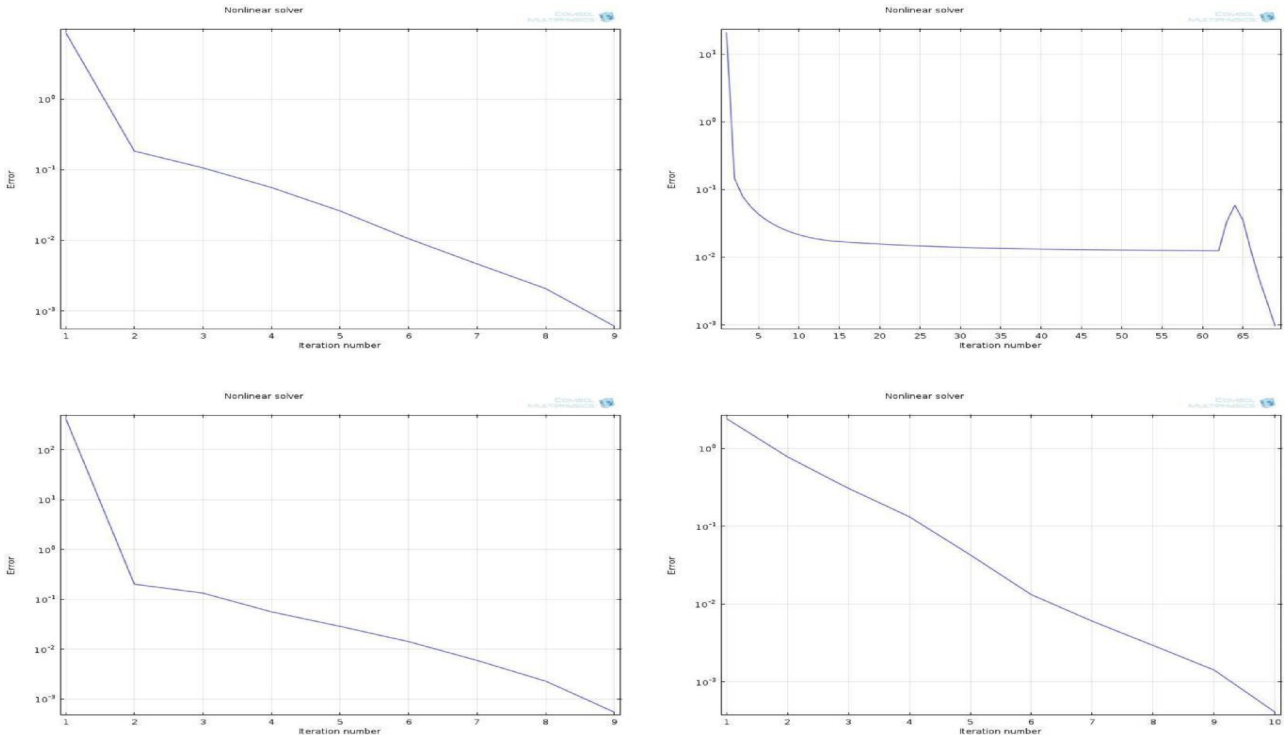

Figure 6: Convergence plots for case 1 to 4 (top to Bottom); pure oil, 0.5%, 1.0%, & 2.0% nano-diamond concentration.

3. THEORY

3.1 Governing Equations

The study balances the heat being generated in the solid steel shell and the spatial component of heat transfer to the left, with the time dependent component on the right side of equation 1.

Energy Heat Transfer $$\rho C_p \mathbf{u} \cdot \nabla T = \nabla \cdot (k \nabla T) + Q \quad (1)$$

The density is given by ρ, specific heat by C_p, k gives the thermal conductivity of steel, del operator dotted with del T represents the divergence of the temperature gradient or Laplacian, the dot product u dot del T models the time dependent advection, and Q represents the heat generation source. It can be seen that the general equations used by the COMSOL stationary solver for the fluids use Naiver Stokes, continuity, and the energy equation. The energy equation generally includes heat and work components added to the left side of the equation not seen in equation 1. For example, if there is convection, which occurs from the outer diameter annular oil pipe to the passing air. Equations 2 and equation 3 seen below, express Naiver Stokes and continuity, respectively.

Naiver Stokes

$$\underbrace{\rho\left(\frac{\partial \mathbf{u}}{\partial t} + \mathbf{u} \cdot \nabla \mathbf{u}\right)}_{1} = \underbrace{-\nabla p}_{2} + \underbrace{\nabla \cdot \left(\mu(\nabla \mathbf{u} + (\nabla \mathbf{u})^T) - \frac{2}{3}\mu(\nabla \cdot \mathbf{u})\mathbf{I}\right)}_{3} + \underbrace{\mathbf{F}}_{4} \quad (2)$$

Continuity $$\nabla \cdot (\rho \mathbf{u}) = 0 \quad (3)$$

Equation 3 represents conservation of mass where density is not variant with time; for the divergence of velocity, the del operator expands with vector u multiplied by the density to form the infinitesimal mass volume density representative of the mass inflow and outflow respective of a control volume, for laminar nearly incompressible flow. Solved simultaneously is equation 2 or Naiver Stokes equation derived by Naiver, Stokes, Saint-Venart, and Poisson sometime around 1827 and 1845 [8]. The equation represents newton's second law for compressible fluids or it can be understood as the conservation momentum equation. From {1} to {4} the terms represent a summation of internal forces, with force components of pressure, viscous force, and external force; μ is the dynamic viscosity, and I is the identity matrix [8]. One case when a term is eliminated is when the viscous force term drops out, if the divergence of the velocity is zero, in the case of incompressible flow for a fluid, such as, engine oil.

4. RESULTS

The analysis produced a more efficient system regarding the addition of the nano- diamond particle engine oil additive. The addition of baffles produced a similar improvement. The max of 17 baffles produced about a 1 % improvement in efficiency, whereas the addition of the 2.0% nano-diamond concentration gave about a 1% improvement in heat transfer efficiency.

5. DISCUSSION

5.1 Effects of Nano-Diamond Implementation

In figure 9, the plane sections of the heat exchanger are shown, the temperature profiles are displayed for each concentration tested. In figure 11 the streamline temperature distributions are presented for comparison. It can be seen that the area to the left of the air inlet, an eddy had formed where the boundary layer was not formed, immediately deflecting off the pipe. The eddy has the effect of

trapping cooling fluid in an isolated region, accumulating heat, with the eventual result of losing effectiveness of heat transfer from these locations overall. Additionally, because these regions trap a bulk of cooling fluid, the limit of the capacity of the fluid running alongside the oil tube is seen, which results in a small quantity of air absorbing as much thermal energy as seen, but only making up a minute total of the outlet air volume; the air running alongside the tube has less cold air molecules to pass thermal energy onto due to a large quantity of cooling fluid being located in the eddy, remaining a non-participant. For this reason, the results observed can lead one to desire a modification to the geometry of a smaller space between the outer shell and the oil pipe to reduce the natural convection produced phenomenon.

The temperature rise has the greatest increase from pure oil with a 0.5% nano-diamond addition. In figures 7- 8 it can be seen that the green 295 K air dominates the outlet air region for pure oil, where the yellow-orange 302 K outlet air dominates in the 0.5% nano-diamond case. The dominant air temperature in the outlet air for the last cases was approximately
303-304 K for 1%, and 305-306 K for the 2% nano-diamond, where the bulk region being spoken of is coming from the bottom of the heat exchanger making up more than half of the air outlet volume. The overall hotter air outlet region (approximately 306-310 K) is closer in temperature through the 4 cases and makes up a smaller percent of the overall air outlet volume.

Overall, as the air and oil move through the cross-flow exchanger the outlet temperature of the air rises and the outlet temperature of the oil approaches the inlet temperature of the oil as the concentration of nano-diamond particle content increases. The rise in oil temperature was due to an increase in conductive properties of the fluid increasing with nanoparticle addition, which was occurring faster than what was being removed via forced air convection in the air chamber figure 10. The largest improvement of heat transfer occurred at the largest concentration of nano-diamonds used, which maxed at only a 1.06% improvement over pure oil, as seen in Table 4. However, the overall effect of the nano-diamond addition decreased with every rise in percent relative to the increase seen from pure oil to 0.5%, showing that there are diminishing returns for every relative increase in nano-diamond particle percent increase. Although, if a plateau exists it was not observed at 2% as a slight increase was still seen between 1.5% and 2%, the proximity to level would be near as the percent increase between the two cases is only 0.2%, relative to each other (figure 9). However, if one observes figure 9 a parabolic trend of an increase in
nano-diamond may be present, according to the R squared term equaling 0.9914 for the simulation data, if this is so, the maximum nano-diamond concentration would be around 1.6 %. However, for one to be conclusive, more data points are needed.

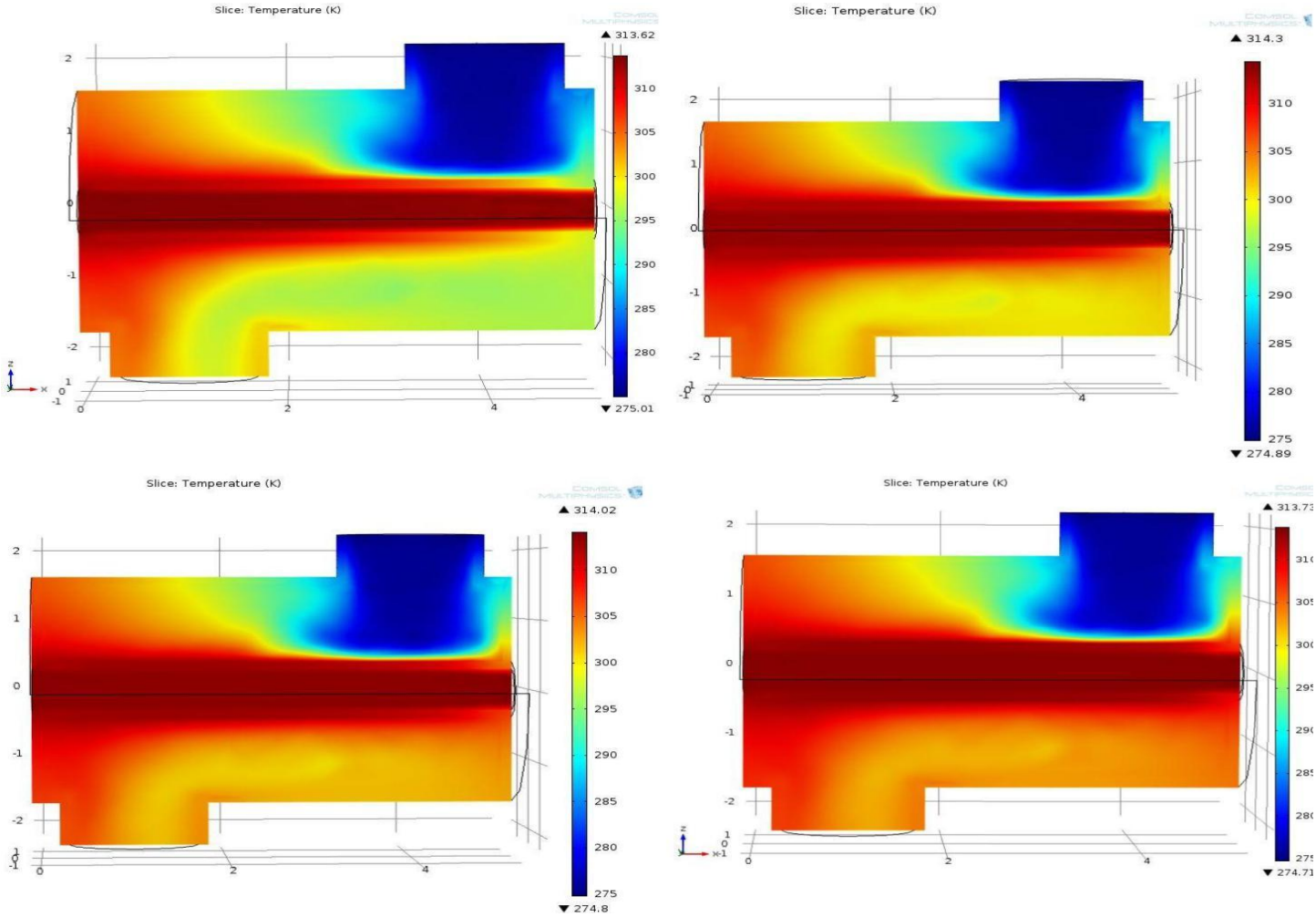

Figure 7: Temperature contour plots for case 1 to 4 (top to Bottom); pure oil, 0.5%, 1.0%, & 2.0% nano-diamond concentration.

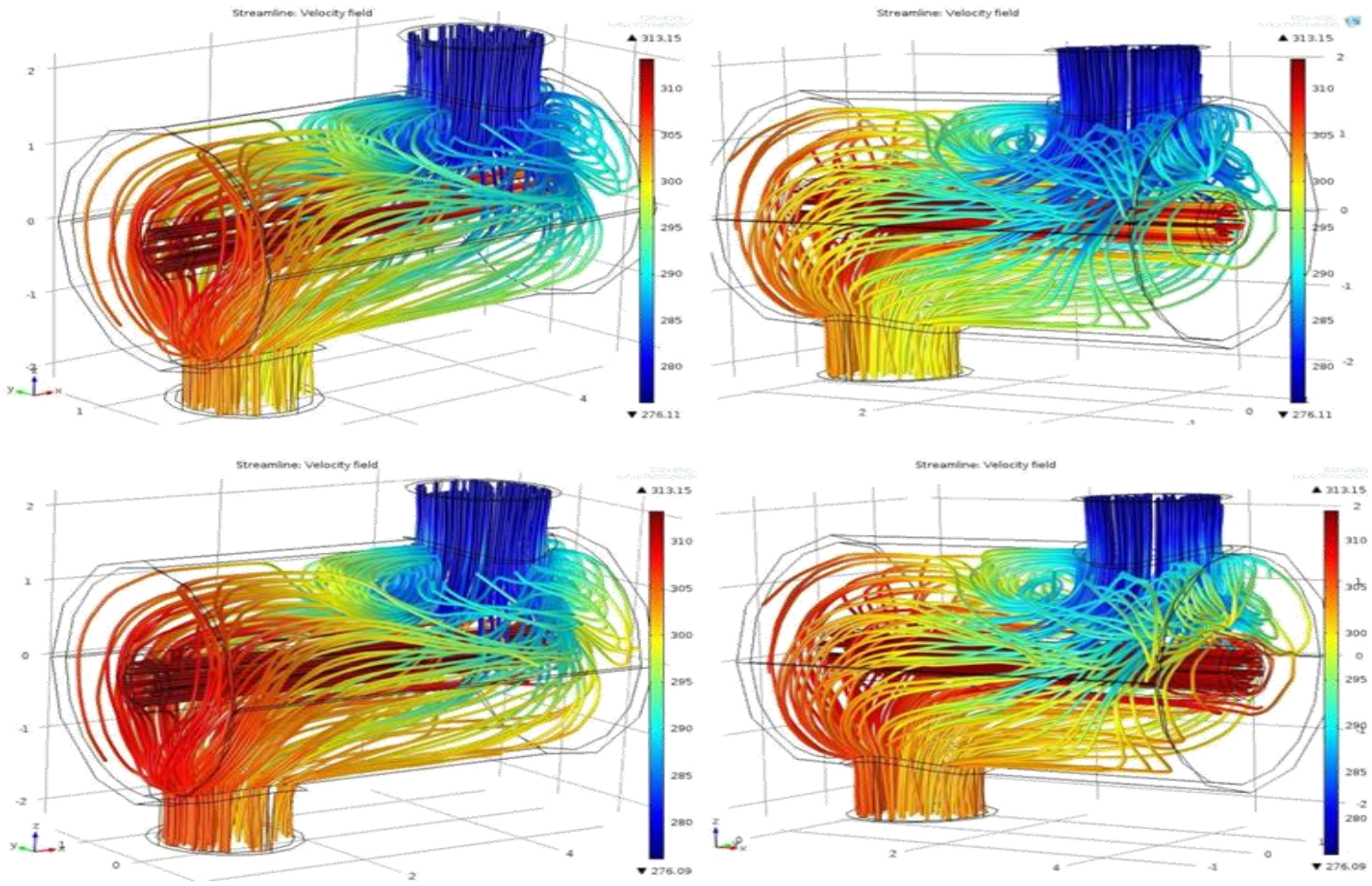

Figure 8: Temperature Streamline Plot No Baffles (Pure oil top) (2% ND bottom)

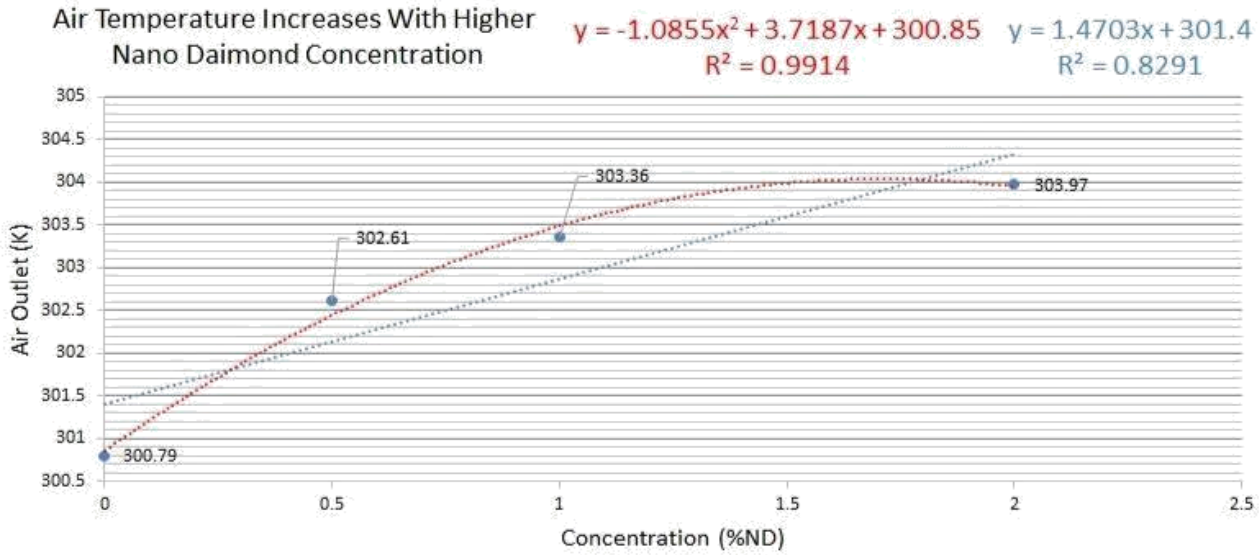

Figure 9: Air Outlet Temperature vs % Nano Diamond Concentration (Increased Heat Transfer)

The initial air inlet temperature was 276.15 K, which means for pure oil the air outlet temperature rose 24.64 K. Whereas, the maximum addition of nanoparticles at 2% increased the air outlet by 27.82 K. The oil on the other hand initially has a decrease in outlet temperature, 5.11 K for pure oil in relation to the inlet 313.15 K. However, as stated the nano-diamond addition promoted conduction within the fluid at a faster rate than what thermal energy could escape through convection with the cold air blowing across the pipe, thus, only a 0.88 K drop occurred. Also, one may note that the initial oil velocity is much faster than that of the air inlet velocity.

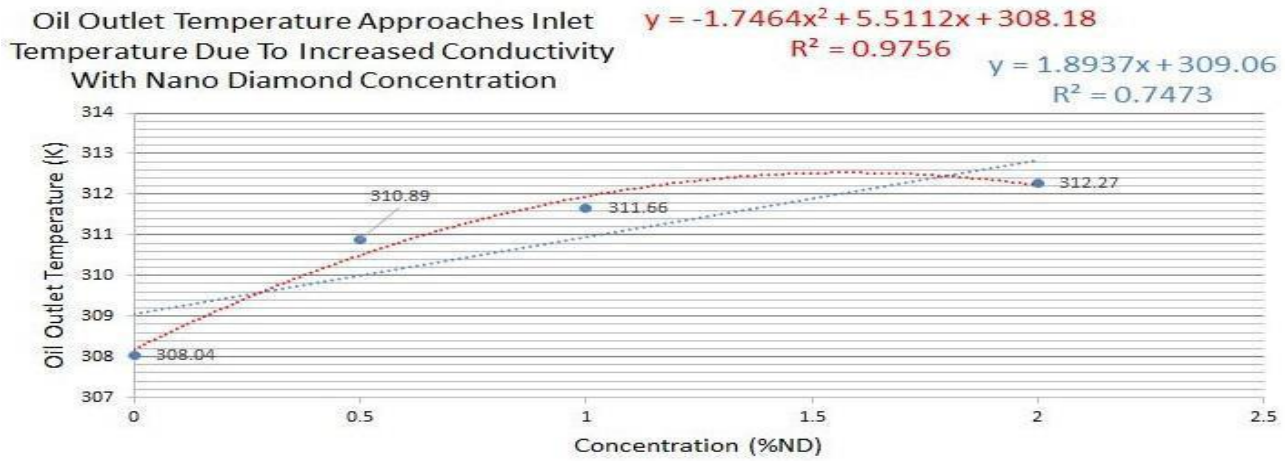

Figure 10: Oil Outlet Temperature vs % Nano Diamond Concentration

Table 4: Oil Outlet Temperature & Increased Efficiency of Heat Transfer due to %ND

Resultant Outlet Temperatures					
Case A	% ND Concentration	Air Outlet [K]	Oil Outlet [K]	Air Difference from caseA1 [K]	% Difference caseA1
1	0	300.79	308.04	0	0.00%
2	0.5	302.61	310.89	1.82	0.61%
3	1	303.36	311.66	2.57	0.85%
4	2	303.97	312.27	3.18	1.06%

5.2 Addition of Baffle/ Fin Comparison

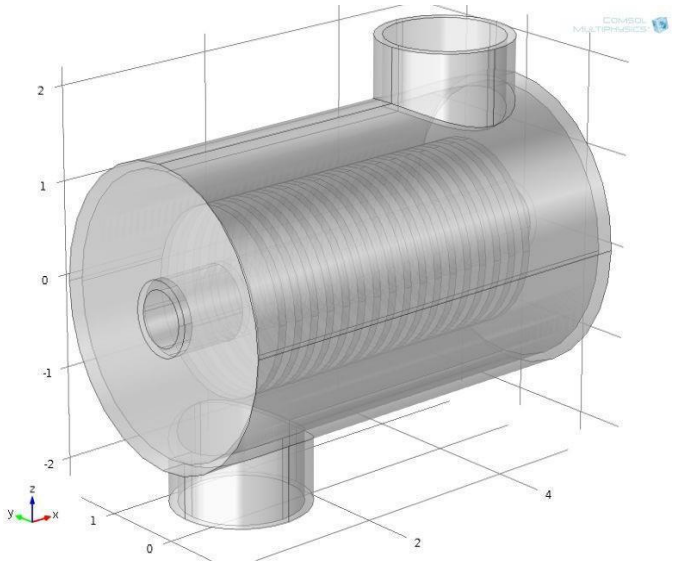

Figure 11: Baffle Dimensions, 2 mm OD 0.8 mm ID & 0.1 mm thickness with 0.25 mm spacings

5.3 Metry Baffle Fin Addition

The addition of heat fin baffles was incorporated to increase heat transfer between the oil and the air in the two-concentric tube heat exchanger; the addition of fins to the outer diameter of the oil pipe offers a comparison of air outlet temperature rise relative to the nanofluid. The geometrical addition has dimensions that follows a symmetric multiplier of two fins opposite a central baffle with a 0.25 mm baffle spacing. Additionally, the baffle seen in figure 11 is a 0.1 mm annular disk, with a 0.8 mm inner diameter, and a 2 mm outer diameter; the disk along with the central oil tube comprise 75% of the radial internal air cavity. At the 17-baffle configuration used for the primary comparison study, the surface area density was calculated as 3835.07 m^2/m^3, which is much higher than the common range of 60 - 500 m^2/m^3.

5.4 General Setup Baffle Fin Addition

It can be noted that to compare the simulations all other components related to the settings and mesh were kept identical to the first geometries simulation. It was desirous to find the point where the effect of adding heat transfer surface area began to negatively impact the performance of the heat exchanger due to the decrease in air volume; the effect was measured relative to the air outlet temperature, which is a sign of heat transfer efficiency of the overall system. Moreover, the initial trials were simulated with pure oil as the hot fluid; the addition of baffles followed the increasing series of: 0, 1, 2, ...n+2 for n is the total baffles present in the last case before it. The series was performed up to 21 baffles and the graphical parabolic trend can be seen in figure 12, with the no baffle case at the left corner of the graph; the parabolic arc starts with 1 baffle and continues to 21. The derivative was set to zero and by taking the ceiling, the maximum for the configuration is found to be 17 baffles.

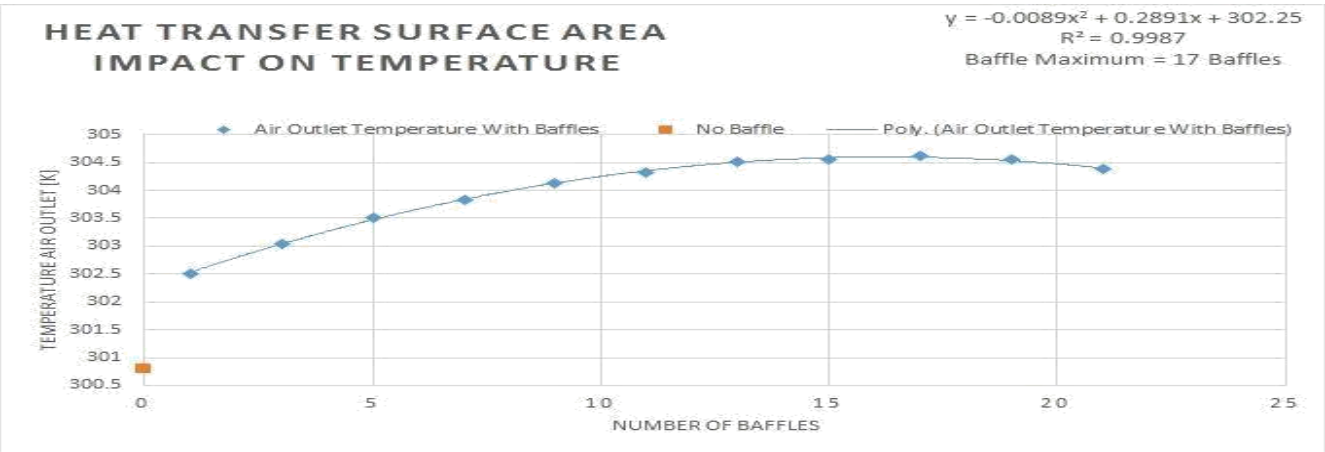

Figure 12: Temperature of air outlet as a function of the number of baffles used. Highest efficiency occurs when 17 baffles are used.

5.5 Effects of a Baffle Fin Alongside Nano-Diamond Implementation

The comparative results of the study show a complete elimination of the eddy currents observed in the non-baffle geometry, and a more symmetric temperature gradient distribution due to less space in the cavity to house the circulation formations; the boundary layer along the shell is formed and retained, seen in figure 14. The effect is a more uniform air outlet temperature, the addition of baffles is for the encouragement of turbulence, thus, greater heat transfer (figure 13). However, the simulation is kept laminar and the baffles are directly mounted to the hot pipe; the baffles physical effect more closely simulate annular heat sink fins, increasing the heat transfer surface area with each additional fin. The overall trends are consistent with the non- baffle case according to the nano-diamond addition. The max percent increase due to the nanoparticle addition is 0.98% relative to the pure oil air outlet temperature, where the previous geometry was 1.06% at 2% nano-diamond. The increase of the air outlet temperature due to the baffle addition was a 1.28 % increase over the non- baffle case for pure oil (Table 5). The temperature increases from the baffles alone respective of the 276.15 K air inlet was a 28.48 K increase, a 0.24 % increase over the 2% nano-diamond case's increase in temperature of 27.82 K. Therefore, the combined effect of baffles and the nano-diamond is roughly double the nano-diamond increase at the 2% case, 2.3% (i.e., an overall 31.48 K air temperature increase from the air inlet temperature) (Table 5).

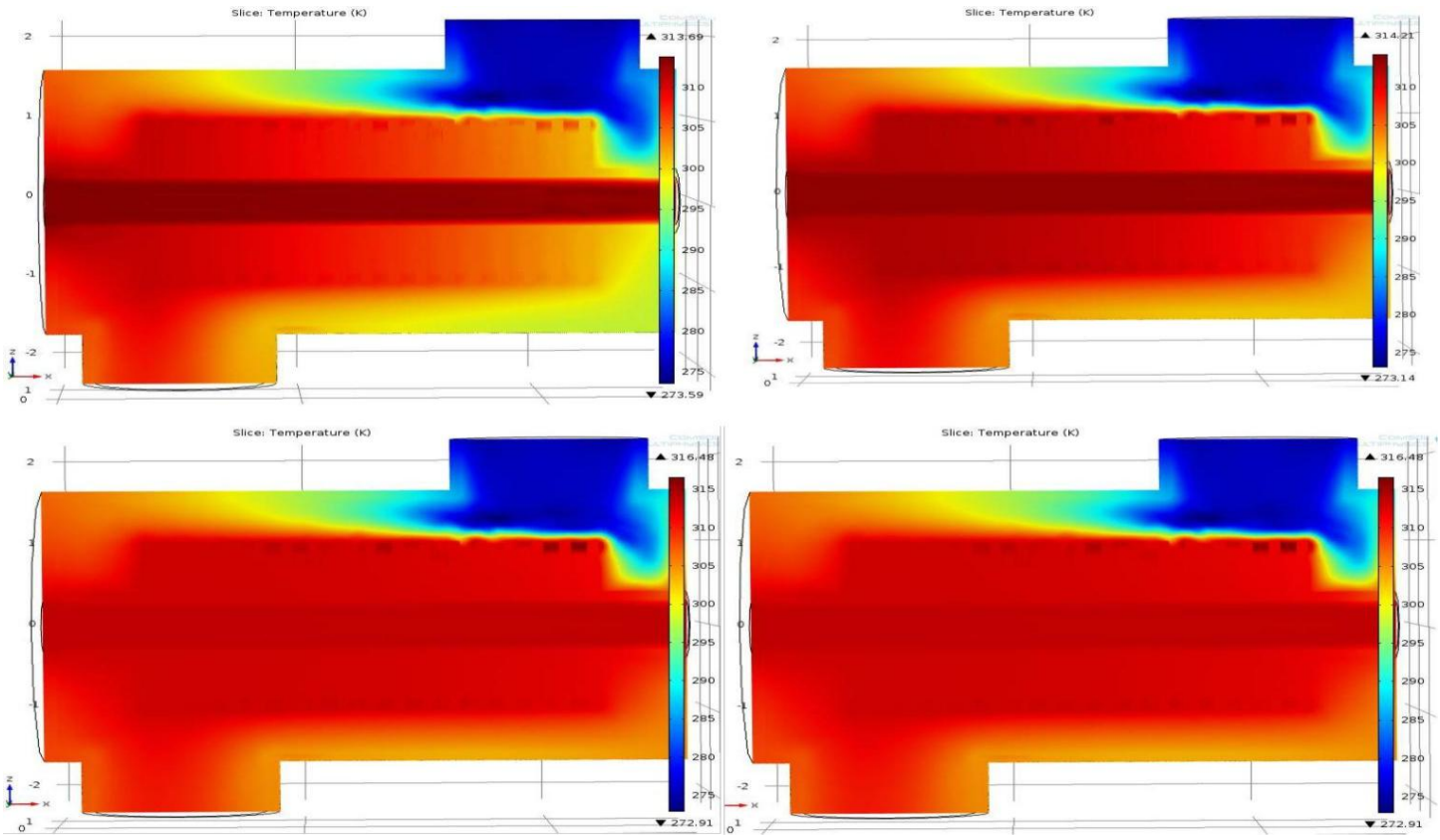

Figure 13: Temperature Distribution of Air with 17 Baffles (ND Concentration: 0,0.5,1,2%, respectively)

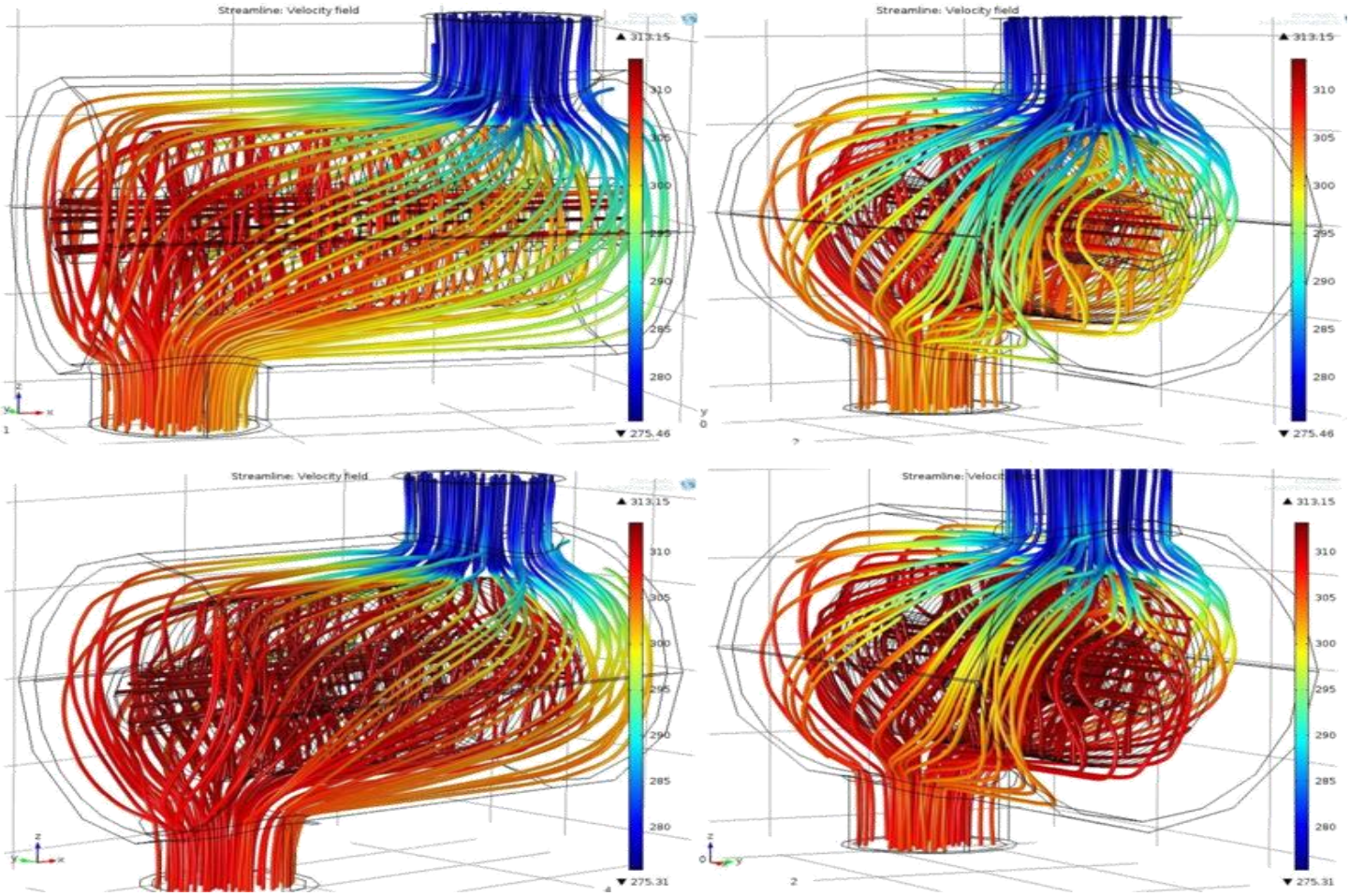

Figure 14: Temperature Streamline Plot 17 Baffles (Pure oil top) (2% ND bottom)

Table 5: Maximum baffles Additional effect on heat transfer (top), Nanoparticles & Maximum Baffles effect on heat transfer (bottom)

Resultant Outlet Temperatures: For Pure Oil				
Cases	Baffles	Air Outlet [K]	Air Difference from caseA[K]	% Difference caseA
A	0	300.79	0	0.00%
B	17	304.63	3.84	1.28%

Resultant Outlet Temperatures: With 17 Baffles				
CaseB	% ND Concentration	Air Outlet [K]	Air Difference from caseB1 [K]	% Difference caseB
1	0	304.63	0	0.00%
2	0.5	306.38	1.75	0.57%
3	1	307.07	2.44	0.80%
4	2	307.63	3	0.98%

The temperature vs % nano-diamond concentration graph can be seen in figure 15 and has information that summarizes the results of all the relevant trials. The lower data is the first case geometry, whereas, the upper curve is representative of the baffle fin geometry. The slope is a direct correlation to the temperature rise for additional nano-diamond concentration. The addition of baffles can then be said to vertically shift the results from the first case up roughly 1.28%.

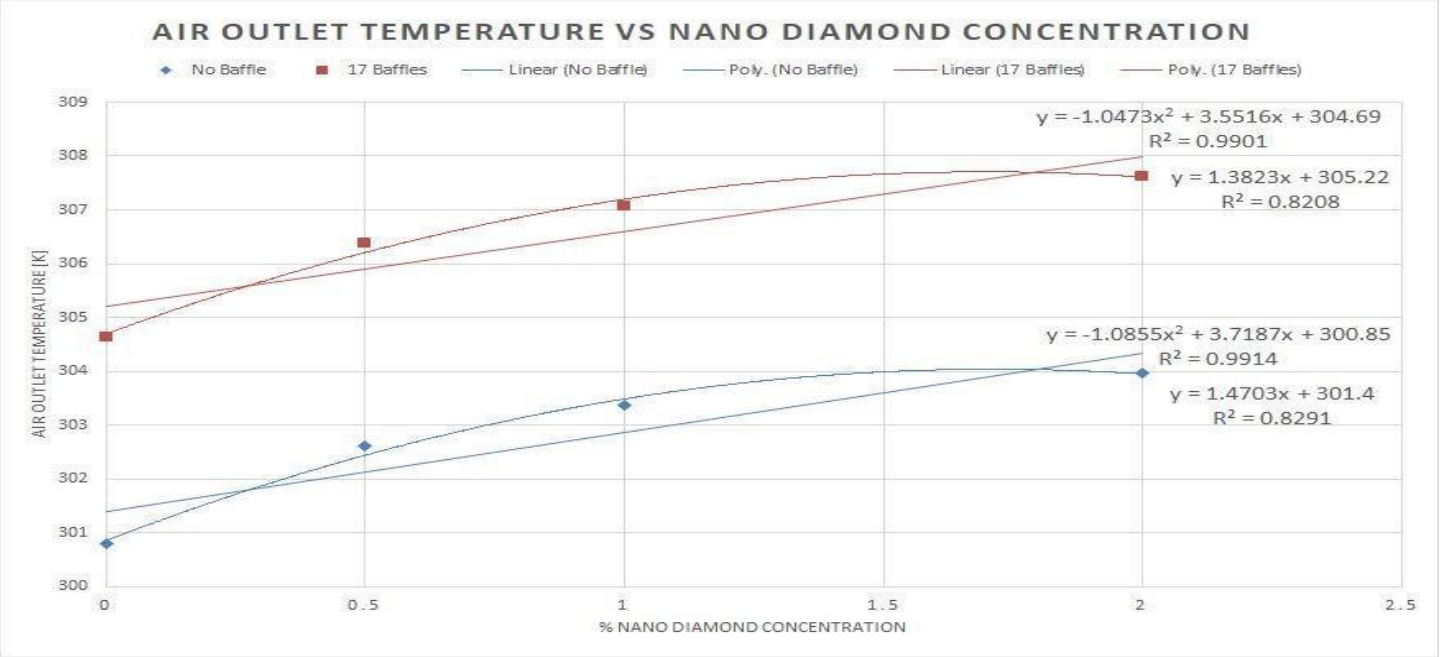

Figure 15: Comparison between Trials

6. CONCLUSIONS

This study set out to determine the effect of nanofluid in conjunction with a shell and tube heat exchanger. The first set of simulations observed the raw effect of nanofluid in a shell and tube heat exchanger hot flowing fluid without any thin member baffle fin structure in the cold fluid chamber, this was done with the purpose of contrasting the relative effect of the methods themselves. Both adding baffle fins or adding a nanofluid can be considered a heat transfer enhancing method in general.

Therefore, the study offers a lens as to their individual benefits, and a lens to the combined effect for this particular geometry. In the shell and tube heat exchanger, an analysis according to the varying amounts of nano-diamond particles that ranged from 0% to 2.0% was conducted, which considered heat transfer changes relative to the increasing nano-diamond concentration effect on: thermal conductivity, specific heat, density, and dynamic viscosity. Second, a baffle system was constructed where the geometries unique max of 17 baffles was found, the max was used to contrast the addition of nanofluid to the addition of baffles. In each investigation there were increases in the overall efficiency of the heat exchanger.

The nano-diamond study showed a 1.06% raise in the heat transfer for the 2.0%. nano-diamond compared to the 0% nano-diamond system. In addition, the context of the stated increase is found in a material property comparison to the original source. The max thermal conductivity of the nanofluid increased about 36% in comparison to the conclusion found in M. Ghazvini, et al's paper, which expresses that the max rise in thermal conductivity of the experimental study was approximately 35% [1]. Similarly, this simulation had a max increase in specific heat of 15%, where the referenced conclusion states the max value to be around a 20 % increase [1]. Thus, this study was conducted at or near the maximum capacity relative to M. Ghazvini, et al's optimal experimental results.

With the same assumptions as the nano-diamond particle simulations utilized on the non-baffle heat exchanger, the baffle simulations were conducted. The baffle study showed asimilar rise in heat transfer with pure oil to the 2% nano-diamond case, respective of the air outlet temperature rise (0.98%); the pure oil baffle case had an increase of 1.28% in air outlet temperature relative to the pure oil no baffle case. Accordingly, it was from the combination of the examinations of 0 to 21 baffles that the most efficient number of baffles for the system was found at 17. The baffle setup shows that the geometry of the shell and tube heat exchanger is just as import as the fluid being fed through the pipes, allowing one to conclude that they both can be considered as respectable options to increase the heat exchangers efficiency. Lastly, it is mentioned that when considering the combined effect of the 17-baffle construction and the 2.0% nano-diamond particle oil addition the system gives an overall increase of 2.34% in air outlet temperature, where each method roughly accounts for half of the increase relative to the pure oil air outlet results for the no baffle geometry. The findings for this geometry suggests that these methods of increasing heat transfer efficiency are comparable and may supply the engineer another respectable option in their desire to add additional efficiency to their system, at the lowest possible cost.

REFERENCES

[1] Ghazvini, M., Akhavan-Behabadi, M. A., Rasouli, E., & Raisee, M. (2012). Heat Transfer Properties of Nanodiamond–Engine Oil Nanofluid in Laminar Flow. Heat Transfer Engineering, 33(6), 525–532. https://doi.org/10.1080/01457632.2012.624858

[2] GalalYehia, Mahmoud & Attia, Ahmed & Ezzat Abdelatif, Osama & Khalil, E.E. (2014). Computational Investigations of Thermal Simulation of Shell and Tube Heat Exchanger. ASME 2014 12th Biennial Conference on Engineering Systems Design and Analysis, ESDA 2014. 3.10.1115/ESDA2014-20005.

[3] Nikhil Deepak Kundnaney& Deepak Kumar Kushwaha (2015). A CriticalReview on Heat Exchangers used in Oil Refinery. Asian International Conference on Science, Engineering & Technology, AAICSET-2015 ISBN: 9-780993-909238

[4] Blake T. Branson, Paul S. Beauchamp, Jeremiah C. Beam, Charles M. Lukehart, and Jim L. Davidson, (2013). Nano diamond Nano fluids for Enhanced Thermal Conductivity www.acsnano.org, Vol. 7, No. 4, pp. 3183–
3189

[5] Choi, U. S., "Enhancing Thermal Conductivity of Fluids with Nanoparticles," Developments and Applications of Non-NewtonianFlows, edited by D. A. Siginer and H. P. Wang, Fluid Engineering Div.-Vol. 231, American Society of MechanicalEngineers, New York, 1995, pp. 99–105.

[6] Hu, Z. S., and Dong, J. X., "Study on Antiwear and Reducing Friction Additive of Nanometer Titanium Oxide," Wear, Vol. 216, No. 1, 1998, pp. 92–96

[7] Huaqing Xie, Wei Yu and Yang Li Thermal performance enhancement in nanofluids containing diamond nanoparticles 2009 J. Phys. D: Appl. Phys. 42 095413

[8] COMSOL (2018). Retrieved December 1,2017, from http://www.comsol.com/multiphysics.

Journal of Mechanical Engineering & Modern Technology
www.jmemt.jarap.org
Volume 1 Issue 1, 30 June 2018
PP. 31-36

HELICAL HEAT EXCHANGER USING PHASE CHANGE MATERIALS WITH EXPANDED GRAPHITE PARTICLES

Hamidreza Ghasemi Bahraseman [1*], Alvah Bickham [2], Matthew Bonilla [2], Justin Hageman [2], Omar Huerta [2], Robert Mann [2] & Marlon Quintanilla [2]

[1] Mechanical Engineering Department, San Diego State University, San Diego, 92182, CA, USA
[2] Mechanical Engineering Department, California State Polytechnic University, Pomona, 91768, CA, USA
*Corresponding authors: Hamidreza Ghasemi Bahraseman, *hghasemibahraseman@sdsu.edu*

Key words

Heat Exchanger
Phase Change Materials
Expanded Graphite Particles

Abstract

This paper focuses and investigates the application of nanoparticle immersion in a phase change material for latent heat energy storage. In a real-world scenario, a helical pipe coil would be wound through an insulated steel tank filled with the composite PCM; heated or cooled water would be pumped to inject or extract heat from the PCM as needed. For simplification, simulation was done using a helical heating element instead. The base of the composite phase change material (PCM) was paraffin wax, and the nano-particle material immersed in the base was expanded graphite. Five total cases were examined with different percentages of expanded graphite in solution, with the first case having no graphite. Simulation and analysis was done using COMSOL Multiphysics 4.3a. Parameters examined were the average temperature of the body, the time to reach the coil temperature, the melted fraction of the PCM, and the time to reach complete melting. The generated data from the selected criteria assist in visualization of the effect of an increased percentage of expanded graphite in heat storage applications.

1. INTRODUCTION

One of the more significant fields in which intensive research has been done in the last century is energy storage. However, the use of current technologies, materials, and other processes to produce energy have been proven detrimental to the environment.[1] The effects of climate change as well as other negative factors have promoted the creation of new technologies to store and transmit energy. Among these new technologies, the use of phase change materials(PCM's) to store latent energy opens a realm of possibilities in increasing the efficiency of energy transfer systems, while reducing the gap between current supply and demand. Although the use of PCM's is new compared with other technologies, it displays a relatively accelerated pace of innovation, as new studies show that combining them with nano-engineered materials make it a promising application. PCM's have been mostly used in three energy storage methods which are sensible heat, latent heat and chemical energy. However, it was found to be more successful in the area of latent heat storage due to its high energy storage capacity and small temperature variation. Materials that show these properties are called heat absorbers. These materials have the ability to undergo phase transition and are becoming more common in the building industry.

In countries where climate varies from temperatures of 5º Celsius in the winters to 45º Celsius in the summer; energy consumption in air conditioning is a major factor in energy cost. For this reason PCM's are being studied and developed for absorbing and releasing large amounts of energy proportionally in order to increase efficiency. PCM's can be used in within building walls so that during the day they absorb energy from the sun keeping the inside relatively cool and releasing the absorbed energy at night keeping the inside relatively warm.

A phase change material is any material that has a high heat of fusion, which means that it absorbs a large amount of thermal energy in the process of melting from solid to liquid. Similarly, it discharges a large amount of heat during solidification. When a PCM absorbs heat from a contact medium, their temperature increase and then they release energy almost to a constant temperature. Some

PCM's are capable of storing from 5 to 14 times more heat per unit volume than a regular material. [3].Phase change materials need to have certain properties, which make them either expensive, and hard to find, or to manufacture. [2] The thermodynamic properties of a PCM include: good phase change temperature, high latent heat of transition and have a good thermal conductivity for heat transfer. Other physical and chemical qualities that characterize good PCM's are high density, small volume change, low vapor pressure, sufficient crystallization rate, inter-substance nonreactivity, nontoxic, and lastly noncombustible. [3]

Phase change materials can be categorized into three main groups. First there are organic materials in which paraffins are the most important. They consist on a mixture of n-alkanes chains that are available on large temperature ranges. Since this type of material is highly reliable and cheap there are several systems that in which they can be used. However, there are also some limitations like low thermal conductivity when they are used alone, they cannot be used in plastic containers as they do not interact well, and finally they are flammable. The next subcategory among organic PCM's are the non-paraffin's, these materials form the largest group because each of them has its own unique properties. Studies like the one conducted by Buddhi and Sawhney[4] identify several organic substances like fatty acids, esters, alcohols and glycols as PCM's due to their potential for energy storage. While having good heat of fusion characteristics and inflammability, some highlighting features of non-paraffin, organic PCM's which disqualify their use are toxicity and being unstable at higher temperatures.

The second group of PCM's, the inorganics, are divided between salt hydrates and metallics. The use of salt hydrates for energy purposes has been the topic of hundreds of recent studies. The results indicate that the biggest issue encountered is the degradation of their thermal energy storage capacity. This occurs after certain number of heating-cooling cycles.[5] Another disadvantage of these materials are their poor nucleation properties which make them prone to supercooling or fast change in phase before crystallization occurs. Although they have high thermal conductivity, are cheap, and have small volume changes when melting, most of the time they need to be mixed with other substances to increase their effectiveness. [6] The group of metallics includes all the low melting metals and metal eutectics, these materials are not considered for energy storage due to their weight and volume as well as many other implications that require the use of extremely high temperatures to achieve a phase change.

The last classification of PCM's are the eutectics. These are a minimum- melting mixture of materials, each of which changes phase congruently during crystallization [7]

The efficiency of both organic and inorganic PCM's as thermal storage systems is generally affected by the same factor: low thermal conductivity. Even though inorganic PCM's have higher thermal conductivity compared their organic counterparts, there are several cases that require a higher thermal exchange improvement. There have been several approaches recently studied to overcome this problem: metal thin strips [9], thin walled rings [10], porous metals [11] porous graphite [12], metal foam matrix [13] and carbon fibers [14,15] are the common techniques proposed to enhance the thermal conductivity of a PCM. In particular carbon fibers are highly promising additions, since they are resistant to corrosion and chemical attacks, conditions that make them adequate to combine with PCM's that present corrosive properties. [8]

2. METHODOLOGY

Using COMSOL Multiphysics 4.3a, a 3D model was generated. The model consisted of a helical copper heating element running through a cylindrical PCM body. The system is assumed to be contained in a well-insulated body and is adiabatic. The material and thermal properties of copper were retrieved from COMSOL's incorporated database, and the properties of the PCM body were introduced on the system depending on each case. Thermal conductivity and latent heat of fusion were determined using published data [17].Specific heat was determined empirically using specific heat values of each pure substance and the percentage of each in each case. Similarly, the density of each case was calculated using the densities of each pure substance. Five cases (0%, 8%, 13%, 19%, and 26%) of added graphite were chosen based on available information from published data [17]. A coarse mesh was applied to the body and simulated. Simulations were conducted over a timeframe of ten seconds in 0.01 second intervals, with the exception of the case of pure paraffin wax, which was simulated for 300 seconds to accommodate the longer melting time. From the obtained results a better understanding of the effects of incorporation of thermally conductive nanoparticles can be understood.

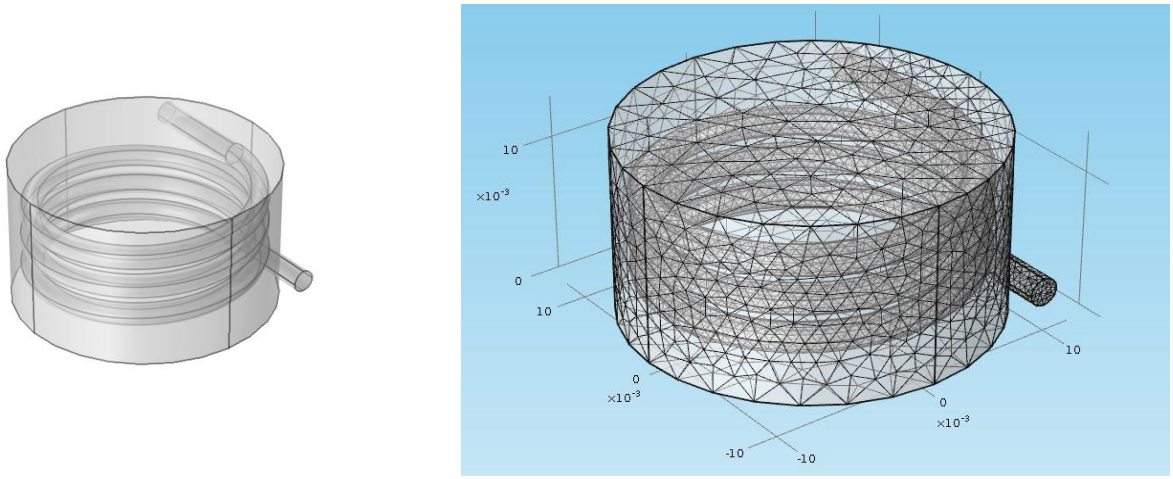

Figure1: Geometry Generated in COMSOL and Corresponding Mesh

As mentioned on previous section, paraffin wax is one of the most accessible forms of PCM's. Paraffins are formed of straight chains of hydrocarbons that have melting temperatures ranging from 73.4 to 152.6 degrees Fahrenheit[18] Commercial grade paraffins are obtained from the distillation of petroleum, they are a combination of several hydrocarbons and the longer the length of the chain, the higher their melting temperature and heat of fusion [19] Even though this material possesses desirable properties like low price, nontoxic, and high latent heat it also has the disadvantage of low thermal conductivity[16]. For this reason, this study focuses on a previously mentioned technique for the enhancement of paraffin conductivity: the mixture of the commonly available paraffin wax and expanded graphite.

For the purpose of this study, several ratios of PCM-graphite were used. The graphite nanoparticles increase the thermal conductivity of the PCM, thus increasing the rate at which the material absorbs heat and reaches its melting temperature.

3. RESULTS AND DISCUSSION

The simulation clearly demonstrates an acceleration of heat absorption for each increase of graphite in solution. Graphite greatly decreases the amount of time for the PCM mixture to completely reach its melting temperature.

Trends show a diminishing return for each percent increase of graphite added to the mixture as seen in figure 4 and 5. This is likely due to the combined properties of the mixture approaching those of the a 100% graphite solution. Due to the extreme difference between the thermal conductivity of the paraffin wax and the graphite, changes in behavior are drastic as graphite is first added.

Table 1: This table shows density and specific heat of the materials used in the mixture

Density (kg/m^3)	
Paraffin Wax	Graphite
800	2090
Specific Heat (J/kg K)	
Paraffin Wax	Graphite
1250	690

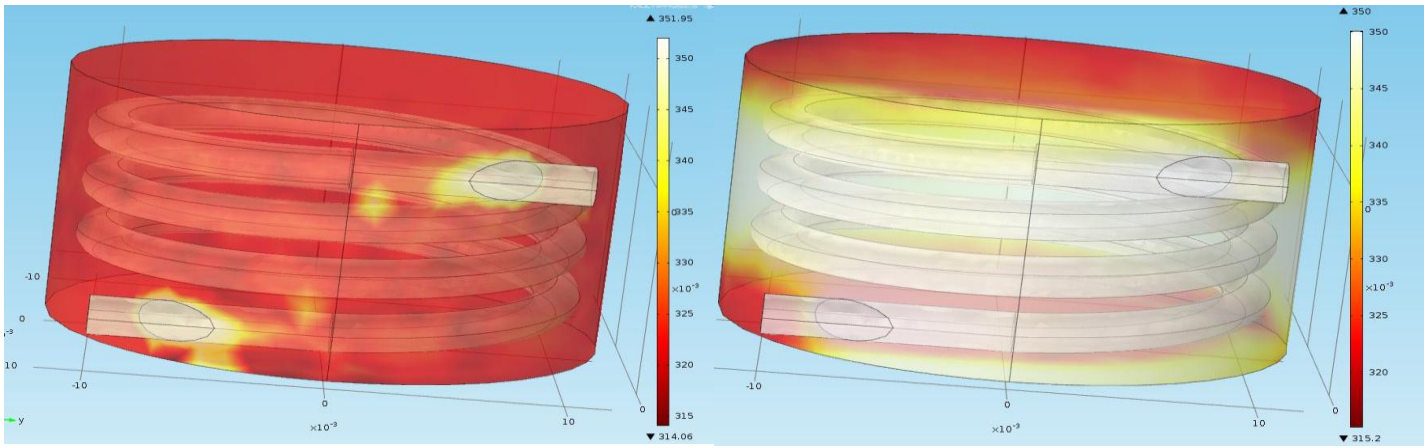

Figure 2: first stage of PCM melting using Helical Heating Element

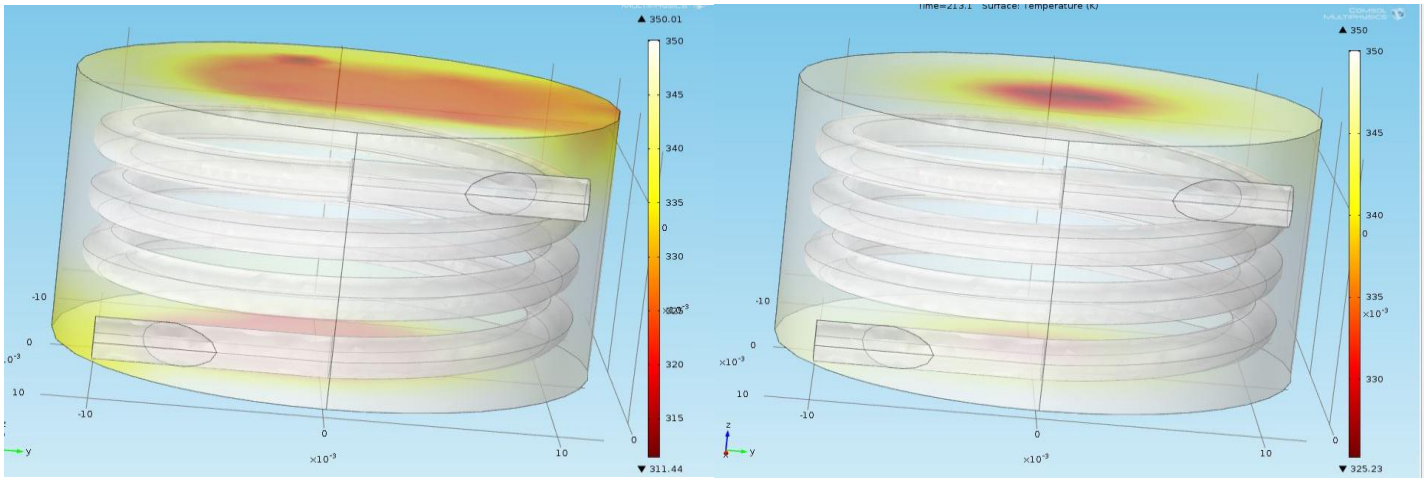

Figure 3 : second stage of PCM melting using Helical Heating Element

Table 2: Material Properties of each Case and the Time to Complete Melting.

	Case 1	Case 2	Case 3	Case 4	Case 5
% PCM	100%	92%	87%	81%	74%
Thermal Conductivity (W/mK)	0.35	10	21	46	66
Latent Heat (J/Kg)	125000	144000	133000	121000	120000
Specific Heat (J/Kg K)	1,250.00	1,205.20	1,177.20	1,143.60	1,104.40
Density of Mixture (kg/m^3)	800.00	903.20	967.70	1,045.10	1,135.40
100% Melted Time (s)	204	9.54	4.34	2.7	1.69

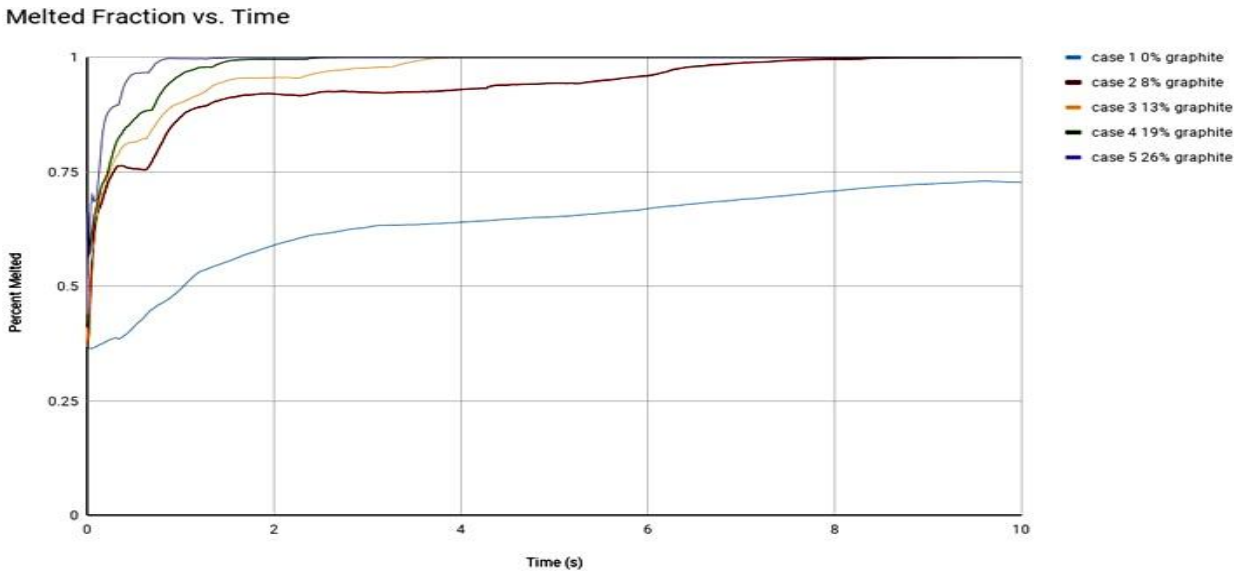

Figure 4: Plot of Average Temperature for each Case

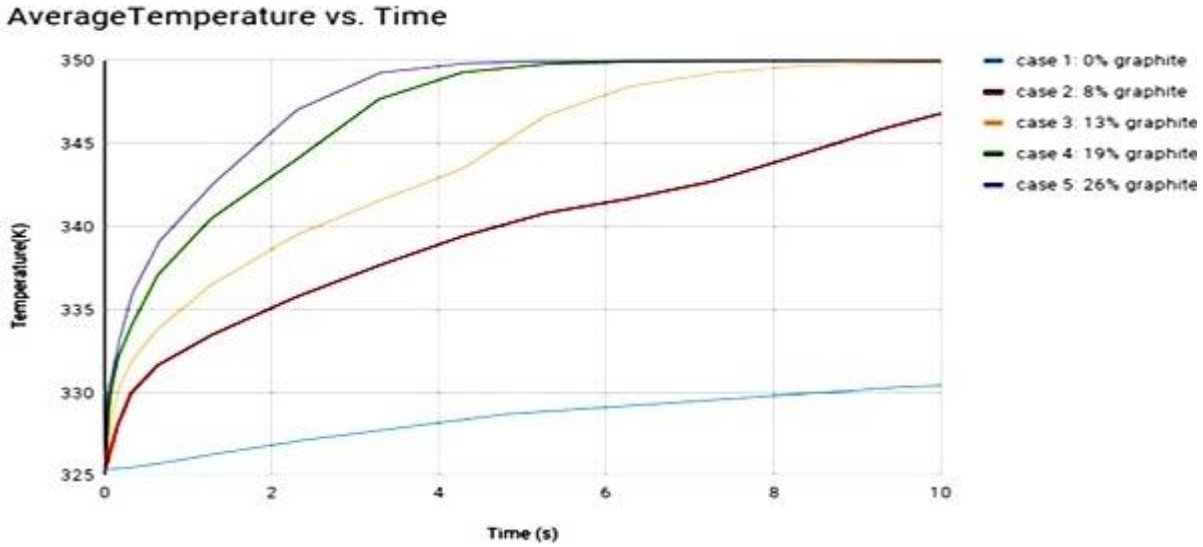

Figure 5: Plot of Melted Fraction versus Time for each Case

This paper studies the role of expanded graphite when added to phase change materials in thermal energy storage systems to enhance the response rate of the TES system. Mixtures of PCM-EG were tested and prepared emperically to assess their heat transfer rate, structural stability, and other thermo-physical properties under a charging cycle. A thermal boundary conditions were used to heat thermal energy to PCM-EG mixtures at various EG percentages. Considerable improvement in melting time were performed when EG added to the PCM. For example, the response rate of the system enhanced about significantly when 26% EG added to the PCM which had a reduction in thermal energy storage of the system, as the penalty. The numerical results used to study the heating cycle for samples clearly portrays the hot zone and development within the composite by time that helps to better understand the melting process. Moreover, the presented data in this paper reveals that the inherent structure of the EG did affect the thermo-physical of composite material.

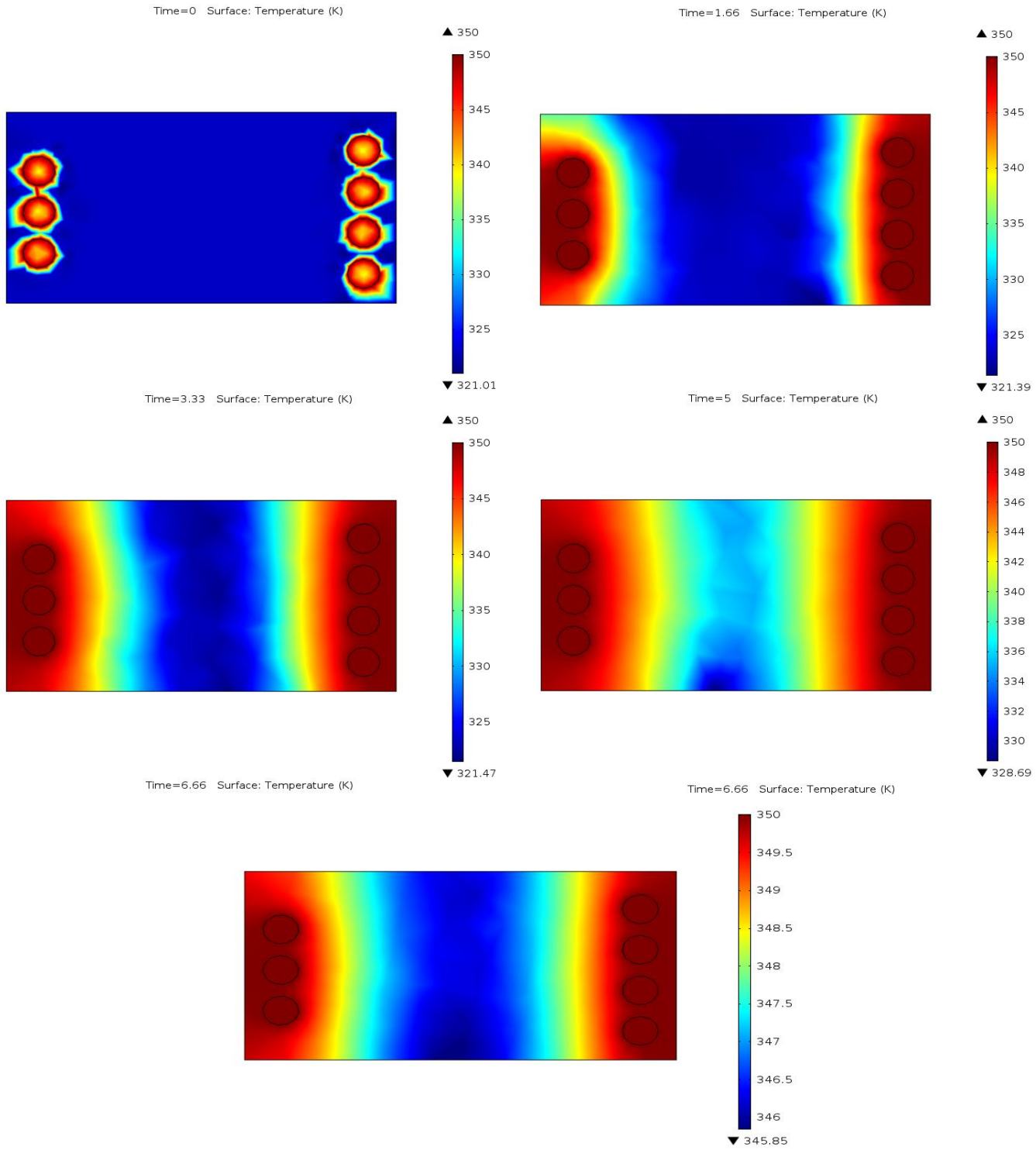

Figure 6: Melted Fraction Over Time for Case 2, 8% Graphite Solution

4. CONCLUSION

The study has combined heat conduction measurements with a fluid dynamics model to numerically calculate the time of melted fraction for a helical pipe coil including a composite phase change material (PCM), paraffin wax, and the nano-particle material immersed in the base was expanded graphite. To our knowledge this is the first time that a numerical model has been applied to enable numerical predictions of performance of latent heat energy storage. Five cases (0%, 8%, 13%, 19%, and 26%) were tested with different percentages of expanded graphite in mixture. Simulation and analysis was done using COMSOL Multiphysics 4.3a. Parameters examined were the average temperature of the body, the time to reach the coil temperature, the melted fraction of the PCM, and the time to reach complete melting. Outcomes perform that a decreasing return for each percent enhance of graphite applied to the mixture. This is mostly due to the mixed thermal and physical features of the composite approaching those of the a 100% graphite solution. Because of the huge discrepancy between the thermal conductivity of the paraffin wax and the graphite, variations in behavior are significantly eye-catching as graphite is first added.

Expanded graphite proved to be a potentially efficient method of increasing thermal storage efficiency for paraffin based heat storage systems. The improvement to thermal conductivity increased exponentially as the graphite was increased. The same is true for the total time required to completely melt the material, which decreased exponentially as graphite increased. After analyzing the trendline of conduction and melting time temperature with an increase in graphene, the conclusion was drawn that a graphite content of 8% by weight was the ideal to increase overall efficiency.

REFERENCES

[1] Hidden Costs of Energy: Unpriced Consequences of Energy Production and Use. National Research Council of the National Academies. The National Academies Press Washington D.C. p 358 2010.

[2] Abhay B. Lingayat, Yogesh R. Suple. Review on Phase Change Materials As Thermal Energy Storage Medium: Materials, Application. Nagpur University, India. IJERA 2013.

[3] Atul Sharma V.V. Tyagi C.R Chen, D.Buddhi. Review on the thermal energy storage with phase change materials and applications. Devi Ahila University India. Sciencedirect 2007

[4] Buddhi. D. Sawhney RL. In: Proceedings on thermal energy storage and energy conversion. 1994

[5] C. Vaccarino, V. Cali, F. Frusteri, A. Parmaliana, Low Temperature Latent Heat Storage with Quasi-eutectic Mixtures containing Ca(N03)2*4H2O J. Solar Energy 109(1987) 176.

[6] Lane G.A. et al Macro Encapsulation of PCM report no. QRO/5117-8 Midland Michigan: Dow Chemical Company 1978 p.152

[7] A. George A. Phase Change Thermal Storage Materials. In Handbook Of Thermal Design. Guyer C, Ed. McGraw Hill Book Co. 1989

[8] F. Frausteri*, V. Leonardi, S. Vasta, G. Restuccia. Thermal Conductivity Measurement of a PCM Based storage System Containing Carbon Fibers. Elsevier Publishings. 2004.

[9] C.J. Hoogendoorn, G.C.J. Bart, Performance and Modeling of latent Heat Stores, Energy 48 (1992)53–58.

[10] R. Velraj, R.V. Seeniraj, B. Hafner, C. Faber, K. Schwarzer, Heat Transfer Enhancement in Latent Heat Storage System, Solar Energy 65 (199) 171-180.

[11] J.A. Weaver, R. Viskanta, Melting of Frozen, Porous Media Contained in a Horizontal or a Vertical, Cylindrical Capsule, Int. J. Heat Mass Transfer 29 (1986) 1943–1951.

[12] A.M. Tayeb, Use of Some Industrial Wastes as Energy Storage Media, Energy Conversion. Manage. 37 (1996) 127–133.

[13] V.V. Calmidi, R.L. Mahajan, The Effective Thermal Conductivity of High Porosity Fibrous Metal Foam, Trans. ASME 121 (1999) 466–471.

[14] J. Fukai, Y. Hamada, Y. Morozumi, O. Miyatake, Effect of Carbon-fiber Brushes on Conductive Heat Transfer in Phase Change Materials, Int. J. Heat Mass Transfer 45 (2002) 4781–4792.

[15] J. Fukai, M. Kanou, Y. Kodama, O. Miyatake, Thermal Conductivity Enhancement of Energy Storage Media Using Carbon Fibers, Energy Conversion. Manage. 41 (2000) 1543–1556.

[16] Farid MM, Khudhair AM, Siddique KR, AL-Hallaj S. A Review on Phase Change Energy Storage: Materials and Applications. Energy Conversion Manage 2004;45:1957-615

[17] Zhong, Yajuan, et al. “Heat transfer enhancement of paraffin wax using compressed expanded natural graphite for thermal energy storage.” *Carbon*, Elsevier, 12 Sep. 2009 300-304

[18] Abhat A. Low temperature latent heat thermal energy storage: heat storage materials. Sol Energy 1983;30:3 13–32

[19] Himran S, Suwono A, Mansori GA. Characterization of alkanes and paraffin waxes for application as phase change energy storage medium. Energ Source 1994;16:117–28.

Journal of Mechanical Engineering and Modern Technology
www.jmemt.jarap.org
Volume 1 Issue 1, 30 June 2018
PP. 37-52

HEAT EXCHANGER TECHNOLOGY AND APPLICATIONS: GROUND SOURCE HEAT PUMP SYSTEM FOR BUILDINGS HEATING AND COOLING

Abdeen Mustafa Omer

Energy Research Institute (ERI), Nottingham, United Kingdom

Key words

Geothermal heat pumps
Direct expansion
Ground heat exchanger
Heating and cooling

Abstract

ome emphasis has recently been put on the utilisation of the ambient energy from ground source and other renewable energy sources in order to stimulate alternative energy sources for heating and cooling of buildings. Geothermal heat pumps (GSHPs), or direct expansion (DX) ground source heat pumps, are a highly efficient renewable energy technology, which uses the earth, groundwater or surface water as a heat source when operating in heating mode or as a heat sink when operating in a cooling mode. It is receiving increasing interest because of its potential to reduce primary energy consumption and thus reduce emissions of the greenhouse gases (GHGs). The main concept of this technology is that it utilises the lower temperature of the ground (approximately <32°C), which remains relatively stable throughout the year, to provide space heating, cooling and domestic hot water inside the building area. The main goal of this study is to stimulate the uptake of the GSHPs. Recent attempts to stimulate alternative energy sources for heating and cooling of buildings has emphasised the utilisation of the ambient energy from ground source and other renewable energy sources. The purpose of this study, however, is to examine the means of reduction of energy consumption in buildings, identify GSHPs as an environmental friendly technology able to provide efficient utilisation of energy in the buildings sector, promote using GSHPs applications as an optimum means of heating and cooling, and to present typical applications and recent advances of the DX GSHPs. The study highlighted the potential energy saving that could be achieved through the use of ground energy sources. It also focuses on the optimisation and improvement of the operation conditions of the heat cycle and performance of the DX GSHP. It is concluded that the direct expansion of the GSHP, combined with the ground heat exchanger in foundation piles and the seasonal thermal energy storage from solar thermal collectors, is extendable to more comprehensive applications.

1. INTRODUCTION

The earth's surface acts as a huge solar collector, absorbing radiation from the sun. In the UK, the ground maintains a constant temperature of 11-13oC several metres below the surface all the year around [1]. Among many other alternative energy resources and new potential technologies, the ground source heat pumps (GSHPs) are receiving increasing interest because of their potential to reduce primary energy consumption and thus reduce emissions of greenhouse gases [2].

Direct expansion GSHPs are well suited to space heating and cooling and can produce significant reduction in carbon emissions. In the vast majority of systems, space cooling has not been normally considered, and this leaves ground-source heat pumps with some economic constraints, as they are not fully utilised throughout the year. The tools that are currently available for design of a GSHP system require the use of key site-specific parameters such as temperature gradient and the thermal and geotechnical properties of the local area. A main core with several channels will be able to handle heating and cooling

simultaneously, provided that the channels to some extent are thermally insulated and can be operated independently as single units, but at the same time function as integral parts of the entire core. Loading of the core is done by diverting warm and cold air from the heat pump through the core during periods of excess capacity compared to the current needs of the building [3-4]. The cold section of the core can also be loaded directly with air during the night, especially in spring and fall when nighttimes are cooler and daytimes are warmer. The shapes and numbers of the internal channels and the optimum configuration will obviously depend on the operating characteristics of each installation. Efficiency of a GSHP system is generally much greater than that of the conventional air-source heat pump systems. Higher COP (coefficient of performance) is achieved by a GSHP because the source/sink earth temperature is relatively constant compared to air temperatures. Additionally, heat is absorbed and rejected through water, which is a more desirable heat transfer medium due to its relatively high heat capacity.

The GSHPs in some homes also provide:

- Radiant floor heating.
- Heating tubes in roads or footbaths to melt snow in the winter.
- Hot water for outside hot tubs and
- Energy to heat hot water.

With the improvement of people's living standards and the development of economies, heat pumps have become widely used for air conditioning. The driver to this was that environmental problems associated with the use of refrigeration equipment, the ozone layer depletion and global warming are increasingly becoming the main concerns in developed and developing countries alike. With development and enlargement of the cities in cold regions, the conventional heating methods can severely pollute the environment. In order to clean the cities, the governments drew many measures to restrict citizen heating by burning coal and oil and encourage them to use electric or gas-burning heating. New approaches are being studied and solar-assisted reversible absorption heat pump for small power applications using water-ammonia is under development [5].

An air-source heat pump is convenient to use and so it is a better method for electric heating. The ambient temperature in winter is comparatively high in most regions, so heat pumps with high efficiency can satisfy their heating requirement. On the other hand, a conventional heat pump is unable to meet the heating requirement in severely cold regions anyway, because its heating capacity decreases rapidly when ambient temperature is below -10°C. According to the weather data in cold regions, the air-source heat pump for heating applications must operate for long times with high efficiency and reliability when ambient temperature is as low as -15°C [6]. Hence, much researches and developments has been conducted to enable heat pumps to operate steadily with high efficiency and reliability in low temperature environments [7]. For example, the burner of a room air conditioner, which uses kerosene, was developed to improve the performance in low outside temperature [8]. Similarly, the packaged heat pump with variable frequency scroll compressor was developed to realise high temperature air supply and high capacity even under the low ambient temperature of –10 to –20°C [9]. Such a heat pump systems can be conveniently used for heating in cold regions. However, the importance of targeting the low capacity range is clear if one has in mind that the air conditioning units below 10 kW cooling account for more than 90% of the total number of units installed in the EU [10].

2. METHODS AND LABORATORY MEASUREMENTS

This communication describes the details of the prototype GSHP test rig, details of the construction and installation of the heat pump, heat exchanger, heat injection fan and water supply system. It also, presents a discussion of the experimental tests being carried out.

2.1. Main Experimental Test Rig

The schematic of the test rig that was used to support the two ground-loop heat exchangers is shown in Figure 1. It consisted of two main loops: heat source loop and evaporation heat pump. Three horeholes were drilled each 30 meters deep to provide sufficient energy. The closed-loop systems were laid and installed in a vertical well. The ground-loop heat exchaners were connected to the heat pump.

2.1.1. Direct expansion heat pump installation

The experimental work undertaken was separated into three parts. The first part dealt with drilling three boreholes each 30 meter deep, digging out the pit and connection of the manifolds and preparation of coils. Holes were grouted with bentonite and sand. The pipes were laid and tested with nitrogen. Then, the pit was backfilled and the heat pump was installed. The second part was concerned with the setting up of the main experimental rig: construction and installation of the heat injection fan, water pump, expansion valve, flow meter, electricity supply, heat exchanger and heat pump. The third part was an installation of refrigerator and measurements.

The aim of this project is to present and develop a GSHP system to provide heating and cooling for buildings (Figure 2). The heat source loop consisted of two earth loops: one for vapour and one for liquid. A refrigeration application is only concerned with the low temperature effect produced at the evaporator; while a heat pump is also concerned with the heating effect produced at the condenser.

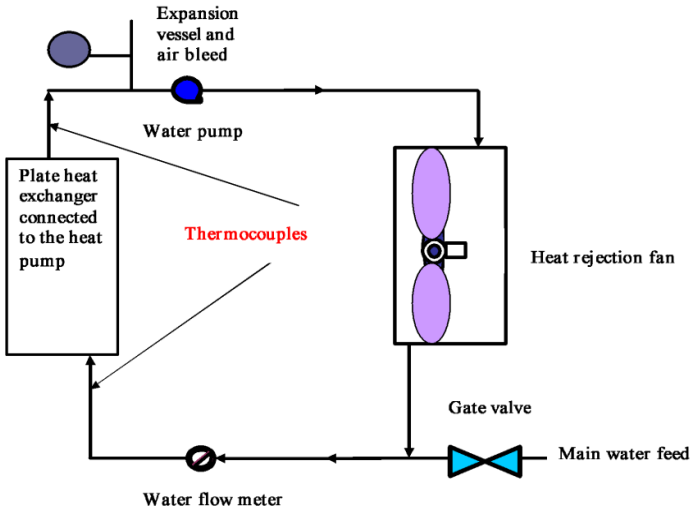

Figure 1. Sketch of installing heat pump**.**

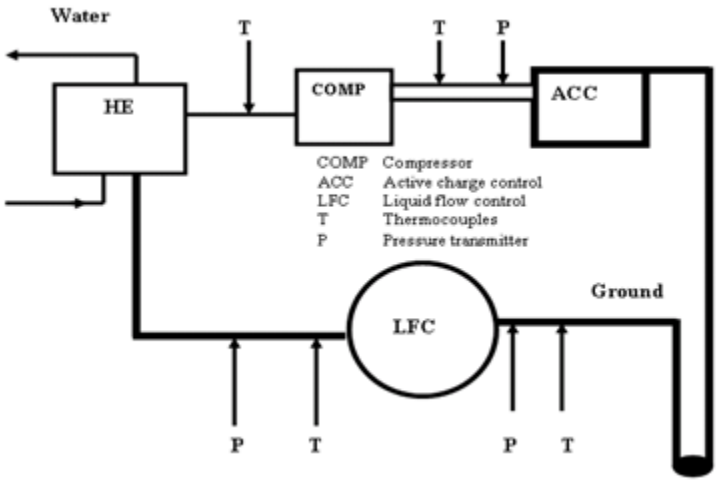

Figure 2.Shows the connections of ground loops to heat pump and heat exchanger.

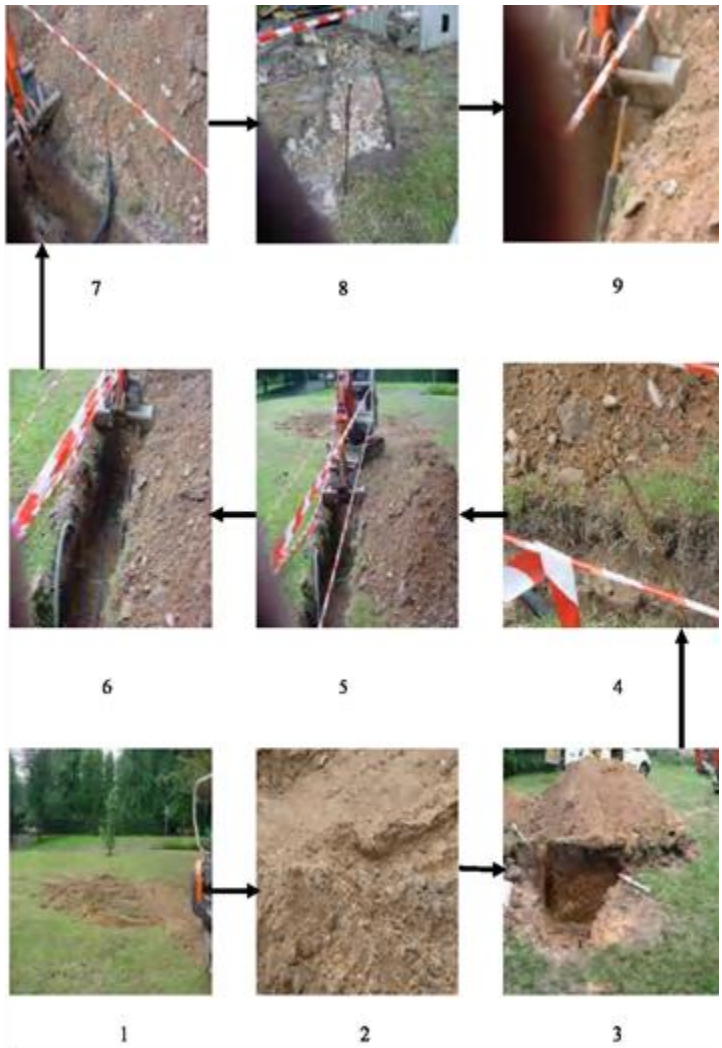

Figure 3. Showing the drilling (1-2) digging of the pit (3), connection of the manifolds (4), grouting, preparation of the coils (5-6) and the source loop, which consists of two earth loops: one for vapour and one for liquid (7-9).

The earth-energy systems, EESs, have two parts; a circuit of underground piping outside the house, and a heat pump unit inside the house. And unlike the air-source heat pump, where one heat exchanger (and frequently the compressor) is located outside, the entire GSHP unit for the EES is located inside the house.

The outdoor piping system can be either an open system or closed loop. An open system takes advantage of the heat retained in an underground body of water. The water is drawn up through a well directly to the heat exchanger, where its heat is extracted. The water is discharged either to an aboveground body of water, such as a stream or pond, or back to the underground water body through a separate well. Closed-loop systems, on the other hand, collect heat from the ground by means of a continuous loop of piping buried underground. An antifreeze solution (or refrigerant in the case of a DX earth-energy system), which has been chilled by the heat pump's refrigeration system to several degrees colder than the outside soil, and circulates through the piping, absorbing heat from the surrounding soil.

The direct expansion (DX) GSHP installed for this study was designed taking into account the local meteorological and geological conditions. The site was at the School of the Built Environment, University of Nottingham, where the demonstration and performance monitoring efforts were undertaken Figures (3-4). The heat pump has been fitted and monitored for one-year period. The study involved development of a design and simulation tool for modelling the performance of the cooling system, which acts a supplemental heat rejecting system using a closed-loop GSHP system. With the help of the Jackson Refrigeration (Refrigeration and Air Conditioning engineers) the following were carried out:

- Connection of the ground loops to the heat pump
- Connection of the heat pump to the heat exchanger
- Vacuum on the system
- Charging the refrigeration loop with R407C refrigerant

2.1.2. Water supply system

The water supply system consisted of water pump, boiler, water tank, expansion and valve flow metre (Figure 4). A thermostatically controlled water heater supplied warm water, which was circulated between the warm water supply tank and warm water storage tank using a pump to keep the surface temperature of the trenches at a desired level.

The ground source heat pump system, which uses a ground source with a smaller annual temperature variation for heating and cooling systems, has increasingly attracted market attention due to lower expenses to mine for installing underground heat absorption pipes and lower costs of dedicated heat pumps, supported by environmentally oriented policies. The theme undertakes an evaluation of heat absorption properties in the soil and carries out a performance test for a DX heat pump and a simulated operation test for the system. In fact, these policies are necessary for identifying operational performance suitable for heating and cooling, in order to obtain technical data on the heat pump system for its dissemination and maintain the system in an effort of electrification. In these circumstances, the study estimated the heat properties of the soil in the city of Nottingham and measured thermal conductivity for the soil at some points in this city, aimed at identifying applicable areas for ground source heat pump system.

Figure 4. Showing preparation of coils (1-2), installation of heat pump (3-6) and connection of water supply system (water pump, flow metre, expansion valve and the boiler) (7-9).

2.2. Design and Installation

Installation of the heat pump system and especially the ground heat exchanger needs to be carefully programmed so that it does not interfere with or delay any other construction activities. The time for installation depends on soil conditions, length of pipe, equipment required and weather conditions. The DX systems are most suitable for smaller domestic applications.

The most important first step in the design of a GSHP installation is accurate calculation of the building's heat loss, its related energy consumption profile and the domestic hot water requirements. This will allow accurate sizing of the heat pump system. This is particularly important because the capital cost of a GSHP system is generally higher than for alternative conventional systems and economies of scale are more limited. Oversizing will significantly increase the installed cost for little operational saving and will mean that the period of operation under part load is increased. Frequent cycling reduces equipment life and operating efficiency. Conversely if the system is undersized design conditions may not be met and the use of top-up heating, usually direct acting electric heating, will reduce the overall system efficiency. In order to determine the length of heat exchanger needed to piping material. The piping material used affects life; maintenance costs, pumping energy, capital cost and heat pump performance

2.3. Heat Pump Performance

The need for alternative low-cost energy resources has given rise to the development of the DX-GSHPs for space cooling and heating. The performance of the heat pump depends on the performance of the ground loop and vice versa. It is therefore essential to design them together. Closed-loop GSHP systems will not normally require permissions/authorisations from the environment agencies. However, the agency can provide comment on proposed schemes with a view to reducing the risk of groundwater pollution or derogation that might result. The main concerns are:

- Risk of the underground pipes/boreholes creating undesirable hydraulic connections between different water bearing strata.
- Undesirable temperature changes in the aquifer that may result from the operation of a GSHP.
- Pollution of groundwater that might occur from leakage of additive chemicals used in the system.

Efficiencies for the GSHPs can be high because the ground maintains a relatively stable temperature allowing the heat pump to operate close to its optimal design point. Efficiencies are inherently higher than for air source heat pumps because the air temperature varies both throughout the day and seasonally such that air temperatures, and therefore efficiencies, are lowest at times of peak heating demand.

A heat pump is a device for removing heat from one place - the 'source' - and transferring it at a higher temperature to another place. The heat pumps consist of a compressor, a pressure release valve, a circuit containing fluid (refrigerant), and a pump to drive the fluid around the circuit. When the fluid passes through the compressor it increases in temperature. This heat is then given off by the circuit while the pressure is maintained. When the fluid passes through the relief valve the rapid drop in pressure results in a cooling of the fluid. The fluid then absorbs heat from the surroundings before being re-compressed. In the case of domestic heating the pressurised circuit provides the heating within the dwelling. The depressurised component is external and, in the case of ground source heat pumps, is buried in the ground. Heat pump efficiencies improve as the temperature differential between 'source' and demand temperature decreases, and when the system can be 'optimised' for a particular situation. The relatively stable ground temperatures moderate the differential at times of peak heat demand and provide a good basis for optimisation.

The refrigerant circulated directly through the ground heat exchanger in a direct expansion (DX) system but most commonly GSHPs are indirect systems, where a water/antifreeze solution circulates through the ground loop and energy is transferred to or from the heat pump refrigerant circuit via a heat exchanger. This application will only consider closed loop systems. The provision of cooling, however, will result in increased energy consumption and the efficiently it is supplied. The GSHPs are particularly suitable for new build as the technology is most efficient when used to supply low temperature distribution systems such as underfloor heating. They can also be used for retrofit especially in conjunction with measures to reduce heat demand. They can be particularly cost effective in areas where mains gas is not available or for developments where there is an advantage in simplifying the infrastructure provided.

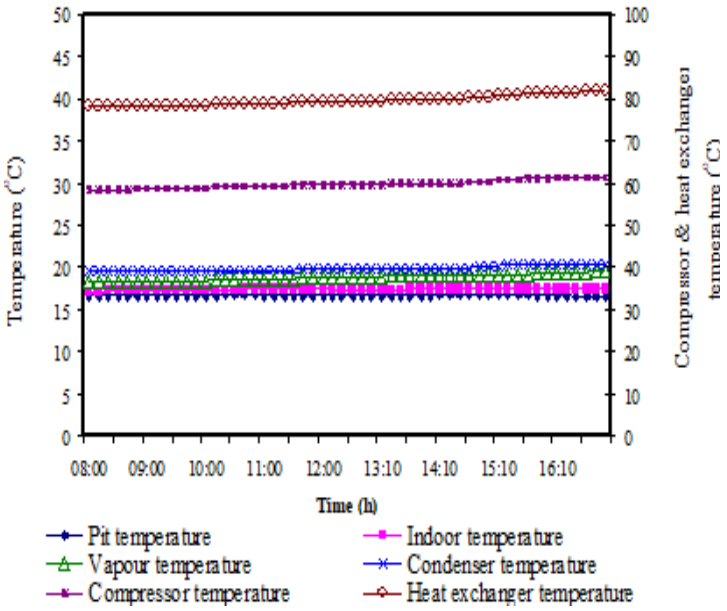

Figure 5. Variation of temperatures per day for the DX system.

2.3.1. Coefficient of performance (COP)

Heat pump technology can be used for heating only, or for cooling only, or be 'reversible' and used for heating and cooling depending on the demand. Reversible heat pumps generally have lower COPs than heating only heat pumps. They will, therefore, result in higher running costs and emissions. Several tools are available to measure heat pump performance. The heat delivered by the heat pump is theoretically the sum of the heat extracted from the heat source and the energy needed to deliver the cycle. Figure 5 shows the variations of temperature with the system operation hours. Several tools are available to measure heat pump performance. The heat delivered by the heat pump is theoretically the sum of the heat extracted from the heat source and the energy needed to derive the cycle. For electrically driven heat pumps the steady state performance at a given set of temperatures is referred to as the coefficient of performance (COP). It is defined as the ration of the heat delivered by the heat pump and the electricity supplied to the compressor:

COP = [heat output (kWth)] / [electricity input (kWel)] (1)

For an ideal heat pump the COP is determined solely by the condensation temperature and the temperature lift:

COP = [condensing temperature (oC)] / [temperature lift (oC)] (2)

Figure 6 shows the COP of heat pump as a function of the evaporation temperature. Figure 7 shows the COP of heat pump as a function of the condensation temperature. As can be seen the theoretically efficiency is strongly dependent on the temperature lift. It is important not only to have as high a source temperature as possible but also to keep the sink temperature (i.e., heating distribution temperature) as low as possible. The achievable heat pump efficiency is lower than the ideal efficiency because of losses during the transportation of heat from the source to the evaporator and from the condenser to the room and the compressor. Technological developments are steadily improving the performance of the heat pumps.

The need for alternative low-cost energy has given rise to the development of the GSHP systems for space cooling and heating in residential and commercial buildings. The GSHP systems work with the environment to provide clean, efficient and energy-saving heating and cooling the year round. The GSHP systems use less energy than alternative heating and cooling systems, helping to conserve the natural resources. The GSHP systems do not need large cooling towers and their running costs are lower than conventional heating and air-conditioning systems. As a result, GSHP systems have increasingly been used for building heating and cooling with an annual rate of increase of 10% in recent years. While in some zones such as hot summer and cold winter areas, there is a major difference between heating load in winter and cooling load in summer. Thus the soil temperature increases gradually after yearly operation of the GSHP system because of the inefficient recovery of soil temperature as the result of imbalance loads (Figure 8). Finally, the increase of soil temperature will decrease the COP of the system.

The first law of thermodynamics is often called the law of conservation of energy. Based on the first law or the law of conservation of energy for any system, open or closed, there is an energy balance as:

[Net amount of energy added to system] =

[Net increase of stored energy in system] (3)

or

[Energy in] – [Energy out] = [Increased of stored energy in system] (4)

In a cycle, the reduction of work produced by a power cycle (or the increase in work required by a refrigeration cycle) equals the absolute ambient temperature multiplied by the sum of irreversibilities in all processes in the cycle. Thus, the difference in reversible and actual work for any refrigeration cycle, theoretical or real, operating under the same conditions becomes:

$W_{actual} = W_{reversible} + T_o \sum I$ (5)

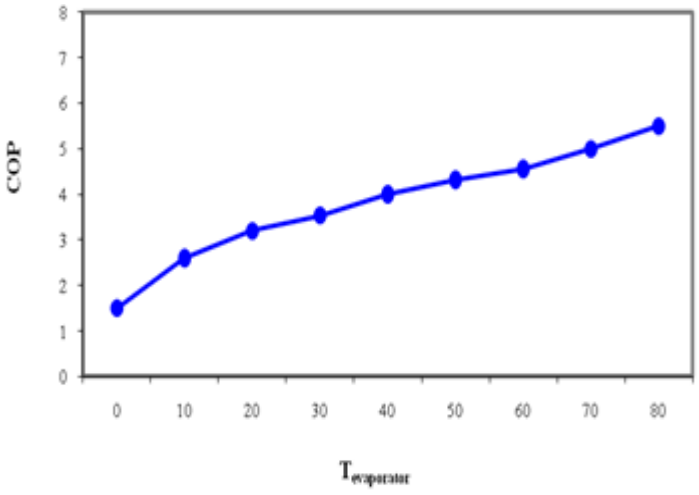

Figure 6. Heat pump performance vs evaporation temperature.

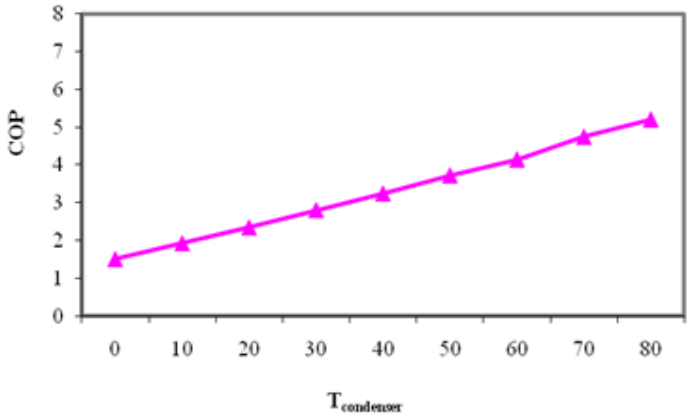

Figure 7.Heat pump performance vs condensation temperature.

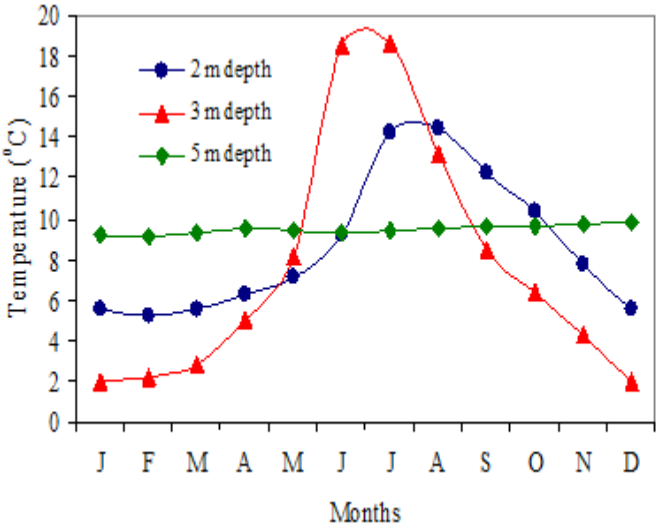

Figure 8.Seasonal temperature variations.

Where:
I is the irreversibility rate, kW/K.
To is the absolute ambient temperature, K
Refrigeration cycles transfer thermal energy from a region of low temperature to one of higher temperature. Usually the higher temperature heat sink is the ambient air or cooling water, at temperature To, the temperature of the surroundings. Performance of a refrigeration cycle is usually described by a coefficient of performance (COP), defined as the benefit of the cycle (amount of heat removed) divided by the required energy input to operate the cycle:
COP = [Useful refrigeration effect]/
[Net energy supplied from external sources] (6)
For a mechanical vapour compression system, the net energy supplied is usually in the form of work, mechanical or electrical and may include work to the compressor and fans or pumps. Thus,
COP = [Qevap] / [Wnet] (7)
In an absorption refrigeration cycle, the net energy supplied is usually in the form of heat into the generator and work into the pumps and fans, or:
COP = (Qevap) / (Qgen + Wnet) (8)
In many cases, work supplied to an absorption system is very small compared to the amount of heat supplied to the generator, so the work term is often neglected. Applying the second law of thermodynamic to an entire refrigeration cycle shows that a completely reversible cycle operating under the same conditions has the maximum possible COP. Table 1 lists the measured and computed thermodynamic properties of the refrigerant. Departure of the actual cycle from an ideal reversible cycle is given by the refrigerating efficiency:
ηR = COP / (COP)rev (9)

2.3.2. Seasonal performance factor (SPF)

There are primary two factors to describe the efficiency of heat pumps. First, the coefficient pf performance (COP) is determined in the test stand with standard conditions for a certain operating point and/or for a number of typical operating points. Second, the seasonal performance factor (SPF), describes the efficiency of the heat pump system under real conditions during a certain period, for example for one year. The SPFs in this case are the ratio of the heat energy produced by the heat pump and the back-up heater and the corresponding energy required of the heat pump. The SPF for individual months and an average value for the year 2008 for the DX GSHP are shown in Figure 9. The assessment of the 2008 measurement data for the GSHP in the buildings providing both heating and cooling reveals a seasonal performance factor (SPF) of 3.8. The SPF of the individual system was in the range of 3.0-4.6.
The preliminary results show that the GSHP are especially promising when it comes to reaching high efficiencies under real conditions. However, there is still a need for optimisation in the integration of the unit in the supply system for the house and for the control strategies of the heat pump. Thus, a poorly integrated heat source or an incorrectly designed heat sink can decrease the seasonal performance factor of the heat pump. The main point to consider is the careful layout of the system as a whole, rather than with respect to single components. High installation costs have been identified as a major barrier to wider application of the GSHPs often referred to as geothermal heat pumps. The primary reason cited for higher cost is the ground loop. Other factors may be high costs of the GSHP heat pump units and supplies, interior installation, and limited competition. The ground-source machine had lower demand (summer and winter) and lower heating energy use than either of the air heat pumps. Comparisons with natural gas must be based on cost since the units for natural gas (therm = 100,000 Btu) are different than electrical energy unit (kWh).

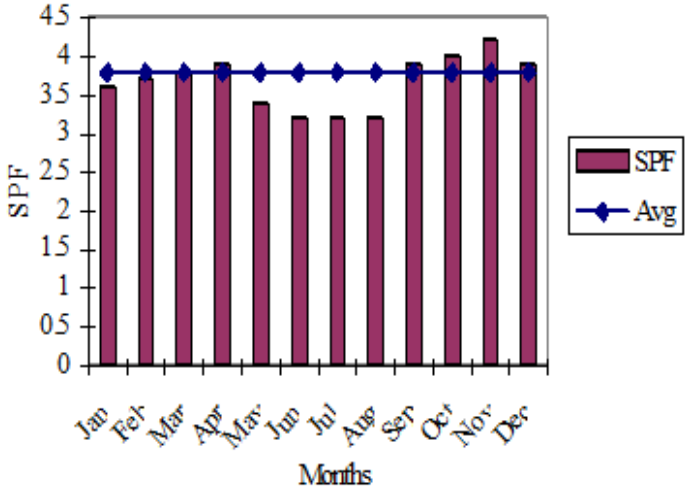

Figure 9. Seasonal performance for individual months and average for 2008.

Table 1. Measured and computed thermodynamic properties of R-22

Measured			Computed		
State	**Pressure (kPa)**	**Temperature (°C)**	**Specific enthalpy (kJ/kg)**	**Specific entropy (kJ/kg°K)**	**Specific volume (m^3/kg)**
1	310	-10	402.08	1.78	0.075
2	304	-4	406.25	1.79	0.079
3	1450	82	454.20	1.81	0.021
4	1435	70	444.31	1.78	0.019
5	1410	34	241.40	1.14	0.0008
6	1405	33	240.13	1.13	0.0008
7	320	-12.8	240.13	1.15	0.0191

3. COMPARISON OF NUMERICAL SIMULATION AND EXPERIMENTS

The GSHPS are generally more expensive to develop, however they have very low operating cost, and justify the higher initial cost. Therefore, it is necessary to have an idea of the energy use and demand of these equipments. The performances are normally rated at a single fluid temperature (0°C) for heating COP and a second for cooling EER (25°C). These ratings reflect temperatures for an assumed location and ground heat exchanger type, and are not ideal indicators of energy use. This problem is compounded by the nature of ratings for conventional equipment. The complexity and many assumptions used in the procedures to calculate the seasonal efficiency for air-conditioners, furnaces, and heat pumps (SEER, AFUE, and HSPF) make it difficult to compare energy use with equipment rated under different standards. The accuracy of the results is highly uncertain, even when corrected for regional weather patterns. These values are not indicators for demand since they are seasonal averages and performance at severe conditions is not heavily weighted.

The American Society of Heating, Refrigerating, and Air-Conditioning Engineers (ASHRAE) (Luo, et al., 2005) recommends a weather driven energy calculation, like the bin method, in preference to single measure methods like seasonal energy efficiency ratio (SEER), seasonal performance factor (SPF), energy efficiency rating (EER), coefficient of performance (COP annual fuel utilisation efficiency rating (AFUE), and heating season performance factor (HSPF). The bin method permits the energy use to be calculated based on local weather data and equipment performance over a wide range of temperatures [10]. Both solid and liquid parts co-existed in one control volume of non-isothermal groundwater flow. It was therefore necessary to integrate the two parts into one energy equation. Accordingly, the governing equation [11] describing non-isothermal groundwater flow in a saturated porous medium was as follows:

$$T(\Delta v) + (\delta T/\delta t)\,\sigma = \alpha t\,\Delta 2T + qt/(\rho Cp)f \quad (10)$$

$$(\rho Cp)t = \psi(\rho Cp)f + (1-\psi)(\rho Cp)s \quad (11)$$

Latent heat during phase changes between freezing soil and thawing soil was regarded as an inner heat source described as follows:

$$WH(\sigma d)\,\delta fs/\delta ts = qs \quad (12)$$

$$(\delta T/\delta t)\,\sigma + Ux\delta Tf/\delta x = \alpha t\,\Delta 2T + qt/(\rho Cp)f \quad (13)$$

Where:

Cp is the specific heat (J kg-1 K-1); q is the internal heat source (Wm-3).

W is the water content in soil (%); T is the temperature (°C).

H is the condensation latent heat of water (J kg-1).

t is the times (s); U is the velocity (ms-1).

fs is the solid phase ratio.

s is the soil; f is the groundwater.

Ψ is the porosity.

α is the convective heat transfer coefficient (Wm-2K-1).

δ is volumetric specific heat ratio.

ρ is the density (kg m-3).

The experiments and calculations are conducted for unsaturated soil without groundwater flow (US), saturated soil without groundwater flow (SS) and saturated soil with groundwater flow (SSG) under same conditions and their results are compared with each other in Figures 10-13. The temperature in vertical boreholes used, as heat source for GSHPs will slowly drop with time, the more so the more energy is extracted. This can be mitigated either by a deeper borehole (in a new installation) or a system to replenish the energy extracted from the hole (in both new and existing installations). Raising the brine temperature from -5°C to 0°C may improve the COP by 10-50% depending on the type of heat pump.

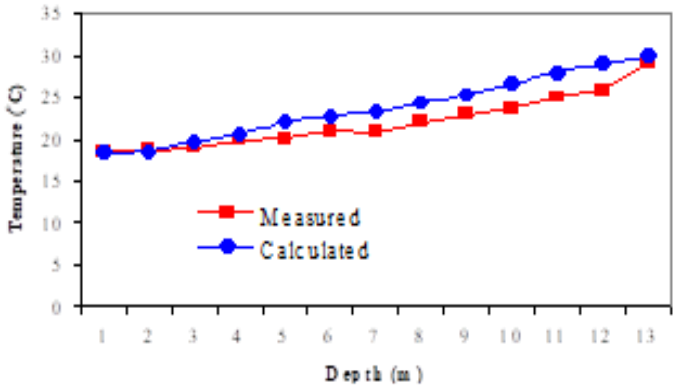

Figure 10. Comparison of calculations and experiments for saturated soil with groundwater flow (SSG).

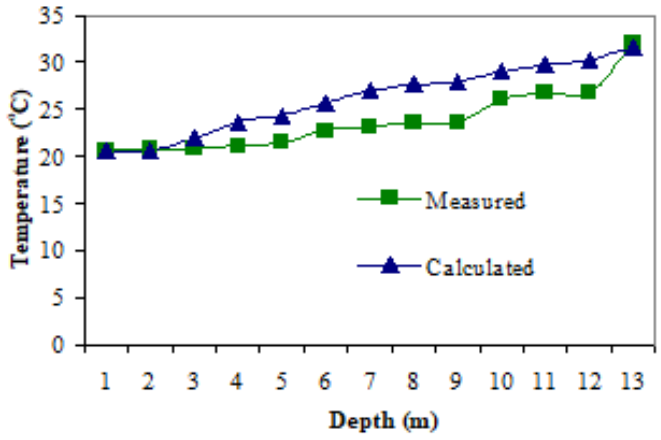

Figure 11. Comparison of calculations and experiments for saturated soil without groundwater flow (SS).

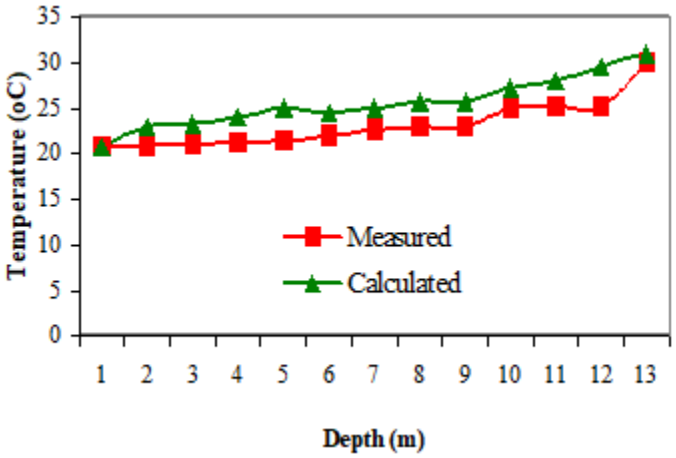

Figure 12. Comparison of calculations and experiments for unsaturated soil without groundwater flow (US).

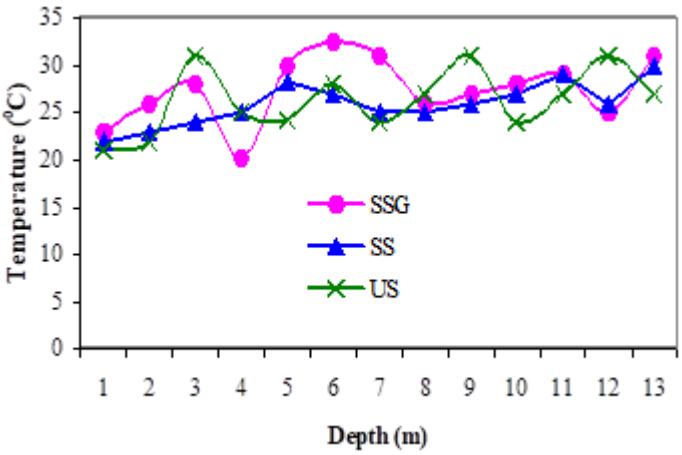

Figure 13. Comparison of experiments for saturated soil with groundwater flow (SSG), saturated soil without groundwater flow (SS) and unsaturated soil without groundwater flow (US).

4. PERFORMANCE ENHANCEMENT OF GSHP

The heat transfer between the GSHP and its surrounding soil affected by a number of factors such as working fluid properties (e.g., 20% glycol) and its flow conditions, soil thermal properties, soil moisture content and groundwater velocity and properties, etc. The GSHP has a great potential to be one of the main energy sources in the future as it can be tapped in a number of different ways and can be used to produce hot water as well as electricity. It has a large spatial distribution with almost all countries having at least low enthalpy resources available (less than 125oC) and many countries around the world in both developing and developed countries are already harnessing it. It is a resource that has always been there and always with be and does not rely on specific factors such as the wind to be blowing or the sun to be shining, as is the case with other forms of renewable energies. The GSHP is inherently clean and environmentally sustainable and will soon become more economical than combustion (fossil fuel) plants as regulations on plant emission levels are tightened and expensive abatement measures such as carbon capture and storage become compulsory. This study urges the need for the GSHP to be considered much more strongly than it currently is in environmental policies as it has been overlooked as a main alternative to fossil fuels and other forms of renewable energies.

Geothermal power utilises the heat energy naturally produced within the earth. Its wide abundance and renewable nature make it an attractive alternative energy source to fossil fuels. The environmental impact of geothermal power plants is negligible in comparison to combustion plants and it is progressively becoming more financially viable as emission regulations are tightened. The technology is increasingly being utilised by countries all over the world, as there are many different ways in which geothermal can be harnessed. Geothermal power is very competitive with other sources of energy when it comes to energy costs. Table 2 shows the globally averaged energy costs in 2008 for different energy sources and shows what the potential future energy costs for different sources will be. As the Table 2 shows, geothermal is already generally more financially viable and cost-effective globally than other forms of renewable power, being on par with hydro-electricity (however, it is important to note that costs will vary between countries) [12].

Table 2. Comparison of energy costs between different energy sources

Energy source	Energy costs (US¢/kWh)	Potential future energy costs (US¢/kWh)
Hydro	2-10	2-8
Biomass	5-15	4-10
Geothermal	2-10	1-8
Wind	5-13	3-10
Solar	25-125	5-25
Tidal	12-18	4-10
Coal	4	.4

Over its first year of operation, the ground source heat pump system has provided 91.7% of the total heating requirement of the room and 55.3% of the domestic water-heating requirement, although only sized to meet half the design-heating load. The heat pump has operated reliably and its performance appears to be at least as good as its specification. The system has a measured annual performance factor of 3.16. The system is quiet and unobtrusive and achieved comfort levels. The heat pump does not reduce the useful space in the laboratory, and there are no visible signs of the installation externally (no flue, vents, etc.). The performance of the heat pump system could also be improved by eliminating unnecessary running of the integral distribution pump. It is estimated that reducing the running time of this pump, which currently runs virtually continuously, would increase the overall performance factor to 3.43. This would improve both the economics and the environmental performance of the system. More generally, there is still potential for improvement in the performance of heat pumps, and seasonal efficiencies for ground source heat pumps of 4.0 are already being achieved. It is also likely the unit costs will fall as production volumes increase.

Energy Efficiency Ratio (EER) is a ratio calculated by dividing the cooling capacity in watts per hour by the power input in watts at any given set of rating conditions. Coefficient of performance (COP) is a ratio calculated for both the cooling (C) and heating (H) capacities by dividing the capacity expressed in watts by the power input in watts (excluding any supplementary heat). Table 3 summarises COP for

different loops. Tables 4-5 present energy efficiency ratios for cooling and heating purposes.

Ground storage systems can be classified in many different ways. One of the most important classifications is in accordance to the temperature of the storage. The ground storage systems are classified as follows:

- The GSHPs, without artificial charging the soil - temperature about 10°C.
- Low temperature ground storage - temperature < 50°C.
- High temperature ground storage - temperature > 50°C.

Table 3. COPs for different loops

Type of system	COP_C	COP_H
Opened loops	4.75 at 15°C	3.6 at 10°C
Closed loops	3.93 at 25°C	3.1 at 0°C
Internal loops	3.52 at 30°C	4.2 at 20°C

Table 4. Energy efficiency ratios for cooling and heating applications

Application	Type of system	Minimum EER	Minimum COP
Cooling	Opened loops (10°C)	13.0	-
	Closed loops (25°C)	11.5	-
Heating	Opened loops (10°C)	-	3.1
	Closed loops (0°C)	-	2.8

Table 5. Direct expansion closed loop ground or water source heat pumps

Application	Type of system	Minimum EER	Minimum COP
Cooling	Opened loops (10°C)	11.0	3.2
	Closed loops (25°C)	10.5	3.1
Heating	Opened loops (10°C)	-	3.0
	Closed loops (0°C)	-	2.5

Table 6 shows COP and EER for different applications. Conserving natural resources benefits everyone now and into the future. For homebuilders, green building means the resource-efficient design, construction, and operation of homes. It represents an approach to both building and marketing homes that highlights environmental quality.

Table 6. Key energy star criteria for ground-source heat pumps

Product Type	Minimum EER	Minimum COP	Water Heating (WH)
Closed-loop	14.1	3.3	Yes
With integrated WH	14.1	3.3	N/A
Open-loop	16.2	3.6	Yes
With integrated WH	16.2	3.6	N/A
DX	15.0	3.5	Yes
With integrated WH	15.0	3.5	N/A

5. HEAT EXCHANGER DESIGN

A heat exchanger is usually referred to as a micro heat exchanger (μHX) if the smallest dimension of the channels is at the micrometer scale, for example from 10 μm to 1 mm. Beside the channel size, another important geometric characteristic is the surface area density ρ (m2/m3), which is defined as the ratio of heat exchange surface area to volume for one fluid. It reflects the compactness of a heat exchanger and provides a criterion of classification. Note that the two parameters, the channel size and surface area density, are interrelated, and the surface area density increases when the channel size decreases. The exchangers that have channels with characteristic dimensions of the order of 100 μm are likely to get an area density over 10 000 m 2/m3 and usually referred to as μHXs [13].

By introducing α in the specific heat exchanger performance equation, the volumetric heat transfer power P/V (W/m 3) can be expressed as follows:

$$P = FUA\,\Delta Tm = FUA\,\rho\,\alpha\,V\,\Delta Tm \quad (14)$$

$$P/V = \rho\,FU\,\Delta Tm \quad (15)$$

Where, U, ΔTm and F refer to the overall heat transfer coefficient (W/m2 K), the mean temperature difference (K) and the dimensionless mean temperature difference correction factor for flow configuration respectively. Note that for a specific heat exchanger performance, high values of α lead to a corresponding high volumetric heat transfer power, larger than that of the conventional equipment by several orders of magnitude. As a result, heat exchanger design by miniaturisation technology has become a common research focus for process intensification [14].

The main advantages of the μHX design are "compactness, effectiveness and dynamic". These properties enable exact process control and intensification of heat and mass transfer [15]:

Compactness: The high surface area density reduces substantially the volume of the heat exchanger needed for the same thermal power. As a result, the space and costly material associated with constructing and installing the heat exchanger could be reduced significantly. Moreover, the fluid holdup is small in a μHX; this is important for security and economic reasons when expensive, toxic, or explosive fluids are involved.

Effectiveness: The relatively enormous overall heat transfer coefficient of the μHXs makes the heat exchange procedure much more effective. In addition, the development of microfabrication techniques [16] such as LIGA, stereolithography, laser beam machining, and electroformation allows designing a μHX with more effective configurations and high pressure resistance.

Dynamic: The quick response time of a μHX provides a better temperature control for relatively small temperature differences

between fluid flows. The quick response (small time constant) is connected to the small inertia of the heat transfer interface (the small metal thickness that separates the two fluids). On the other hand, the exchanger as a whole, including the “peripheric” material, usually has a greater inertia than conventional exchangers, entailing a large time-constant. Thus the response of one fluid to a temperature change of the other fluid comprises two “temperature-change waves”, with very distinct time-constants. In conventional exchangers, it is possible that the two responses are blurred into one.

However, the μHXs are not without shortcomings. On one hand, the high performance is counterbalanced by a high pressure drop, a rather weak temperature jump and an extremely short residence time. On the other hand, those fine channels (~100 μm) are sensitive to corrosion, roughness and fouling of the surfaces. Moreover, the distinguishing feature of the μHXs is their enormous volumetric heat exchange capability accompanied with some difficulties in realisation. The μHXs design optimisation lies, on one hand, in maximising the heat transfer in a given volume taking place principally in microchannels, while, on the other hand, minimising the total pressure drops, the dissipations, or the entropy generation when they function as a whole system. Moreover, difficulties such as the connection, assembly, and uniform fluid distribution always exist, all of which should be taken into account at the design stage of the μHXs. All these make the optimisation of the μHXs design a multi-objective problem, which calls for the introduction of multi-scale optimisation method [17] to bridge the microscopic world and the macroscopic world. In recent years, the fractal theory [17] and constructal theory [18] are introduced to bridge the characteristics of heat and mass transfer that mainly takes place in micro-scale and the global performance of the heat exchanger system in macro-scale [19].

The concept of multi-scale heat exchanger is expected to have the following characteristics [20]:

- A relatively significant specific heat exchange surface compared to that of traditional exchangers;
- A high heat transfer coefficient, as heat transfer is taking place at micro-scales and meso-scales;
- An optimised pressure drop equally distributed between the various scales;
- A modular character, allowing assembly of a macro-scale exchanger from microstructured modules.

Some difficulties still exist. On one hand, the properties of flow distribution in such an exchanger are still unknown [21]. A lot of research work still needs to be done for the equidistribution optimisation. On the other hand, 3-D modelling of heat transfer for such an exchanger requires a thorough knowledge of the hydrodynamics and profound studies on elementary volume (smallest scale micro channels). Finally, maintenance problems for this type of integrated structures may become unmanageable when fouling; corrosion, deposits or other internal perturbations are to be expected. Figures 14-16 show the connections of the heat exchanger, water pump, heat rejection fan and expansion valve.

The present DX GSHP system has been designed taking into account the local metrological and geological conditions and then systems was installed, using the ground source as a heat source. This project yielded considerable experience and performance data for the novel methods used to exchange heat with the primary effluent. The heat pump have also fitted in dry, well-ventilated position where full access for service was possible and monitored the performance of a number of the DX GSHPs, including one so-called "hybrid" system that included both ground-coupling and a cooling tower.

Figure 14. Shows the heat exchanger.

Figure 15. Shows the connections of the heat exchanger, water pump, heat rejection fan and expansion valve.

Figure 16. Shows the connections of the heat exchanger and expansion valve.

The GSHPs provide an effective and clean way of heating buildings worldwide. They make use of renewable energy stored in the ground, providing one of the most energy-efficient ways of heating buildings. They are suitable for a wide variety of building types and are particularly appropriate for low environmental impact projects. They do not require hot rocks (geothermal energy) and can be installed in most of the world, using a borehole or shallow trenches or, less commonly, by extracting heat from a pond or lake. Heat collecting pipes in a closed loop, containing water (with a little antifreeze) are

used to extract this stored energy, which can then be used to provide space heating and domestic hot water. In some applications, the pump can be reversed in summer to provide an element of cooling. The only energy used by the GSHP systems is electricity to power the pumps. Typically, a GSHP will deliver three or four times as much thermal energy (heat) as is used in electrical energy to drive the system. For a particularly environmental solution, green electricity can be purchased. The GSHP systems have been widely used in other parts of the world, including North America and Europe, for many years. Typically they cost more to install than conventional systems; however, they have very low maintenance costs and can be expected to provide reliable and environmentally friendly heating for in excess of 20 years. Ground source heat pumps work best with heating systems, which are optimised to run at a lower water temperature than is commonly used in the UK boiler and radiator systems. As such, they make an ideal partner for underfloor heating systems.

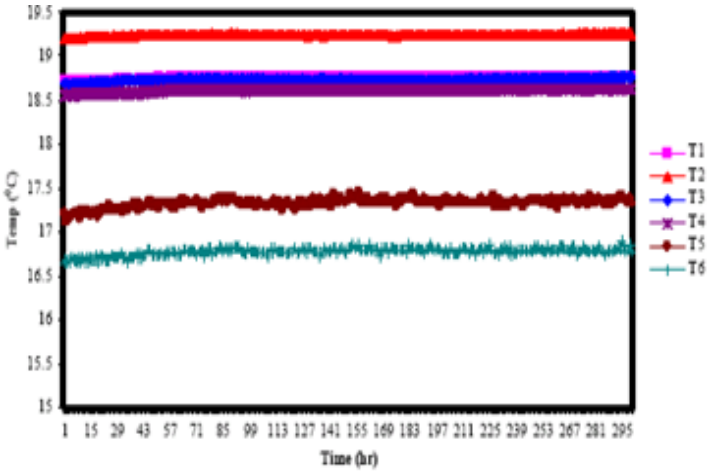

Figure 17. Variation of temperatures for heat exchanger for two weeks.

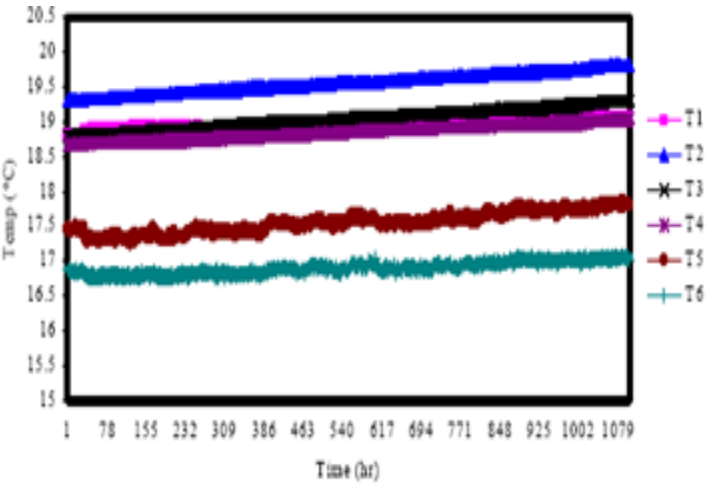

Figure 18. Variation of temperatures for heat exchanger for 45 days.

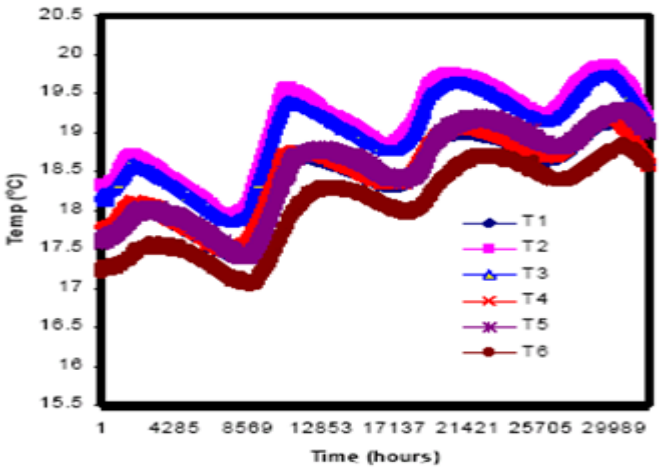

Figure 19. Variation of temperatures for heat exchanger for year.

T1 is the Heat exchanger temperature
T2 is the compressor temperature
T3 is the condenser temperature
T4 is the vapour temperature
T5 is the indoor temperature
T6 is the pit temperature

Figures 17-19 show daily system temperatures for a sample day in each period and the periods of operation of the auxiliary heater and the immersion heater. The performance of the heat pump is inversely proportional to the difference between the condensation temperature and the evaporation temperature (the temperature lift). Figure 20 shows the output of the heat pump for a range of output (condensation) temperatures. These are stable operating conditions, but not true steady state conditions. At output temperatures greater than 40°C, the heat pump was providing heating to the domestic hot water. The scatter in the points is largely due to variations in the source temperatures (range 0.2°C to 4.3°C). These results indicate that the system performance meets and possibly exceeds the specified rating for the heat pump of 3.7 kW at an output temperature of 45°C. Two different control mechanisms for the supply of energy from the heat pump for space heating were tested. From March 2015 until July 2016, the supply of energy from the heat pump to the space heating system was controlled by a thermostat mounted in the room. From August 2008, an alternative control using an outside air temperature sensor was used. This resulted in the heat pump operating more continuously in cold weather and in considerably less use of the auxiliary heater. The amount the auxiliary heater is used has a large effect on the economics of the system. Using the outdoor air temperature sensor results in the return temperature being adjusted for changes in the outdoor temperature and good prediction of the heating requirement. Very stable internal temperatures were maintained. Figure 20 shows the daily total space heating from the heat pump and the auxiliary heater for the two heating control systems. The same period of the year has been compared, using the room temperature sensor and an outdoor air temperature sensor. The operating conditions were not identical, but the average 24-hour temperatures for the two periods were quite similar at 9.26°C and 9.02°C respectively.

6. PERFORMANCE OF THE GROUND COLLECTOR

The flow rate in the ground coil is 0.23 l/s. The heat collection rate varies from approximately 19 W to 27 W per metre length of collector coil. In winter,

the ground coil typically operates with a temperature differential of about 5°C (i.e., a flow temperature from the ground of 2°C to 3°C and a return temperature to the ground coil of -1°C to -2°C). Icing up of the return pipework immediately below the heat pump can be quite severe. The ground coil temperatures are considerably higher in summer when, for water heating, the temperature differential is similar but flow and return temperatures are typically 11°C and 6°C respectively. When the heat pump starts, the flow and return temperatures stabilise very quickly. Even over sustained periods of continuous operation the temperatures remained stable. The ground coil appears adequately sized and could possibly be oversized. Figure 20 shows the variation of ground source heat pump against ground temperatures.

A residential GSHP system is more expensive to install than a conventional heating system. It is most cost-effective when operated year-round for both heating and cooling. In such cases, the incremental payback period can be as short as 3–5 years. A GSHP for a new residence will cost around 9-12% of the home construction costs. A typical forced air furnace with flex ducting system will cost 5-6% of the home construction costs. Stated in an alternative form, the complete cost of a residential GSHP system is $3,500-$5,500 per ton. Horizontal loop installations will generally cost less than vertical bores. For a heating dominated residence, figure around 550 square feet/ton to size the unit. A cooling dominated residence would be estimated around 450 square feet/ton. The Table 3 compares three types of systems.

6.1. Geothermal Energy: Electricity Generation and Direct Use at the End 2008

Concerning direct heat uses, Table 7 shows that the three countries with the largest amount of installed power: USA (5,366 MWt), China (2,814 MWt) and Iceland (1,469 MWt) cover 58% of the world capacity, which has reached 16,649 MWt, enough to provide heat for over 3 million houses [22] Out of about 60 countries with direct heat plants, beside the three above-mentioned nations, Turkey, several European countries, Canada, Japan and New Zealand have sizeable capacity.

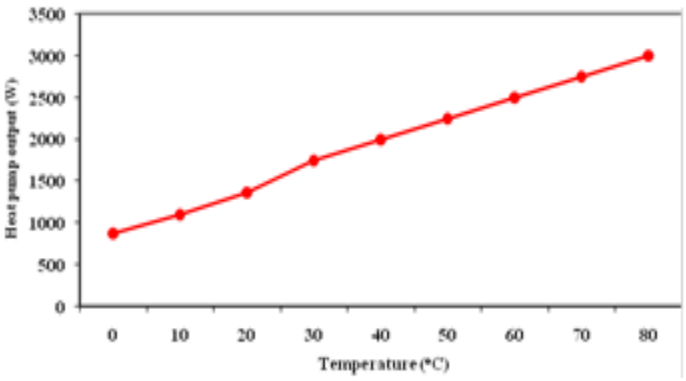

Figure 20. Variation of heat pump output with temperature.

Table 7. Geothermal Energy: Electricity Generation and Direct Use at the End 2008 [23]

Regions	Electricity generation			Direct use		
	Installed capacity	Annual output	Annual capacity factor	Installed capacity	Annual output	Annual capacity factor
	Mw_e	GWh		MW_t	GWh	
Algeria				100	441	0.50
Ethiopia	9	30	0.40			
Kenya	45	390	0.99	1	3	0.25
Tunisia				20	48	0.28
Total Africa	**54**	**420**	**0.89**	**121**	**492**	**0.46**
Canada				378	284	0.09
Costa Rica	115	804	0.80			
El Salvador	161	552	0.39			
Guadeloupe	4	25	0.67			
Guatemala	33	216	0.74	3	30	1.00
Honduras				1	5	0.76
Mexico	750	5 642	0.86	164	1 089	0.76
Nicaragua	70	583	0.95			
United States of America	2 228	16 813	0.86	5 366	5 640	0.12
Venezuela				1	4	0.63
Total North America	**3 361**	**24 635**	**0.84**	**5 913**	**7 052**	**0.14**
Argentina	1	N.A	0.67	26	125	0.55
Chile				N.A	2	0.55
Colombia				13	74	0.63
Peru				2	14	0.65
Total South America	**1**	**N.A**	**0.67**	**41**	**215**	**0.60**
China	29	100	0.39	2 814	8 724	0.35
Georgia				250	1 752	0.80
India				80	699	1.00
Indonesia	590	4 575	0.89	7	12	0.19
Japan	547	3 451	0.72	258	1 621	0.72
Korea (Republic)				51	299	0.67
Nepal				1	6	0.66
Philippines	1 863	10 594	0.65	1	7	0.79
Thailand	N.A	1	0.38	1	4	0.68
Turkey	15	81	0.62	820	4 377	0.61
Total Asia	**3 044**	**18 802**	**0.71**	**4 283**	**17 501**	**0.47**
Austria				255	447	0.20

Table 7. (Continued)

Regions	Electricity generation			Direct use		
	Installed capacity	Annual output	Annual capacity factor	Installed capacity	Annual output	Annual capacity factor
	Mw_e	GWh		MW_t	GWh	
Belgium				4	30	0.87
Bulgaria				107	455	0.48
Croatia				114	153	0.15
Czech Republic				13	36	0.33
Denmark				3	15	0.52
Finland				81	167	0.24
FYR Macedonia				81	142	0.20
France				326	1 365	0.48
Germany				397	436	0.13
Greece				57	107	0.21
Hungary				328	1 400	0.49
Iceland	170	1 138	0.76	1 469	5 603	0.44
Italy	621	4 403	0.81	680	2 500	0.42
Lithuania				21	166	0.90
Netherlands				11	16	0.17
Norway				6	9	0.17
Poland				69	76	0.13
Portugal	20	79	0.45	6	10	0.20
Romania				110	120	0.12
Russian Federation	23	85	0.42	307	1 703	0.63
Serbia and Montenegro				80	660	0.94
Slovakia				132	588	0.51
Slovenia				103	300	0.33
Spain				70	292	0.47
Sweden				377	1 147	0.35
Switzerland				547	663	0.14
United Kingdom				3	10	0.38
Total Europe	**834**	**5 705**	**0.78**	**5 757**	**18 616**	**0.37**
Israel				63	476	0.86
Jordan				153	428	0.32
Total Middle East				**216**	**904**	**0.48**
Australia	N.A	1	0.60	10	82	0.90
New Zealand	410	2 323	0.65	308	1 967	0.73
Total Oceania	**410**	**2 324**	**0.65**	**318**	**2 049**	**0.74**
Total Oceania	**410**	**2 324**	**0.65**	**318**	**2 049**	**0.74**

The GSHPs energy cost savings vary with the electric rates, climate loads, soil conditions, and other factors. In residential building applications, typical annual energy savings are in the range of 30 to 60 percent compared to conventional HVAC equipment.

Most systems have less than 15 kWth heating output, and with ground as heat source, direct expansion systems are predominant. Ground-source heat pumps had a market share of 95% in 2006 [24] (Figure 21). Figure 22 illustrates the monthly energy consumption for a typical household in the United Kingdom. Unlike air source units, GSHP systems do not need defrost cycles nor expensive backup electric resistance heat at low outdoor air temperatures. The stable temperature of a ground source is a tremendous benefit to the longevity and efficiency of the compressor.

The energy used to operate this pump could be reduced if it was controlled to operate only when the heat pump was supplying heat. The improvement in efficiency would be greatest in summer when the heat pump is only operating for a short period each day. If this pump were controlled to operate only when the heat pump is operating, it is estimated that the overall annual performance factor of the heat pump system would be 3.43, and that the average system efficiencies for the period November to March and April to September would be 3.42 and 3.44 respectively [25-28].

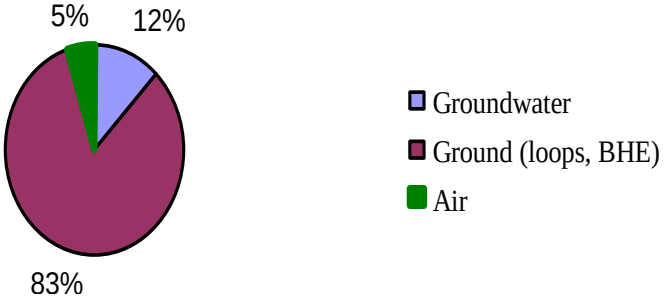

Figure 21. Distribution of heat sources for heat pumps (for space heating).

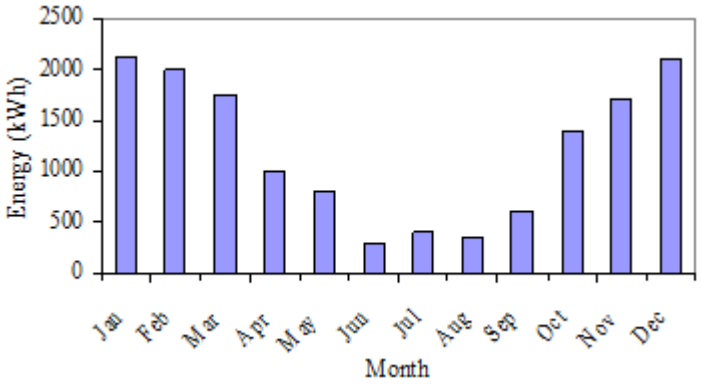

Figure 22. Monthly heating energy demands.

Under these conditions, it is predicted that there would only be a small variation in the efficiency of the heat pump system between summer and winter. This is explained by the fact that although the output temperature required for domestic water heating is higher than that required for space heating, the ground temperatures are significantly higher in the summer than in the winter.

There is clearly a lot more that must be done to support distribution GSHPs in general especially from the perspective of buildings in the

planning and operation, and distribution GSHP systems (Figures 23-25).

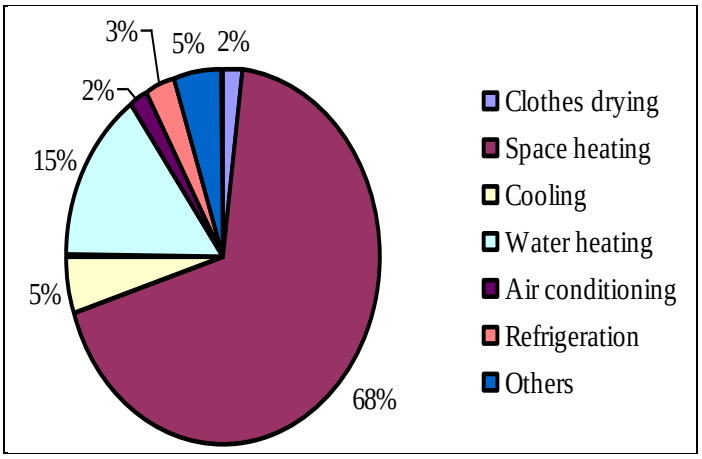

Figure 23. Residential energy consumptions according to end use.

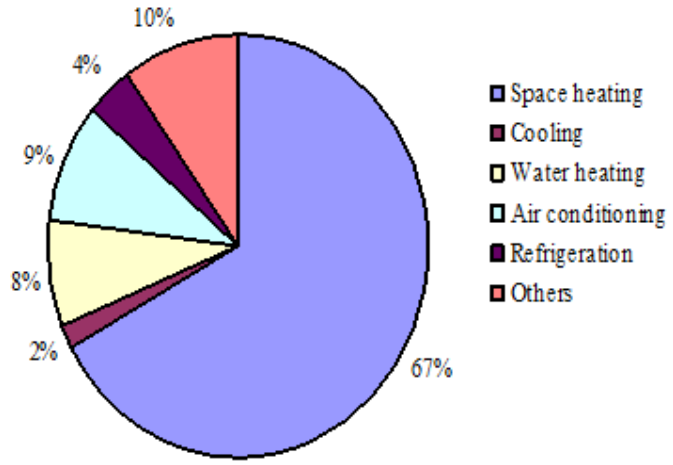

Figure 24. Commercial energy consumptions according to end use.

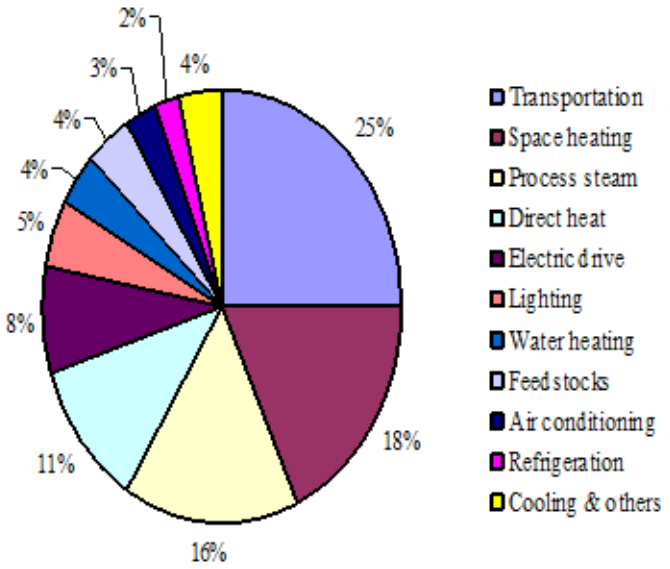

Figure 25. Energy consumptions according to end use.

6.2. Applications of Geoexchanger System

Geoexchanger energy is a natural resource, which can be used in conjunction with heat pumps to provide energy for heating and hot water. CO2 emissions are much lower than gas fired boilers or electric heating systems. Geothermal heating is more expensive to install initially, than electrical or gas fired heating systems. However it is cheaper to run, has lower maintenance costs, and is cleaner in use than other sources of heating.

The temperature of the earth under 2 metres of the surface is a fairly constant 10ºC throughout the year. At a depth of about 100 metres, the temperature of any water or rock is at about 12ºC throughout the year. The heat stored at this depth comes largely from the sun, the earth acting as a large solar collector. For very deep wells, in excess of about 170 metres, there is an added component of heat from the core of the earth. As an approximation, one can add 3ºC of heat gain for every 100 metres of depth drilled into the earth.

A closed loop system takes the heat gained from the bedrock itself. In a vertical system a borehole of a diameter of about 150mm is drilled, depth varies between 32 and 180 metres but will depend on the energy requirements. Multiple boreholes can be drilled. A pair of pipes with a special U-bend assembly at the bottom is inserted into the borehole and the void between pipe and hole backfilled with a special grout solution so that the pipe is in close contact with the rock strata or earth. Fluid (referred to as 'brine' is then circulated through this loop and is heated up by the bedrock. Different rock types will give different results. In some cases a number of boreholes will be made (for example, over a car park) to provide sufficient energy for the heat pump supply. If the ground is not suitable, horizontal loops can be laid or even trench filled 'slinky' loops, which are very simple to install. However trench filled systems and horizontal systems require much more ground than vertical systems. If one has a pond or lake nearby then can lay a closed loop at the base of the pond (it needs to be about 2 metres deep), or simply extract the water directly out of the lake at low level and re-distribute it elsewhere in the lake.

Heat pumps can be cheaper to operate than other heating systems because, by tapping into free heat in the outdoor air, ground or water supply, they give back more energy-in the form of heat-than the equivalent amount of electrical energy they consume. For example, in heating mode, a highly efficient heat pump could extract energy from the earth and transfer it into a building. For every 1 KWh of electrical energy used to drive the heat pump, around 3 to 4 kWh of thermal energy will be produced. In cooling mode, the heat pump works in reverse and heat can be extracted from a building and dissipated into the earth. Heat pumps which work in a heating mode are given a 'coefficient of performance' or 'COP' calculated by dividing the input kWh into the output kWh. This will give a COP figure, which varies with the input temperature and is the ratio of energy in to energy out. In cooling mode, the ratio is called the 'energy efficiency ratio' or 'EER'. When the EER and COP ratios higher, the more efficient the unit. Geothermal/GSHPs are self-contained systems. The heat pump unit is housed entirely within the building and connected to the outside-buried ground loop.

Conventional heating or cooling systems require energy from limited resources, e.g., electricity and natural gas, which have become increasingly more expensive and are at times subjects to shortages. Much attention has been given to sources subject to sources of energy that exist as natural phenomena. Such energy includes geothermal

energy, solar energy, tidal energy, and wind generated energy. While all of these energy sources have advantages and disadvantages, geothermal energy, i.e., energy derived from the earth or ground, has been considered by many as the most reliable, readily available, and most easily tapped of the natural phenomena.

This study has dealt with the modelling of vertical closed-loop and ground source heat pump system. The challenges associated with the design of these systems originate from the fact that they present a unique type of heat transfer problem. First, there are inherent inabilities to make direct observations in the subsurface environment with respect to both space and time. Second, heat transfer within the subsurface environment can be highly transient. Consequently, a considerable amount of research in the past decade has been geared towards optimising the design and performance of GSHP systems and this study is part of those efforts.

The installation and operation of a geothermal system may be affected by various factors. These factors include, but are not limited to, the field size, the hydrology of the site the thermal conductivity and thermal diffusivity of the rock formation, the number of wells, the distribution pattern of the wells, the drilled depth of each well, and the building load profiles. The performance of the heat pump system could also be improved by eliminating unnecessary running of the integral distribution pump. This would improve both the economics and the environmental performance of the system.

The results of soil properties investigation have also demonstrated that the moisture content of the soil has a significant effect on its thermal properties. When water replaces the air between particles it reduces the contact resistance. Consequently, the thermal conductivity varied from 0.25 W/m/K for dry soil to 2.5 W/m/K for wet soil. However, the thermal conductivity was relatively constant above a specific moisture threshold. In fact, where the water table is high and cooling loads are moderate, the moisture content is unlikely to drop below the critical level. In Nottingham, where the present study was conducted, soils are likely to be damp for much of the time. Hence, thermal instability is unlikely to be a problem. Nevertheless, when heat is extracted, there will be a migration of moisture by diffusion towards the heat exchanger and hence the thermal conductivity will increase.

7. CONCLUSION

The direct expansion (DX) ground source heat pump (GSHP) systems have been identified as one of the best sustainable energy technologies for space heating and cooling in residential and commercial buildings. The GSHPs for building heating and cooling are extendable to more comprehensive applications and can be combined with the ground heat exchanger in foundation piles as well as seasonal thermal energy storage from solar thermal collectors. Heat pump technology can be used for heating only, or for cooling only, or be 'reversible' and used for heating and cooling depending on the demand. Reversible heat pumps generally have lower COPs than heating only heat pumps. They will, therefore, result in higher running costs and emissions and are not recommended as an energy-efficient heating option. The GSHP system can provide 91.7% of the total heating requirement of the building and 55.3% of the domestic water-heating requirement, although only sized to meet half the design-heating load. The heat pump can operate reliably and its performance appears to be at least as good as its specification. The system has a measured annual performance factor of 3.16. The heat pump system for domestic applications could be mounted in a cupboard under the stairs and does not reduce the useful space in the house, and there are no visible signs of the installation externally (no flue, vents, etc.).

The performance of the heat pump system could also be improved by eliminating unnecessary running of the integral distribution pump. It is estimated that reducing the running time of the pump, which currently runs virtually continuously, would increase the overall performance factor to 3.43. This would improve both the economics and the environmental performance of the system. More generally, there is still potential for improvement in the performance of heat pumps, and seasonal efficiencies for ground source heat pumps of 4.0 are being achieved. It is also likely the unit costs will fall as production volumes increase. By comparison, there is little scope to further improve the efficiency of gas- or oil-fired boilers.

REFERENCES

[1] Allan, M. L., & Philappacopoulus, A. J. (1999). Ground water protection issues with geothermal heat pumps. Geothermal Resources Council Transactions, 23, 101-105.

[2] Anandarajah, A. (2003). Mechanism controlling permeability changes in clays due to changes in pore fluids. Journal of Geotechnical and Geo environmental Engineering, 129(2), 163-172.

[3] ASHRAE, (1995). Commercial/Institutional Ground Source Heat Pump Engineering Manual. American Society of heating, Refrigeration and Air-conditioning Engineers, Inc. Atlanta, GA: USA.

[4] Bejan, A. (2000). Shape and Structure, from Engineering to Nature. Cambridge University Press: London. The many faces of protease-protein inhibitor interaction. EMBO J. 7, 1303-1130. 2000.

[5] Bergles, A. E. (1988). Some perspectives on enhanced heat transfer - second generation heat transfer technology. Journal of Heat Transfer, 110, 1082-1096.

[6] Bowman, W. J. & Maynes, D. (2001). A Review of Micro-Heat Exchangers Flow Physics, Fabrication Methods and Application. Proc. ASME IMECE, New York, USA, HTD-24280.

[7] EPRI and NRECA, (1997). Grouting for vertical geothermal heat pump systems: Engineering design and field procedures manual. Electric Power Research Institute TR-109169, Palo Alto, CA, and National Rural Electric Cooperative Association, Arlington, VA.

[8] Fahlen, Per. (1997). Cost-effective heat pumps for Nordic countries, and heat pumps in cold climates. The 3rd International Conference, Acadia University, Wolfville, Canada. 1997.

[9] Fridleifsson, I. B. (2003). Status of geothermal energy amongst the world's energy sources. Geothermics, 30, 1-27.

[10] Jo, H. Y., Katsumi, T., Benson, C. H., &Edil, T. B. (2001). Hydraulic conductivity and swelling of nonprehydrated GCLs permeated with single-species salt solutions. Journal of Geotechnical and Geoenvironmental Engineering, 127(7), 557-567.

[11] Kalbus, E., Reinstrof, F., &Schirmer, M. (2006). Measuring methods for groundwater surface water interactions: a

review. Hydrology and Earth System Sciences, Vol. (10), pp. 873-887.

[12] Knoblich, K., Sanner, B., & Klugescheid, M. (1993). Ground source heat pumps. Giessener Geologische Schriften, 49, pp. 192, Giessen.

[13] Li, J., Zhang, J., Ge, W. & Liu, X. (2004). Multi-scale methodology for complex systems. Chemical Engineering Science, 59, 1687-1700.

[14] Luo, L., &Tondeur, D. (2005). Multiscale optimisation of flow distribution by constructal approach. Particuology, 3, 329-336.

[15] Luo, L., Tondeur, D., Le Gall, H., & Corbel, S. (2007). Constructal approach and multi- scale components. Applied Thermal Engineering, 27, 1708-1714.

[16] Luo, L., Fan, Y. &Tondeur, D. (2007). Heat exchanger: from micro to multi- scale design optimisation, International Journal of Energy Research, 31, 1266-1274.

[17] Mandelbrot, B. (1982). The Fractal Geometry of Nature, 2nd Ed., W. H. Freeman, San Francisco, California.

[18] McCray, K. B. (1997). Guidelines for the construction of vertical boreholes for closed loop heat pump systems. Westerville, OH, National Ground Water Association, pp. 43.

[19] Petrov, R. J., Rowe, R. K., & Quigley, R. M. (1997). Selected factors influencing GCL hydraulic conductivity, Journal of Geotechnical and Geoenvironmental Engineering, 123(8): 683-695.

[20] Philappacopoulus, A. J., & Berndt, M. L. (2001). Influence of debonding in ground heat exchangers used with geothermal heat pumps. Geothermics, 30(5), 527-545.

[21] Rafferty, K. (2003). Why do we need thermally enhanced fill materials in boreholes? National Ground Water Association.

[22] Ramshaw, C. (1995). Process Intensification in the Chemical Industry, Mechanical Engineering Publications Ltd, London.

[23] Rybach, L. &Hopkirk, R. (1995). Shallow and Deep Borehole Heat Exchangers - Achievements and Prospects. Pro. World Geothermal Congress 1995: 2133-2139.

[24] Rybach, L., &Eugster, W. J. (1997). Borehole Heat Exchangers to Tap Shallow Geothermal Resources: The Swiss Success Story. In: S. F. Simmons, O. E.

[25] Shah, R. K. (1991). Compact Heat Exchanger Technology and Applications, in Heat Exchange Engineering, Volume 2, Compact Heat Exchangers: Techniques of Size Reduction, eds. E. A. Foumeny and P. J. Heggs, pp. 1–23, Ellis Horwood Limited, London.

[26] Smith, M. D., & Perry R. L. (1999). Borehole grouting: Field studies and therm performance testing. ASHRAE Transactions, 105(1), 451-457.

[27] USEPA, (1997). A short primer and environmental guidance for geothermal heat pumps. U.S.A Environmental Protection Agency EPA 430-K-97-007, pp. 9.

[28] USGAO, (1994). Geothermal energy: outlook limited for some uses but promising for geothermal heat pumps, USA General Accounting Office RECD -94-84.

Nomenclatures

ACH	Air changes Per hour
GSHP	Ground source heat pump
HRV	Heat recovery ventilator
DC	Direct current
HSPF	Heating season performance factor
SEER	Seasonal energy efficiency ratio
Btu	British thermal unit
EER	Energy efficiency rating
DX	Direct expansion
GS	Ground source
EPA	Environmental Protection Agency
HVAC	Heating, ventilating and air conditioning
DETR	Department of the Environment Transport and the Regions
DTI	Department of Trade and Industry
AFUE	Annual fuel utilisation efficiency rating
ARI	The Air-conditioning and Refrigeration Institute
COP	Coefficient of performance (%)
GHP	GEOTHERMAL HEAT PUMP
GL	Ground loop
HP	Heat pump
N	Air change per hour (ACH) (h-1)
P	Pressure (Pa) (kPa)
Q	Heat (thermal energy) (J)
Qc	Capacity (thermal power) (W)